SIGNAL PROCESSING TECHNIQUES
FOR ULTRASONIC INSPECTION

BY

ØIVIND MOEN

Submitted for the Degree
of
Doctor of Philosophy
at
The University of Aston in Birmingham

October
1981

ACKNOWLEDGEMENTS

I would like to thank the Director of the Atomic Energy Research Establishment, Harwell for financial support during the period of research leading to this thesis.

Without the moral support and advice of my two supervisors Dr. J. F. W. Bell and Dr. G. J. Curtis this thesis would not have appeared.

I would also thank my wife, Marion, who had to bear with me during many difficult periods, always giving kind suggestions; and finally being an excellent and patient advisor for the intricacies of the English Language.

CONTENTS

Page

APPENDICES

LIST OF FIGURES

Figure Page

CHAPTER ONE

INTRODUCTION

This thesis discusses the need for nondestructive testing and highlights some of the limitations in present day techniques. Special interest has been given to ultrasonic examination techniques and the problems encountered when they are applied to thick welded plates. Some suggestions are given using signal processing methods.

Chapter 2 treats the need for nondestructive testing as seen in the light of economy and safety. A short review of present day techniques in nondestructive testing is also given. The special problems using ultrasonic techniques for welded structures is discussed in Chapter 3 with some examples of elastic wave propagation in welded steel.

The limitations in applying sophisticated signal processing techniques to ultrasonic NDT are mainly found in the transducers generating or receiving the ultrasound. Chapter 4 deals with the different transducers used.

One of the difficulties with ultrasonic testing is the interpretation of the signals encountered. Similar problems might be found with SONAR/RADAR techniques and Chapter 5 draws some analogies between SONAR/RADAR and ultrasonic nondestructive testing. This chapter also includes a discussion on some on the techniques used in signal processing in general. A special signal processing technique found useful is cross-correlation detection and this technique is treated in Chapter 6. Electronic digital computers have made signal processing techniques easier to implement - Chapter 7 discusses the use of digital computers in ultrasonic NDT.

Experimental equipment used to test cross-correlation detection of ultrasonic signals is described in Chapter 8.

Chapter 9 summarises the conclusions drawn during this investigation.

CHAPTER TWO

A SHORT REVIEW OF NONDESTRUCTIVE TESTING

2.1 THE NEED FOR NONDESTRUCTIVE TESTING

Nondestructive testing is probably as old as man. The inspection of tracks and caves for their safe use has been performed by looking at them and making a comparison with what is expected. Present day nondestructive testing is based on the same ideas, but there is a clearer division between the individual operations involved in making an assessment of the safety of a structure.

The first operation consists of locating any material defects (often referred to as flaws) present in the structure; and then making an estimate of the size and the orientation of the flaw. The engineering construction details give information about the mechanical properties of the material as well as the geometrical shape of the structure and the working stress distributions. This information facilitates an analysis of the safety of the structure in the presence of the flaw and a decision can be taken for the need of repair.

2.1.1 Critical Crack Size - Stress Analyses and Fracture Mechanics

Flaws will inevitably be present in engineering structures even from the time of production. These flaws can be tolerated, but to a limit.

The fracture stress of a brittle material is given by$^{(1)}$:

$$\sigma_f = \left(\frac{EG_{crit}}{\pi(1-\gamma^2)d}\right)^{\frac{1}{2}} \qquad (2.1)$$

where

E	is Young's modulus
γ	is Poisson's ratio
$2d$	is the crack length
G_{crit}	is the materials fracture toughness

When the applied stress exceeds the fracture stress the crack can propagate catastrophically. Depending on the orientation of the flaw with respect to the local stress distribution different size flaws can be tolerated. For a given working stress the crack will not propagate before its critical size is reached.

The stress in an engineering structure is not constant. The stress can be represented by a constant and a cyclic part. The cyclic stress will cause a fatigue of the material lengthening any cracks present. The growth of a crack due to fatigue can be represented as in Fig. 2.1, where the crack length is drawn against the number of constant amplitude stress cycles. The crack propagates at first relatively slowly, after which it accelerates with the number of stress cycles. When the crack length reaches the critical length it will propagate quickly under the influence of the constant stress.

To anticipate the crack reaching the critical length,

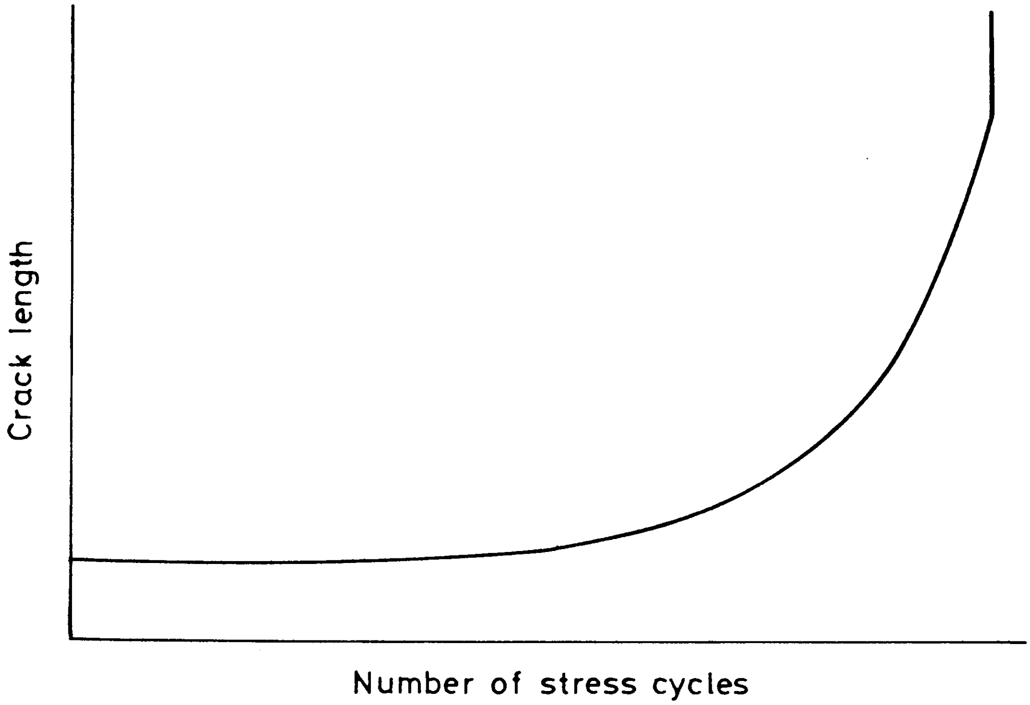

Figure 2.1 Crack length versus the number of fatigue stress cycles.

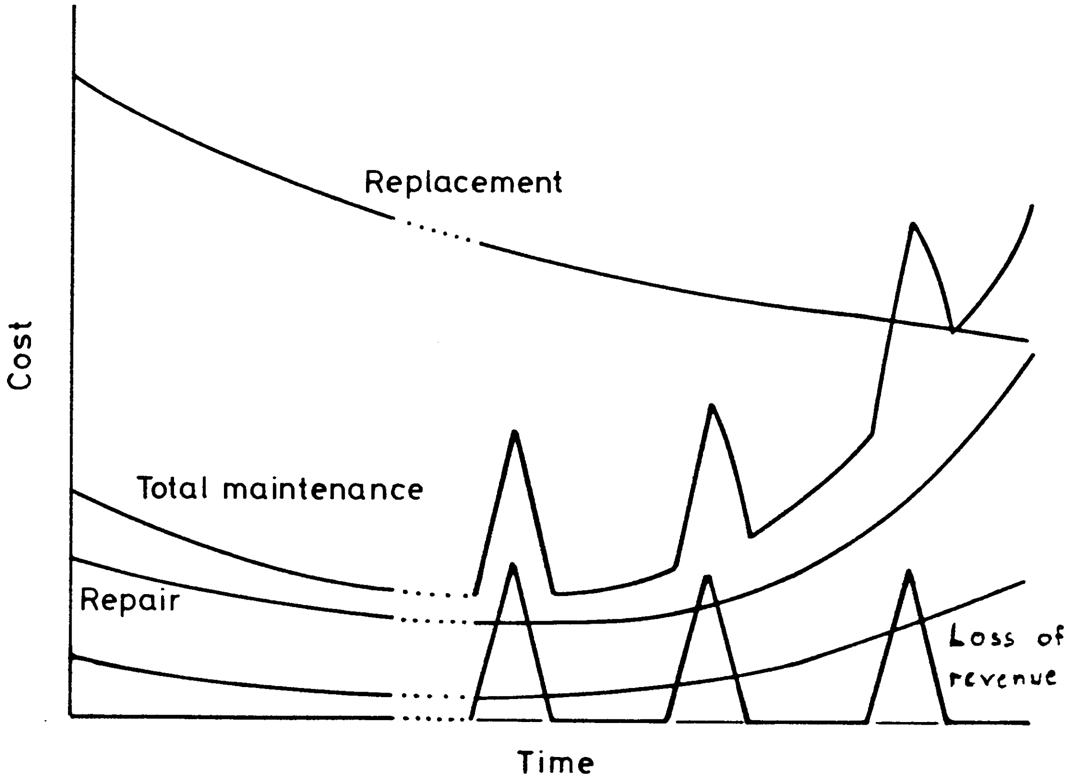

Figure 2.2 The idealized maintenance cost of an engineering structure as a function of time.

monitoring of its growth is required. This is, in principle, achieved by periodic inspection. As the age of the structure is increased the number of fatigue stress cycles is also increased. The accelerated growth of the crack at high stress cycles requires more frequent inspection to be performed towards the predictable end of an engineering structures life.

Before the completion of an engineering structure stringent inspections will be performed to map all sizable material defects. From this data and the calculated stress distribution, the anticipated time for a crack to reach its critical size can be calculated and thence interval between inspections decided.

Using equation (2.1) the critical crack length might be found for a low alloy steel with the following elastic properties: $E = 210\ 10^9\ (N/m^2)$, $\gamma = 0.3$, and $G_{crit} = 24\ 10^3\ (J/m^2)$. Assuming that a thick section of this steel is used in a structure under a working stress of $800\ 10^6 (N/m^2)$; the critical crack length, 2d, is $5.2\ 10^{-3}$(m). To account for fatigue crack growth during the operation period, smaller defects than this need to be found in the construction stage. Such an exchange indicates the order of magnitude of crack size which must be determined by nondestructive methods.

Modern engineering materials will also have ductility, complicating the calculation for critical crack lengths. The understanding of ductile fracture is not yet complete. Assessments of critical flaw sizes are therefore usually performed by experimental fracture tests.

2.1.2 Economic and Safety Considerations

The cost of testing engineering structures must be seen in the light of the cost to replace the structures or the cost of repairing the old one. The idealised maintenance cost of an engineering structure as a function of time is shown in Fig. 2.2. This assumes that no inflation is present. The cost of replacement gradually decreases with time as more efficient production techniques and installation methods are developed. The maintenance cost is initially high as faults from the production are repaired. After the installation period the maintenance cost decreases and keeps constant until faults due to wear start to appear, when it again increases. The economical working life of a structure is exceeded when the maintenance cost exceeds the cost of replacing the structure with a new installation. The working life of an installation can be increased by reducing the cost of maintaining it.

The maintenance cost can be divided into three parts:

(i) The cost of repair.
(ii) The cost of nondestructive testing.
(iii) The loss of revenue during shutdown of a plant due to maintenance.

The maintenance cost can be ideally eliminated during the operation period of the plant if all flaws are characterised during the fabrication period. And the stress analysis and fracture mechanics calculations are performed well during the design stage. The time for the cracks to reach their critical size is then known and no inspection or repair during the operation period is required. Clearly this is not the case in practice as accidentally high stress situations will always occur and the initial evaluation of the flaws is never perfect.

The discussion in this thesis will only be concerned with the nondestructive testing. It is therefore of interest to investigate methods of inspection which are economical and at the same time make reliable measurements of the flaw which do not lead to uneconomical repairs. The cost of repair and loss of revenue during shutdown can easily be extremely high. The loss of revenue from a nuclear power plant of 500 MW power output and at an energy price of 1 pence per kWh will be £120,000 per day.

Certain engineering structures can cause danger to the user and the environment during failure. Examples of such structures are aeroplanes and nuclear power plants. The need for safe operation of such structures makes the inspection requirements more stringent since economy is no longer the sole consideration. Safety factors are introduced in the fracture mechanical calculations increasing the frequency of inspection.

2.2 REVIEW OF TECHNIQUES IN NONDESTRUCTIVE TESTING

The object of this chapter is not to give a detailed history or a review of current NDT techniques, they are adequately assessed elsewhere(2). The object is rather to briefly indicate what is available and the capability and limitations.

2.2.1 Visual Inspection Techniques

The simplest inspection procedure is performed by looking at the structure for surface indications of defects, and is, in many industries, the only one used. A suitably colour contrasting penetrating liquid can be applied to the material surface, thereby increasing the sensitivity for small defects. To improve the sensitivity, magnetic particles, infra-red light or ultra-violet light are commonly used(2).

But clearly defects can also appear in the material having no opening to the surface making them impossible to detect by visual inspection.

2.2.2 Radiographic Inspection Techniques

X-rays (electromagnetic waves with a wavelength in the region 10^{-8} - 10^{-12} (m)) readily penetrate materials and thereby provide a means of probing for deep flaws. The radiographic inspection technique relies on the difference in the attenuation of x-rays between the metal and the flaw. The intensity, I, of x-rays decreases exponentially with the distance travelled:(3)

$$I = I_o e^{-\mu d} \qquad (2.2)$$

The absorption coefficient, μ, depends on the density of the material, and as flaws are often air or oxide filled there is a wide difference in density between flaws and the surrounding metal.

Radiographic equipment is divided into; an x-ray source which is placed on one side of the specimen to be investigated and a detector on the other side. The detector can be a photographic film or an image converter. Both coarse and fine resolution can be achieved. A simple source and photographic plate technique has a resolving power better than millimeters while x-ray microscopes can achieve a resolving power in the order of 0.25 (μm).

The technique is one of the commonly applied NDT methods, but it has limitations both in principle and in applications. On complicated engineering constructions such as on in-service nuclear reactor, access to both sides of the construction might be impossible. (Nevertheless radiographic techniques play a fundamental role at the construction stage and form part of the coded inspection procedures e.g. the American code ASME VIII).

The limitation of principles is that the x-ray visibility of, for example, a planar crack is greatest in the plane of the crack. To size lateral dimensions of the crack ultrasonic inspection is needed. This is an example of the complimentary nature of radiographic and ultrasonic testing, as the latter is not at all accurate in sizing the thickness of the laminar defect.

2.2.3 Ultrasonic Inspection Techniques

The application of high frequency elastic waves (ultrasound) to the nondestructive testing of materials started with Sokoloff's(4) transmission techniques in the 1930's. This technique has similarities with x-ray techniques in that it relies on the difference in attenuation of the elastic wave for the flaw and the surrounding material. The intensity, I, of ultrasound decreases exponentially with the distance, d, travelled:

$$I = I_o \; e^{-\alpha d} \tag{2.3}$$

(compare with equation (2.2))

The attenuation coefficient, α, varies from material to material. For example the attenuation coefficient for air is in the order of dB/mm and that for steel is in the order of dB/cm, at frequencies normally used for ultrasonic NDT.

In Sokoloff's original work, the source and detector were both made of thin plates of quartz which has piezoelectric properties. When quartz is placed in an electric field it will contract and expand in harmony with the applied electric field, hence a generation of elastic waves is achieved. The reverse property is also present in quartz, i.e. when subjected to an elastic wave an electric field is generated thereby yielding a receiver for elastic waves.

The elastic wave propagates with a relatively low velocity when compared to the velocity of electromagnetic waves, the longitudinal elastic wave velocity in steel is approximately 6000 (m/s).

The advancement of electronic equipment during the 1930's enabled a pulse-echo concept to be implemented. Firestone (5) made an apparatus named the Reflectoscope during the early part of the 1940's which relied on this concept. The Reflectoscope sent a short burst of elastic waves into the material and after a short time received any reflected waves from inhomogeneites present in the material. This pulse-echo approach is at present the usual technique for nondestructive testing of materials with ultrasound. One of the advantages over other inspection methods is that access to only one side of the material is required.

The intensity, I, of an elastic wave is given by (6):

$$I = \frac{p^2}{2\rho c}$$

where p is the peak pressure of the elastic wave and ρc the characteristic impedance, z, of the material, i.e. $z = \rho c$. When the elastic wave meets an impedance discontinuity in the material parts of the wave will be reflected. For a plane normally incident wave the ratio of the intensity of the reflected to the incident wave is given by:

$$r_r^2 = \left(\frac{z_2 - z_1}{z_2 + z_1}\right)^2$$

where r_r is the amplitude reflection coefficient and z_2 the impedance of the material causing the inhomogeneity; z_1 the impedance of the surrounding material. When the impedance of the surrounding material is known, the impedance of the flaw causing the reflection can be found from the amplitude of the reflected signal. This enables properties of the flaw to be found.

The lateral position of the flaw can be found by the position of the transducer. The ultrasonic beam sent from a transducer has a finite width so the amplitude of the received signal will be reduced when only the edge of the flaw is in the beam. The amplitude of the reflected signal has also to be used to assess the lateral position of the flaw.

The position in thickness can be found from the transit time, t, of the wave; to the flaw and back.

$$R = \frac{ct}{2}$$

Good thickness resolution requires that the transit time should be accurately measured.

Engineering structures have often maximum stress perpendicular to the thickness of the material and the thickness is also usually the smallest dimension. For inspection during the operational life of the structure, early warnings of critical defects are required. Fatigue cracks have slow changes in dimensions before the crack length reaches its critical length, Fig. 2.1. The requirement for an accurate measurement of the thickness is therefore of utmost importance. Present day thickness measurements rely on the use of short electric pulses, approximating impulses and pulse detection methods. These can measure flaw thickness in the order of millimeters in steel.

The thickness position depends also on the velocity of the elastic wave in the material. This is not always constant as engineering materials are not elastically homogeneous. Welded structures can exhibit relatively large variations in the elastic wave velocities. Such effects are the subject of the next chapter.

CHAPTER THREE

INSPECTION OF WELDS WITH ULTRASOUND

3.1 THE V-SHAPED BUTT WELD

A weld, be it manually or automatically produced, is made by laying down a series of melted pools (beads) in the prepared space, between the parts to be joined. A commonly occurring weld is the V-shaped butt weld shown in Fig. 3.2. This is produced by first laying weld beads at the apex of the V, followed by successive weld runs gradually building up the weld.

3.2 FERRITIC AND AUSTENITIC WELD METAL STRUCTURES

Ferritic welds produced by the submerged arc and manual metal arc processes have grains growing along the maximum thermal gradient in the bead along a [100] crystallographic axis. Deposition of subsequent weld metal reheats the bead and the columnar grain structure is destroyed by the austenitic-ferritic phase transformation that occurs as the solid cools. Fig. 3.1 shows a photomachrograph of a typical ferritic weld. The columnar grain structure which started at the edge of the weld is destroyed further into the weld. This gives a randomly or equiaxed grain structure.

Austenitic welds produced by the submerged arc process develop a texture during the multipass build up of weld metal. Macroscopic examination shows that the weld consists of highly aligned columnar grains which originate at the fusion boundary. Fig. 3.2 shows macrographs of a single V preparation weld. Fig. 3.2(a) is for the width-through thickness plane of the weld. Fig. 3.2(b) is for the length-through thickness plane of the weld. Fig. 3.2(c) is for the length-width of the weld. Close examination shows that only the grains which are situated near to the weld surface, or those which lie on the very centre of the weld, are arranged with their longitudinal axis, (i.e. C axis or [100] direction) normal to the free surface of the weld. The orientation of the grain growth is very much dependent upon the heat flow patterns built up as welding proceeds. In fact near to the surface of the weld the grains are not quite vertical, but tilt over in the direction of welding as they follow the heat flow. Away from the surface and the central axis of the weld, the grains are curved and almost continuous from the fusion faces. Epitaxial growth from bead-to-bead exists and is well shown in Fig. 3.2(a). It will be seen that in places the grains deviate from the vertical by as much as 45°. Observations of Fig. 3.2(b) and 3.2(c) indicates that a grain grows epitaxially with strong curvature in the width-through thickness plane, it only slightly deviates from the vertical in the two mutually perpendicular planes. As will be discussed later, such a texture will yield ultrasonic velocities which vary with direction within the material. It is, however, useful to consider the nature of the texture and x-ray pole figures help to define it. Fig. 3.3(a) shows a pole figure for the point shown in Fig.3.2(a)in the width-thickness plane of the weld. As will be seen the texture could be described as one where the individual body centred cubic crystallites have aligned themselves with their [100] axes parallel and normal to the face surface of the weld, but with their [010] and [001] axes randomly oriented around the normal. Fig. 3.3(c) shows a pole figure for a point on the free surface of the weld, and it represents isotropy. Near to the surface, the pole figure evidence suggests that the weld can be considered to have an orthotropic texture. If however, a point such as 8 in Fig.3.2(b)is examined the pole figure shown in Fig. 3.3(b) is obtained. It will be seen that the [100] axis has tilted by 45° with randomised [010] and [001] axes. This correlates with the visual evidence of the macrograph for this point. In general the weld texture might be described as orthotropic, but with spatially variable tilting of the aligned [100] axes of the crystallites.

The elastic constants are different for different directions of the crystals giving different propagation velocities and modes of propagation for the elastic wave. Interpretation of the returned flaw echo will obviously be effected by the differences in the propagation directions. A review of elastic wave propagation in crystalline metals

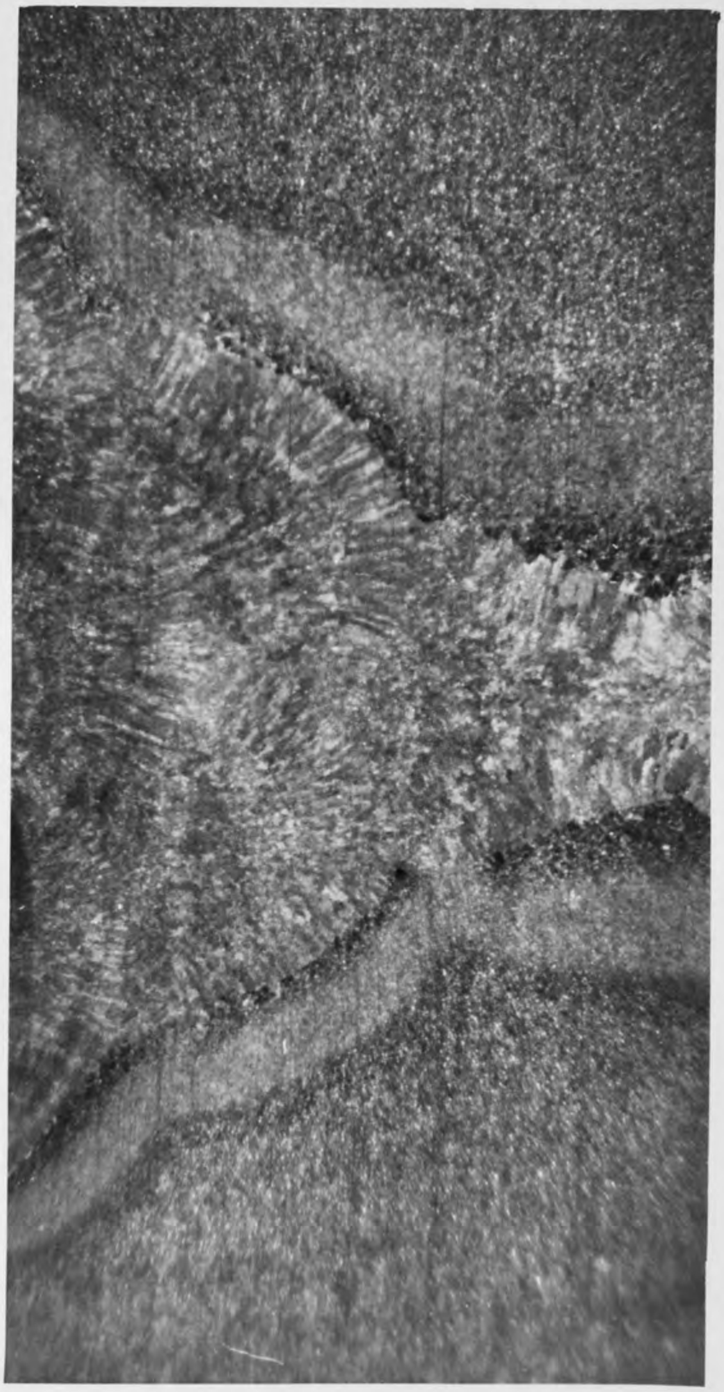

Figure 3.1 Photomacrograph of a ferritic weld.

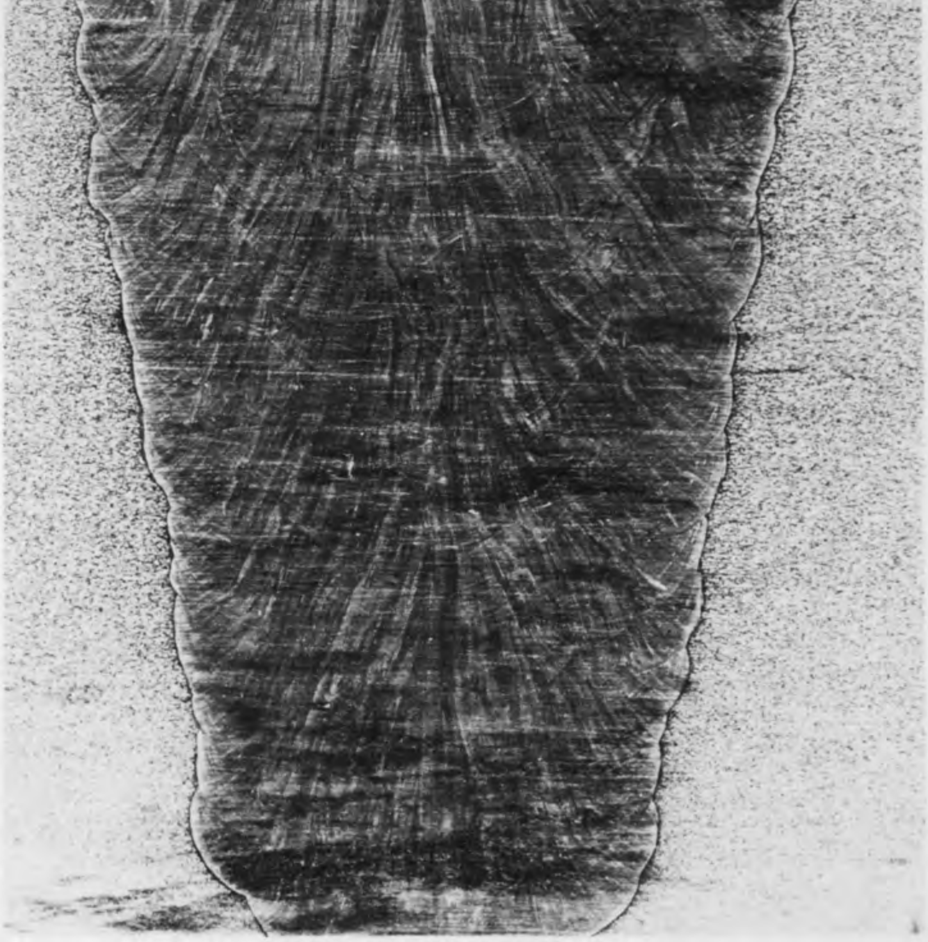

Figure 3.2 Photomacrograph of a V-shaped austenitic weld showing orientation of crystals.

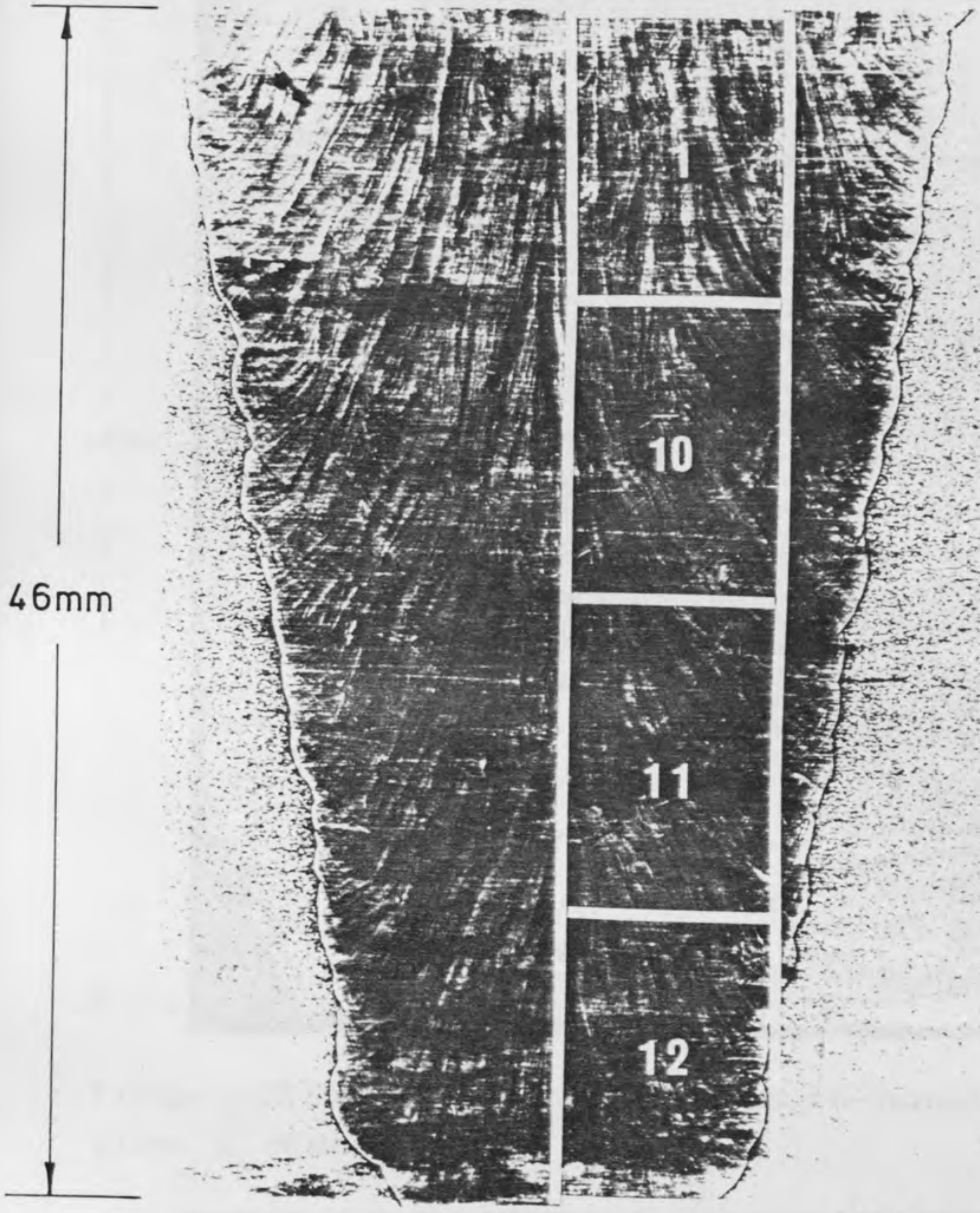

Figure 3.2(a) Photomacrograph of width-thickness plane of weld.(after G.J. Curtis)

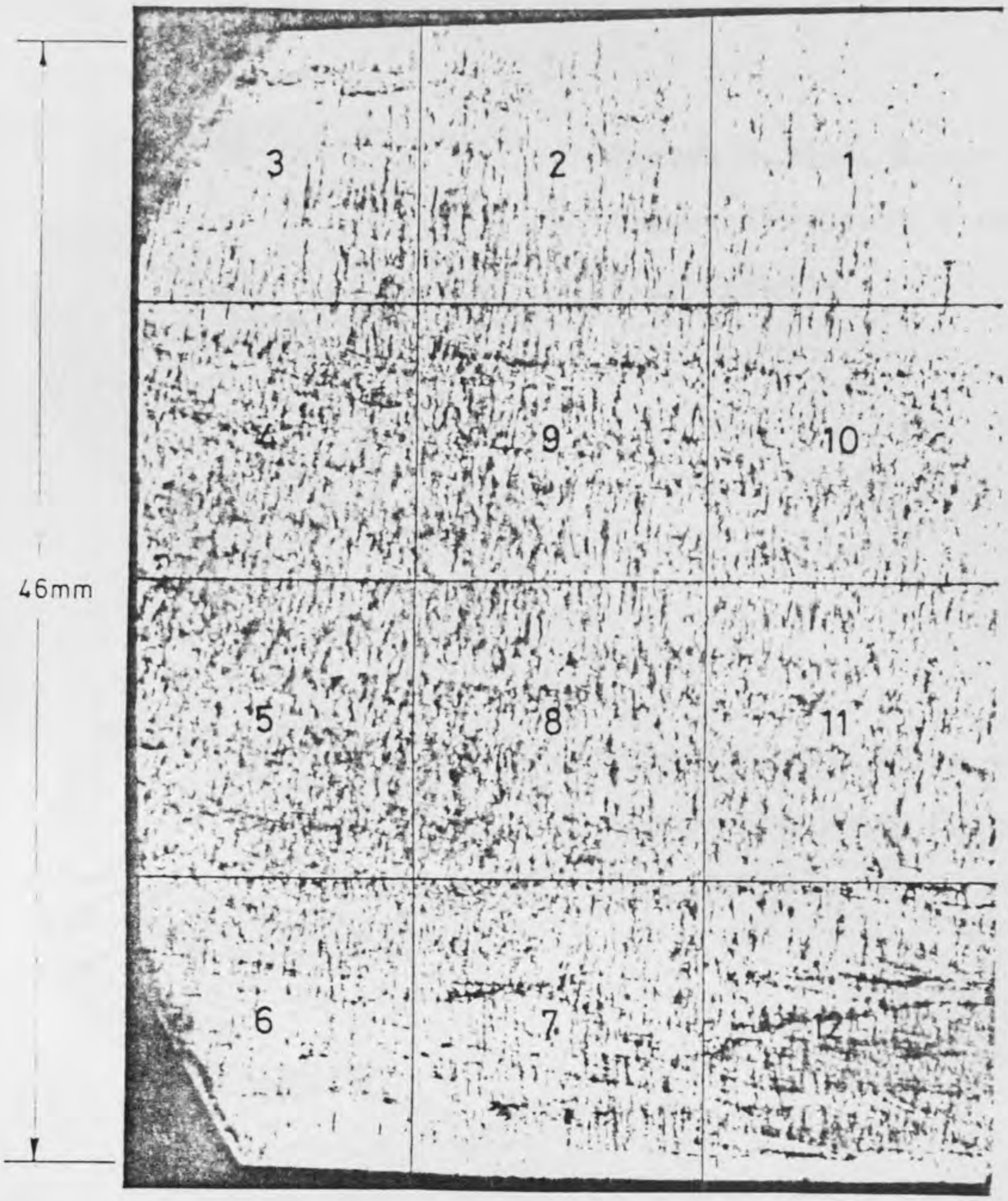

Figure 3.2(b) Photomacrograph of length-thickness plane of weld.

Figure 3.2(c) Photomacrograph of length-width plane of weld.

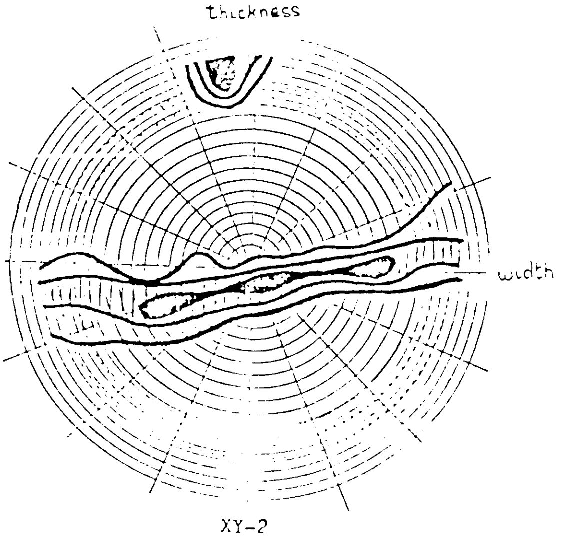

Figure 3.3(a). X-ray pole figure for point 1 in Fig. 3.2(a).

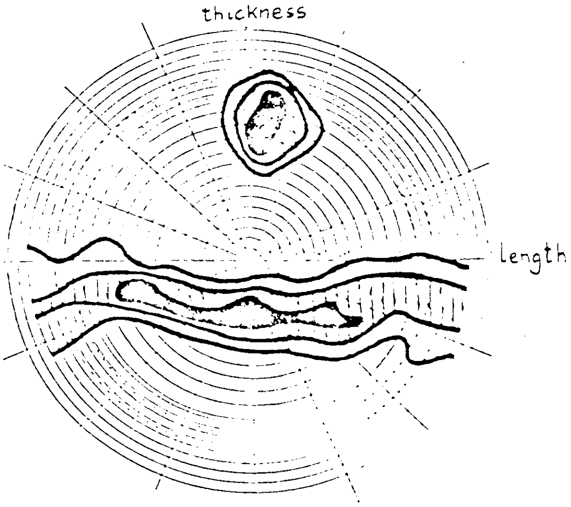

Figure 3.3(b).X-ray pole figure for point 8 in Fig. 3.2(b).

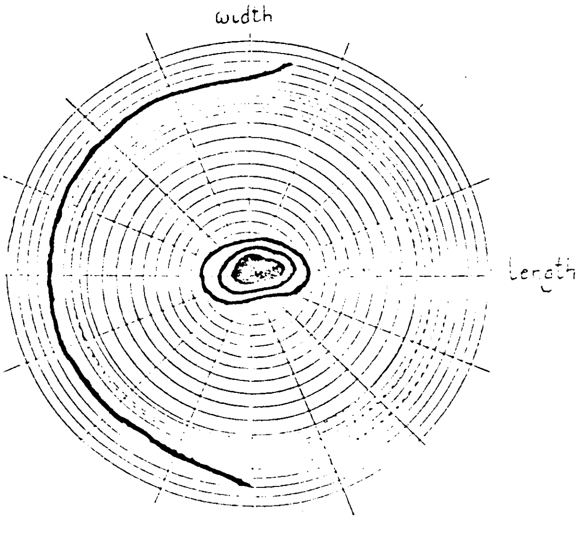

Figure 3.3(c). X-ray pole figure for point 2 in Fig. 3.2(c).

follows to enlighten the interpretation of the wave returned from material defects.

3.3 ELASTIC WAVE PROPAGATION IN CRYSTALLINE METALS

When a force acts upon a body, small displacements in its material will occur. These displacements may be related to the stress caused by the force with the aid of Hooke's Law. For convenience tensor notation is used.

$$\sigma_{ik} = C_{ik\ell m} \frac{1}{2}\left(\frac{\partial u_\ell}{\partial x_m} + \frac{\partial u_m}{\partial x_\ell}\right) \tag{3.1}$$

Hooke's Law assumes that the applied force is small so that it does not permanently deform the material.

Combining Hooke's Law with Newton's second law of motion;

$$\frac{\partial \sigma_{\ell m}}{\partial x_k} = \rho \ddot{u}_i$$

gives

$$\rho \ddot{u}_i = \frac{1}{2} C_{ik\ell m}\left(\frac{\partial}{\partial x_k} \frac{\partial}{\partial x_m} u_\ell + \frac{\partial}{\partial x_k} \frac{\partial}{\partial x_m} u_m\right) \tag{3.2}$$

The elastic constant $C_{ik\ell m}$ is symmetrical in ℓ and m since no total motion of the material is assumed to take place.

Equation (3.2) can hence be written as

$$\rho \ddot{u}_i = C_{ik\ell m} \frac{\partial}{\partial x_k} \frac{\partial}{\partial x_\ell} u_m \tag{3.3}$$

If a sinusoidal force is applied and the displacements are observed far away from this force, a plane sinusoidal wave is observed of the form:

$$u_i = A_i \exp(j(k_i x_i - \omega t)) \tag{3.4}$$

Substituting this into (3.3) gives:

$$\rho \omega^2 u_i = C_{ik\ell m} k_k k_\ell u_m \tag{3.5}$$

The velocity of the wave is given by $c=\omega/k$. Re-arranging equation (3.5) gives:

$$(\rho c^2 \sigma_{im} - C_{ik\ell m} n_k n_\ell) u_m = 0 \tag{3.6}$$

To simplify notation Christoffel's stiffnesses, $\lambda_{im} = C_{ik\ell m} n_k n_\ell$, are introduced. The solution of equation (3.6) requires that the determinant of this equation is zero:

$$|\rho c^2 \sigma_{im} - \lambda_{im}| = 0 \quad , \quad \sigma_{im} \begin{array}{lll} = 0 & \text{when} & i \neq m \\ = 1 & \text{when} & i = m \end{array} \tag{3.7}$$

which in full becomes:

$$\begin{vmatrix} \rho c^2 - \lambda_{11} & \lambda_{12} & \lambda_{13} \\ \lambda_{21} & \rho c^2 - \lambda_{22} & \lambda_{23} \\ \lambda_{31} & \lambda_{32} & \rho c^2 - \lambda_{33} \end{vmatrix} = 0$$

The Christoffel's stiffnesses are given below. The compressed notation form for the elastic constants is used.

$$\lambda_{11} = C_{11}n_1^2 + C_{66}n_2^2 + C_{55}n_3^2 + 2C_{16}n_1n_2 + 2C_{15}n_1n_3 + 2C_{56}n_2n_3$$

$$\lambda_{12} = \lambda_{21} = C_{16}n_1^2 + C_{26}n_2^2 + C_{45}n_3^2 + (C_{12}+C_{66})n_1n_2 + (C_{14}+C_{56})n_1n_3 + (C_{25}+C_{46})n_2n_3$$

$$\lambda_{13} = \lambda_{31} = C_{15}n_1^2 + C_{46}n_2^2 + C_{35}n_3^2 + (C_{14}+C_{56})n_1n_2 + (C_{13}+C_{55})n_1n_3 + (C_{36}+C_{45})n_2n_3$$

$$\lambda_{22} = C_{66}n_1^2 + C_{22}n_2^2 + C_{44}n_3^2 + 2C_{26}n_1n_2 + 2C_{46}n_1n_3 + 2C_{24}n_2n_3$$

$$\lambda_{23} = \lambda_{32} = C_{56}n_1^2 + C_{24}n_2^2 + C_{34}n_3^2 + (C_{25}+C_{46})n_1n_2 + (C_{36}+C_{45})n_1n_3 + (C_{23}+C_{44})n_2n_3$$

$$\lambda_{33} = C_{55}n_1^2 + C_{44}n_2^2 + C_{33}n_3^2 + 2C_{45}n_1n_2 + 2C_{35}n_1n_3 + 2C_{34}n_2n_3$$

To solve equation (3.7) for all the possible elastic constants is time consuming; fortunately practical solids exhibit symmetry, simplifying the solution.

3.4 ELASTIC WAVE PROPAGATION IN CUBIC CRYSTALS

Iron crystals are cubic. Cubic crystals have only three independent elastic constants.

$$C_{11} = C_{22} = C_{33}$$

$$C_{12} = C_{21} = C_{13} = C_{31} = C_{23} = C_{32}$$

$$C_{44} = C_{55} = C_{66}$$

The other constants are zero.

Only three of the infinite possible propagation directions will be discussed. These directions are shown in Fig. 3.4.

3.4.1 Propagation in the |100| Direction

In this direction $n_1=1$, $n_2=0$ and $n_3=0$; equation (3.7) becomes:

$$\begin{vmatrix} \rho c^2 - C_{11} & 0 & 0 \\ 0 & \rho c^2 - C_{44} & 0 \\ 0 & 0 & \rho c^2 - C_{44} \end{vmatrix} = 0$$

The three roots give the velocities as:

$$C_1 = \left(\frac{C_{11}}{\rho}\right)^{\frac{1}{2}} \quad , \quad C_2 = C_3 = \left(\frac{C_{44}}{\rho}\right)^{\frac{1}{2}}$$

The particle motion is parallel to the propagation direction for C_1 i.e. a longitudinal wave. C_2 and C_3 on the other hand have a particle motion perpendicular to the wave propagation direction giving a shear wave.

3.4.2 Propagation in the |110| Direction

In this direction $n_1=n_2=\sqrt{2}$ and $n_3=0$ equation (3.7) becomes:

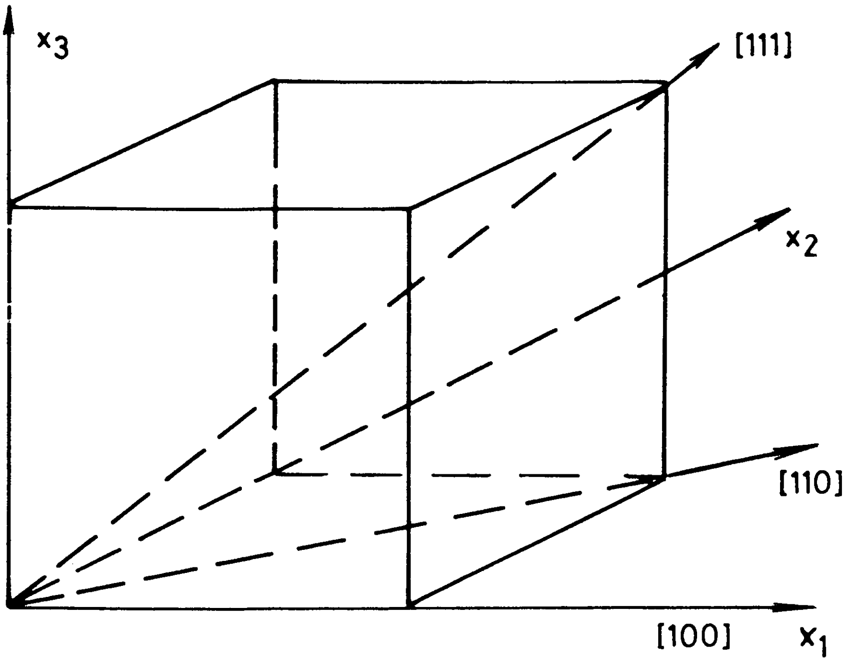

Figure 3.4 ⟨100⟩, ⟨110⟩, ⟨111⟩ wavepropagation directions in cubic crystals.

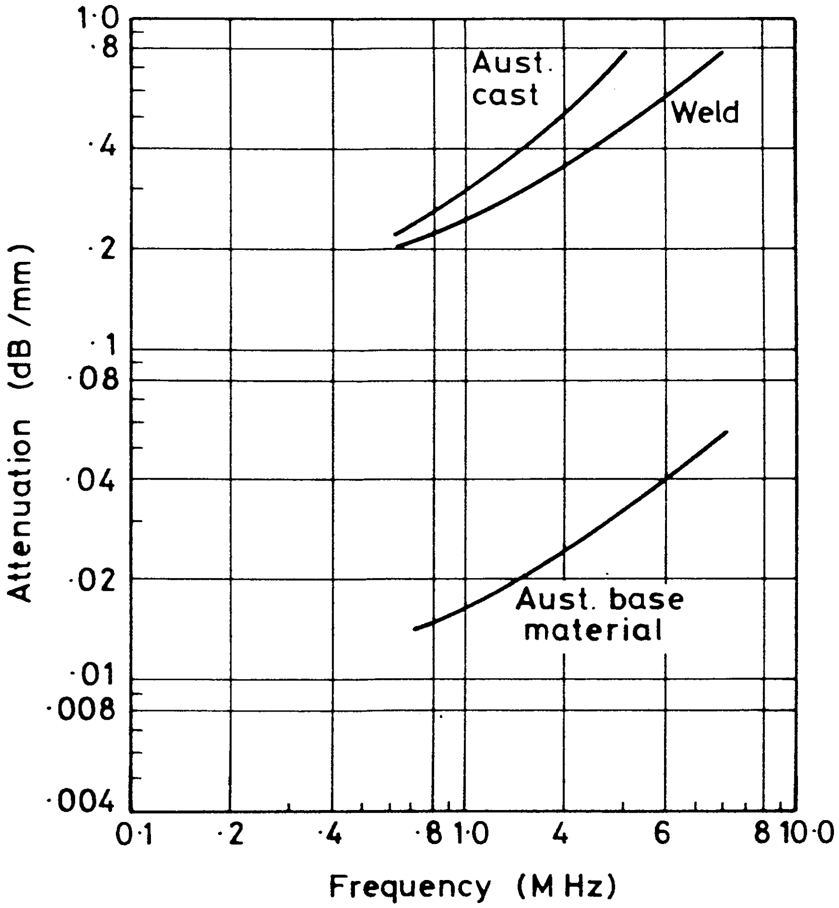

Figure 3.5 Attenuation in austenitic metals. (after Neuman)

$$\begin{vmatrix} \rho c^2 - \frac{1}{2}(C_{11}+C_{44}) & \frac{1}{2}(C_{12}+C_{44}) & 0 \\ \frac{1}{2}(C_{12}+C_{44}) & \rho c^2 - \frac{1}{2}(C_{11}+C_{44}) & 0 \\ 0 & 0 & \rho c^2 - C_{44} \end{vmatrix} = 0$$

The three roots give the velocities as:

$$C_1 = \left(\frac{C_{11}+C_{12}+2C_{44}}{2\rho}\right)^{\frac{1}{2}}; \quad C_2 = \left(\frac{C_{44}}{\rho}\right)^{\frac{1}{2}}; \quad C_3 = \left(\frac{C_{11}-C_{12}}{2\rho}\right)^{\frac{1}{2}}$$

The visualisation of the particle motion is more complicated for this direction, but Pollard(2) has shown that C_1 corresponds to a longitudinal wave and C_2 and C_3 to a shear wave.

3.4.3 Propagation in the |111| Direction

In this direction $n_1=n_2=n_3=\sqrt{3}$. The three roots of equation (3.7) give the velocities as:

$$C_1 = \left(\frac{C_{11}+2C_{12}+4C_{44}}{3\rho}\right)^{\frac{1}{2}}; \qquad C_2 = C_3 = \left(\frac{C_{11}-c_{12}+C_{44}}{3\rho}\right)^{\frac{1}{2}}$$

C_1 is the velocity of a longitudinal wave. While C_2 is the velocity of a quasi-longitudinal wave.

3.5 ELASTIC WAVE PROPAGATION IN 316 AUSTENITIC WELD METAL

The elastic constants of 316 austenitic weld metal have been estimated to be(3);

$C_{11} = 223\ 10^9\ |N/m^2|$

$C_{12} = 132\ 10^9\ |N/m^2|$

$C_{44} = 110\ 10^9\ |N/m^2|$

$\rho = 7850\ |kg/m^3|$

It has to be observed that these constants are not obtained from measurements on single crystals. These cannot therefore be taken to have high accuracy. For estimating the maximum and minimum of the elastic wave velocity in the three previously mentioned directions they will however suffice.

The maximum longitudinal velocity occurs in the |111| direction with $C_\ell = 6275$ (m/s) and the minimum longitudinal velocity is in the |100| direction with $C_\ell = 5330$ (m/s). The variation between the maximum and the minimum velocity is hence in the order of 15%. Experimental measurements of the velocity of 316 weld metal(4) gives the same order of variation as these figures indicate.

The maximum shear velocity occurs in the |110| direction with $C_s = 3745$ (m/s) and the minimum in the |100| direction with $C_s = 2410$ (m/s). The variation between the maximum and minimum shear velocity is hence in the order of 35%.

As seen in Fig. 3.2 the weld consists of a number of small crystals of differing shape and size. The orientation of the crystals also changes through the weld. When an elastic wave propagates through the crystals at different orientations this leads to a change in the propagation velocity of the wave.

The orientation of the crystals in the weld is so that a gradual change in the velocity occurs. This leads to a refraction of the wave towards areas of lower velocity, similar to that observed in the top layer of the sea when using SONAR equipment. Experimental evidence for this is presented by Wagg(5) showing that a longitudinal wave may be re-directed in the order of 45°.

3.6 ATTENUATION OF ELASTIC WAVES IN POLYCRYSTALLINE METALS

The loss of energy from a propagating elastic wave may be divided into :

(i) The loss of energy due to redirection of the energy through scattering when the wave impedance of the material changes.

(ii) The conversion of motion energy into thermal energy through internal friction losses.

Ultrasonic NDT applies elastic waves in the lower end of the megahertz range. The major cause of attenuation in polycrystalline metals is scattering losses(6).

3.6.1 Scattering of Elastic Waves

Scattering of the elastic wave originates from the change in elastic wave impedance between nearby crystals. The elastic wave impedance for a plane wave is given by:

$$Z = \rho c$$

where ρ is the specific density of the material

c is the velocity of the elastic wave.

As seen previously in this chapter, the velocity of the elastic wave depends on the orientation of the crystals with respect to the wave direction. The weld consists of a number of crystals of different orientation. Thereby the individual crystals will have different wave impedances causing a reflection of the incident wave. The crystals are random in form giving a random boundary between the crystals. The incident wave is therefore scattered in random directions.

Considerable attention (6-10) has been paid to the characterisation of scattering in polycrystalline metals. Early work showed that the attenuation due to scattering depends on the frequency of the wave and the mean grain diameter. The individual crystals are often referred to as grains. The fundamental dependence for the attenuation can be tabulated as;

TYPE OF SCATTERING	$\frac{\text{WAVELENGTH}}{\text{MEAN GRAIN DIAMETER}} (\frac{\lambda}{\bar{D}})$	ATTENUATION PROPORTIONAL TO
Rayleigh	$>>1$	$\bar{D}^3 \ f^4$
Stochastic	≈ 1	$\bar{D}^2 \ f^2$
Diffusion	<1	$1/\bar{D}$

Serabian and Williams(11) have discussed the Roney generalised theory of scattering attenuation, this gives a general theory for the entire range of wavelength to grain diameter ratio. A short discussion will be given of the Roney theory, it is discussed in more detail in the reference.

Roney's general equation is:

$$\alpha_s D = \frac{2}{\mu^2} \overline{\left(\frac{\Delta k}{k} \right)^2} \sum_{m=0}^{\infty} (2m+1) \sin^2 \sigma_m \tag{3.8}$$

where

α_s = scattering attenuation coefficient

D = grain diameter, all grains are of the same diameter.

$\mu = \frac{\pi D}{\lambda}$

$\frac{\Delta k}{k}$ = a constant, representative of the anisotropy involved and a measure of the average change in elastic properties.

$$\sigma_m = \mathrm{Tan}^{-1} \frac{mJ_{m-1}(\mu) - (m+1)J_{m+1}(\mu)}{mN_{m-1}(\mu) - (m+1)N_{m+1}(\mu)}$$

J & N are the Bessel and Neuman functions respectively.

For the two extremes, Rayleigh and diffusion scattering, equation (3.8) becomes:

Rayleigh $\lambda >> D$

$$\alpha_s D = \frac{8}{9} \overline{\left(\frac{\Delta k}{k} \right)^2} \mu^4$$

$$\alpha_s = \frac{8}{9} \overline{\left(\frac{\Delta k}{k} \right)^2} \frac{\pi^4 D^4}{\lambda^4 D}$$

$$= \frac{8}{9} \frac{\pi^4}{\lambda^4} \overline{\left(\frac{\Delta k}{k} \right)^2} D^3$$

$$= \frac{8}{9} \frac{\pi^4}{C^4} \overline{\left(\frac{\Delta k}{k} \right)^2} D^3 f^4 \qquad (3.9)$$

Diffusion $\lambda << D$

$$\alpha_s D = \frac{1}{2} \overline{\left(\frac{\Delta k}{k} \right)^2}$$

$$\alpha_s = \frac{1}{2} \left(\frac{\Delta k}{k} \right)^2 \frac{1}{D} \qquad (3.10)$$

Equations (3.9) and (3.10) agree well with the traditional scattering formulas given in the previous table of scattering attenuation.

The virtue of Roney's approach is that it yields a single equation for the attenuation due to scattering whatever the value of the wavelength to grain size ratio. What has been published so far shows that it can describe quite accurately experimental observations of attenuation coefficients. Like all the theories thus far developed, it simplifies the shape of the grains it describes. In real-life grains are not always good approximation to spheres of one fixed diameter.

3.6.2 Practical Effects of Scattering for NDT Inspection

Neuman (12) has presented experimental attenuation figures for austenitic metal. These are shown in Fig. 3.5. As can be seen from this graph the attenuation is in the order of 700 dB/m at 5 MHz.

This makes practical nondestructive testing difficult. The signal returned from the material defect is often masked by scattered signals from the grain boundaries. The display of the returned waveform will often be completely non-interpretable with a number of signals forming the base-line as "grass". The scattered signals from grain boundaries are often referred to as grass by the NDT operators. Serious material defects in welds can therefore be missed causing serious danger.

The masking of signals by scattered noise occurs in SONAR and RADAR as well. These navigational techniques are discussed in Chapter 5.

CHAPTER FOUR

THE GENERATION AND RECEPTION OF ULTRASOUND

Several methods are used for the generation and the reception of ultrasound in ultrasonic NDT. The generation of ultrasound may be divided into four main categories:

(1) Electromagnetic field methods

(2) Electrical field methods

(3) Heating of the specimen surface

(4) Mechanical excitation methods.

With the exception of (3) the reciprocity principle applies to the energy storage of the devices and they can be used equally as drivers and detectors.

4.1 ELECTROMAGNETIC FIELD METHODS

By inducing eddy currents in the material and applying a steady magnetic field, Lorentz forces set the material into vibrations. The eddy currents are induced by a coil near to the surface and fed with a high power radio frequency generator.(1) No contact with the specimen is needed, but any air gap introduces losses and should be kept to a minimum. The sensitivity of the transducer is small compared to that of electrostrictive ceramics. The received signal strength is reported to be down by 40 dB(1) with respect to the piezoelectric plate transducer.

4.2 ELECTRICAL FIELD METHODS

A metal plate placed parallel and close to a conducting surface forms with the surface a capacitor. An elastic wave can be generated in the surface by the application of an electric field between the two plates. The pressure, P, of the wave is(2):

$$P = \frac{1}{2}\varepsilon_o E^2 \qquad (4.1)$$

where ε_o is the dielectric constant of air

E is the electric field strength.

In the absence of a biassing field the elastic wave generated is at twice the frequency of the applied electric field.

This capacitance transducer can also be used as a detector of elastic waves. The distance between the surface and the plate changes as an elastic wave reaches this surface. Providing an electric potential is maintained between the plate and the surface, a change in the stored charge is induced by the elastic wave. This change in the stored charge is then converted to an electrical voltage by a charge-to-voltage converter.

To increase the generated pressure and the sensitivity of the detector, a material having a higher dielectric constant than air might be placed between the surfaces of the capacitor. Curtis(3) used polyethyleneteraphtalate foil metallised on one side in different types of transducer configurations. The foil is flexible and can adhere to different geometrical shapes. The constant electric field between the specimen surface and the metallised side of the foil; sets up forces such that the foil adheres to the specimen. Even with this improvement the capacitive transducer gives small sensitivity and compared to a lead zirconate titanate plate transducer,a reduction in sensitivity of 30 dB is reported.(3)

4.3 HEATING OF THE SURFACE

By a rapid heating of a small spot on a heat absorbing surface the material covered by this spot will expand and thereby cause an elastic wave to be generated. The rapid heating is achieved by focussing a laser beam on the surface.(4) By de-focussing the laser beam different sizes of the heated spot are obtained, thereby changing the intensity distribution of the elastic wave generated.

Conventional transducers are mostly used for the reception of the elastic wave. Due to the expense of the laser equipment only very special applications make use of this technique.

4.4 MECHANICAL EXCITATION METHODS

This technique uses a plate vibrating at the frequency of the wave to be sent. These vibrations are transmitted through a coupling layer into the material to be investigated. This usually means that the plate is made of a material which under the influence of an electric field contracts or expands in harmony with this field. Different materials exhibit the piezoelectric property, among these are; quartz, barium titanite, lithium niobate and lead zirconate titanate(5).

The plate may be made in different shapes to obtain the mode of vibration of interest. The most common transducer used is the circular thickness vibrating lead zirconate titanate plate transducer. This generates longitudinal elastic waves. Fig. 4.1 shows the ideal behaviour of a thickness vibrating plate when excited with an electrical edge. The stress distribution along the vibrating plate for a sinusoidal excitation at the resonant frequency of the plate is also shown.

4.4.1 The Thickness Vibrating Plate Transducer

The thickness vibrating plate transducer generates, ideally, a train of elastic pulses for a single electric pulse(6) as illustrated in Fig. 4.2. The first elastic pulse is generated by the front face moving forward; at a time ℓ/c, later the pulse generated by the rear face of the

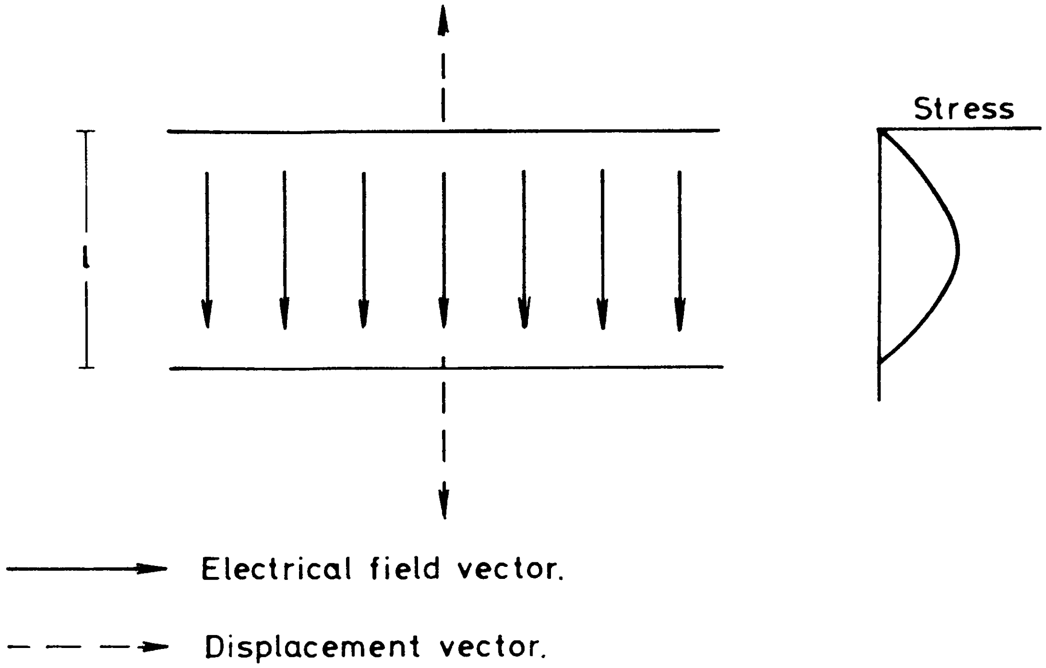

Figure 4.1 Electric field and displacement vectors for a thickness mode transducer.

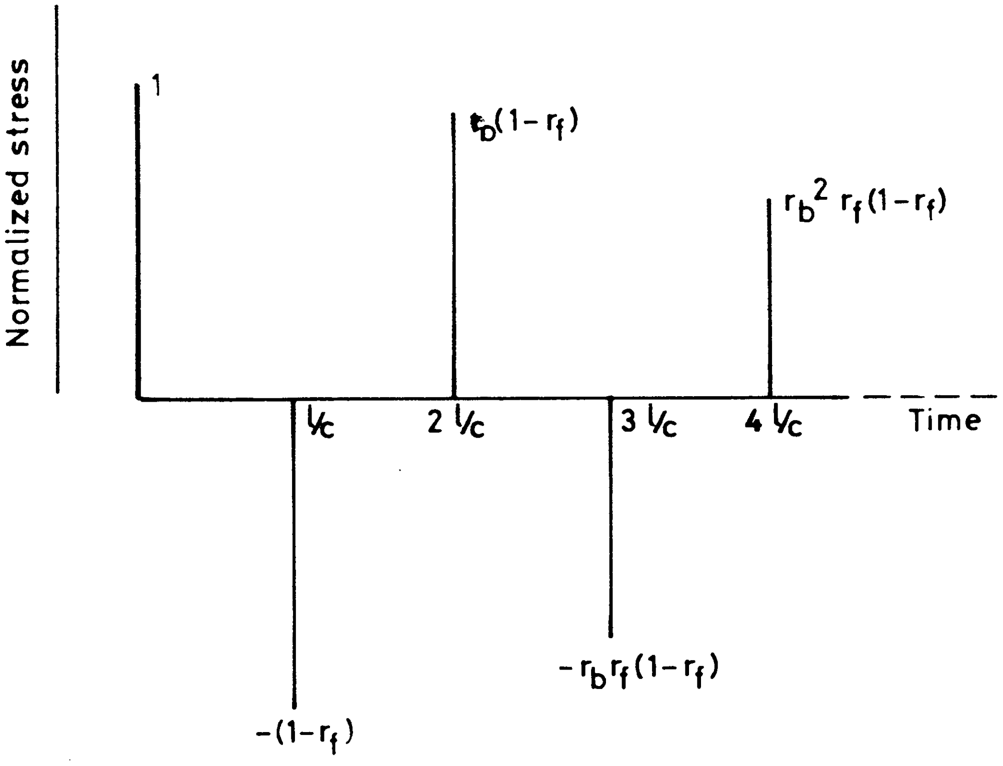

Figure 4.2 The mechanical response of a thickness vibrating plate transducer to one electrical impulse.

plate reaches the front material and part of the pulse is sent into this. The successive pulses are due to the reverberation of the elastic pulse inside the plate. The amplitude reflection coefficients at the plate are given by:

$$r_f = \frac{Z_f - Z_p}{Z_f + Z_p} \tag{4.2}$$

$$r_b = \frac{Z_b - Z_p}{Z_b + Z_p} \tag{4.3}$$

The mechanical impedances are denoted in Fig. 4.3, assuming for the time that the adhesive layer of the backing material has negligible thickness. Depending on the ratio of the boundary impedances Z_f and Z_b to the plate impedance Z_p, phase changes of the generated pulses can take place. Fig. 4.2 is drawn for Z_f and Z_b less than Z_p. If an ideal mechanical matching exists between the plate and its surrounding material, (i.e. $Z_f = Z_p$ and $Z_b = Z_p$) only the two generated pulses appear in the front material.

The ideal behaviour of a transducer would however be that one electric pulse generates one elastic pulse. This can be achieved by making the transducer with only the front face active. Different methods have been considered for obtaining this. One method is to place the rear electrode at the side of the transducer(7) thereby reducing the force generated perpendicular to the rear face. Another proposed method(8) is to make the piezoelectric material with a non-uniform distribution of the piezoelectric

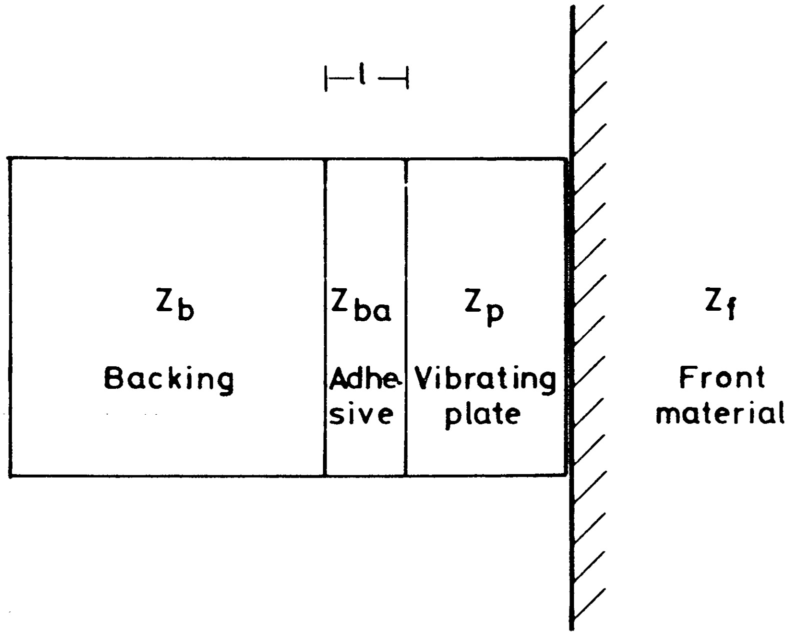

Figure 4.3 The impedances of a backed vibrating plate transducer.

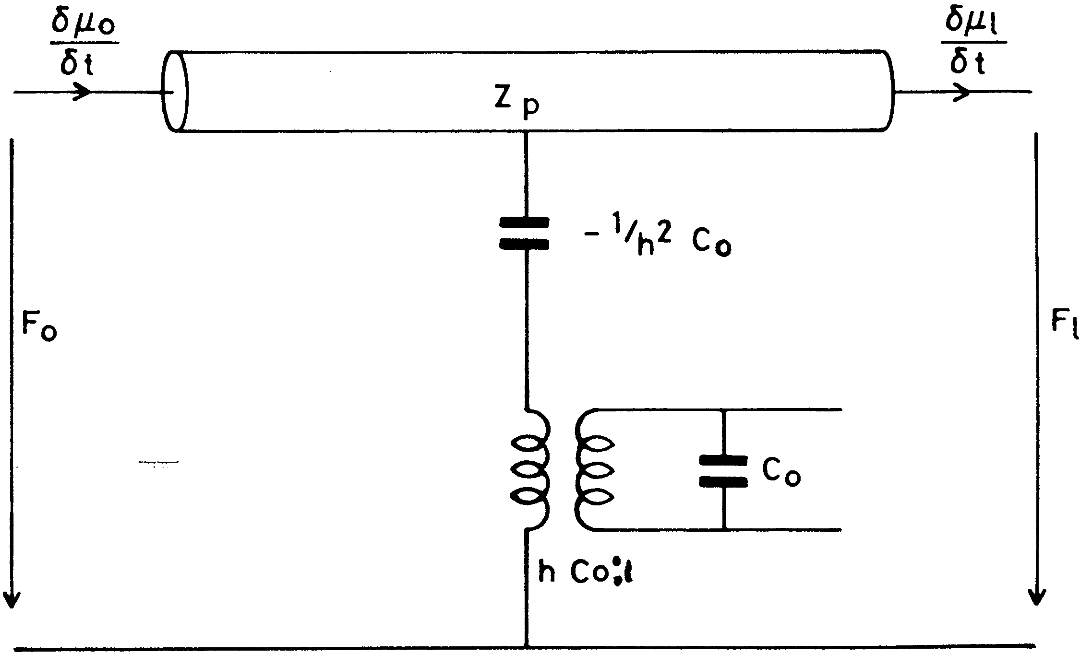

Figure 4.4 The distributed delay line equivalent circuit, for a thickness mode transducer.

conversion constant. As the generated force is proportional to the gradient of the product of the electric field and the piezoelectric conversion constant; the piezoelectric material is manufactured so that the steepest gradient is at the front face of the plate. Theoretical studies have shown that this transducer does not have a resonance frequency as occurs with transducers having a uniform distribution of the piezoelectric conversion constant.

These methods of obtaining ideal transducers are however difficult to engineer. The most common method is to mechanically match the rear face of the vibrating plate, the front face is however not matched and causes reflections of the elastic pulse generated at the rear face. The matching of the rear face is achieved with the application of a material of equal specific impedance as the vibrating plate and covering the same area as the plate. The backing material should at the same time have a high attenuation for elastic waves, so that any waves reflected from the back of the material are adequately attenuated.

Different types of backing materials have been considered. The most widely used is small tungsten particles supported in an epoxide resin. The mechanical impedance of this mixture is dependent on the ratio of tungsten to epoxide resin. Bainton(9) has shown that the amount of tungsten should be higher than the amount at present normally used.

The mixing of the resin must also be exercised with care to prevent air bubbles being trapped in the mixture.

Other backing materials given consideration are different solids with an appropriate mechanical impedance to that of the vibrating plate.$^{(10)}$ The backing solid should at the same time have a large grain structure giving scattering attenuation of the wave propagated into the backing material.

The application of a solid as the backing material requires that an adhesive bond is formed between the vibrating plate and the solid. The thickness of this bond affects the transmission of the elastic wave into the solid.

The amplitude transmission coefficient through a layer is given by$^{(11)}$;

$$t = \frac{H}{H\cos(k_{ba}\ell) + \left(\frac{z_{ba}}{z_p} + \frac{z_p}{z_{ba}}\right)^2 \sin^2(k_{ba}\ell)} \qquad (4.4)$$

where

$$k_{ba} = \frac{2\pi}{\lambda_{ba}}, \quad z_{ba} = \rho_{ba}c_{ba}, \quad z_p = \rho_p c_p$$

This equation assumes no loss in the adhesive and that only plane wave propagation with normal incident waves is present. It is also assumed that the mechanical impedance of the backing material and the plate is the same i.e. $z_b = z_p$.

A commonly occurring adhesive is the epoxide resin 'Araldite'. The volume density for 'Araldite' is $\rho_{ba} \approx 1.2\ 10^3 (kg/m^3)$ and the longitudinal velocity is $c_{ba} \approx 2600\ (m/s)^{(9)}$. The specific elastic impedance becomes then $z_{ba} \simeq 3.12\ 10^6 (kg/m^2 s)$. The vibrating plate material lead zirconate titanate (PZT-5A) has $\rho_p \approx 7.75\ 10^3 (kg/m^3)$ and $c_p \simeq 4350 (m/s)$,$^{(12)}$ giving $z_p \approx 33.71\ 10^6 (kg/m^2 s)$. Using equation (4.4) the amplitude transmission coefficient is found to be $t = 0.99$ for $\ell = \lambda_{ba}/400$ and $t = 0.69$ for $\ell = \lambda_{ba}/50$.

At a frequency of 5 (MHz) the wavelength in the adhesive is 520 (μm). If an amplitude reflection coefficient of 1% at the bonding layer is accepted, the thickness of the bonding layer should by 1.3 (μm). The engineering difficulties in achieving such small reflection coefficients are large, as the surface roughness of the vibrating plate easily exceeds this.

4.4.2 Electrical Equivalent Circuit of the Thickness Vibrating Plate Transducer

Ultrasonic transducers are connected to electrical generators and amplifiers, it is therefore convenient to represent the transducer in terms of an electrical circuit. The piezoelectric plate vibrator can be described by the following equations$^{(13)}$;

$$\sigma_x = C_x \frac{\delta u_x}{\partial x} - hD_x \qquad (4.5)$$

$$E_x = -h \frac{\partial u_x}{\partial x} + D_x/\varepsilon_x \qquad (4.6)$$

where x indicates the thickness expansion direction and h is piezoelectric constant.

To simplify the analysis it is assumed that the driving frequency is well away from any other vibrational modes of the plate than the thickness expansion mode. Coupling to other modes will however always be present due to the effect of Poisson's ratio, but can be neglected when the modal frequencies of the plate are well separated. The application of a backing material helps separate the modal frequencies.

Assuming that the elastic wave in the plate is sinusoidal, the particle displacement can be represented by:

$$u_x = A\, e^{j(\omega t-kx)} + B\, e^{j(\omega t+kx)} \qquad (4.7)$$

inserting this into equation (4.5) gives:

$$J_x + hD_x = (-jC_x kAe^{-jkx} + jC_x kBe^{jkx})\; e^{j\omega t}$$

but as there is no free charge within the plate:

$$Q = D_x a$$

and using the following notation

$\sigma_x = F_x a$ and

$$C_x ka = \frac{\omega}{c} .\rho \frac{C_x}{\rho} .\; a = \omega\rho c.a = Z_p \omega$$

gives

$$F_x + hQ = jZ_p\omega(-Ae^{-jkx} + Be^{jkx})e^{j\omega t} \qquad (4.8)$$

Differentiating equation (4.7) with time gives

$$\frac{\partial u_x}{\partial t} = j\omega\ (Ae^{-jkx} + Be^{jkx})\ e^{j\omega t} \qquad (4.9)$$

The term hQ represents a force, this can be related to the applied voltage by integrating equation (4.6) with respect to x giving:

$$V = \int_{\partial}^{\ell} E_x d_x = \int_{\partial}^{\ell} (D_x/\varepsilon_x - h\ \frac{\partial \mu_x}{\partial_x})\ dx$$

$$= \frac{D_x \ell}{\varepsilon_x} - h(\mu_\ell - u_o)$$

but $\frac{D_x \ell}{\varepsilon_x} = \frac{Q}{C_o}$ and assuming sinusoidal motion:

$$hQ = hC_oV + \frac{h^2 c_o}{j\omega}\ (\frac{\partial u_\ell}{\partial t} - \frac{\partial u_o}{\partial t}) \qquad (4.10)$$

Equations (4.8) and (4.9) represent a delay line driven with an equivalent external force of F_x. The voltage to force conversion is represented from equation (4.10) by a negative capacitor of value $1/h^2C_o$ and a transformer with a turn ratio $h\ C_o:1$. From equation (4.10) the current entering the transducer can be written.

$$i = j\omega C_oV + hC_o(\frac{\partial u_\ell}{\partial t} - \frac{\partial u_o}{\partial t})$$

This equation represents a current flowing into a capacitor of value C_o and the previously mentioned transformer.

A diagramatical representation of this circuit is given in Fig. 4.4.

4.4.3 Electrical Series Impedance of the Thickness Vibrating Plate Transducer

The equivalent circuit in Fig. 4.4 can be used to find the electrical series impedance of the plate, but certain transformations simplify the derivation. The delay line can be represented by a T-network.$^{(14)}$ with two impedances of $jZp \tan(\frac{\pi \ell}{\lambda})$ and the centre impedance $-jZp \csc(\frac{2\pi\ell}{\lambda})$. Fig. 4.5 shows the transformed circuit with the mechanical impedances Z_b and Z_f appearing at the front and back of the plate.

This form of the equivalent circuit is similar to Mason's equivalent circuit.$^{(15)}$ Following Gooberman's$^{(13)}$ simplification the electrical series impedance is given by:

$$R_s = \frac{(\frac{Z_b + Z_f}{4}) \left(\frac{1}{\omega C_o Z_p} \right)^2}{b^2 C_o^2 (\frac{Z_b + Z_f}{4Z_p})^2 + \frac{1}{4} \cot^2 (\frac{\pi\ell}{\lambda})} \qquad (4.11)$$

$$X_s = - \frac{1}{\omega C_o} + \frac{\frac{1}{\omega^2 C_o^2} \cot(\frac{\pi\ell}{\lambda})}{h^2 C_o^2 2Z_p ((\frac{Z_b + Z_f}{4Z_p})^2 + \frac{1}{2} \cot^2 \frac{\pi\ell}{\lambda})} \qquad (4.12)$$

where R_s is the real part and X_s is the imaginary part of the impedance.

Assuming that $(Z_f + Z_b) << Z_p$ the Argand diagram for R_s and X_s will form a circle as shown in Fig. 4.6.

The diameter of the circle is given by:

$$\frac{4}{\omega^2 h^2 C_o^4 (Z_b + Z_f)}$$

This diameter is reduced by increasing the mechanical impedance of the backing and front material. The variation in the electrical series impedance will hence be smaller, simplifying the matching of the receiver and driver to the vibrating plate transducer. For maximum power transfer perfect matching should be present between the receiver/driver equipment and the transducer. However this requirement can be made less stringent in experimental equipment where interest is not in the matching of transducers to electrical equipment.

Kossoff(10) has shown that using a resistive loading for the vibrating plate transducer does not degrade the bandwidth of the transducer very much. The sensitivity of the transducer is however reduced by not matching the receiver/driver and the transducer. In experimental equipment this reduction in sensitivity can be overcome by increasing the gain of the ultrasonic equipment. This method was chosen for its simplicity.

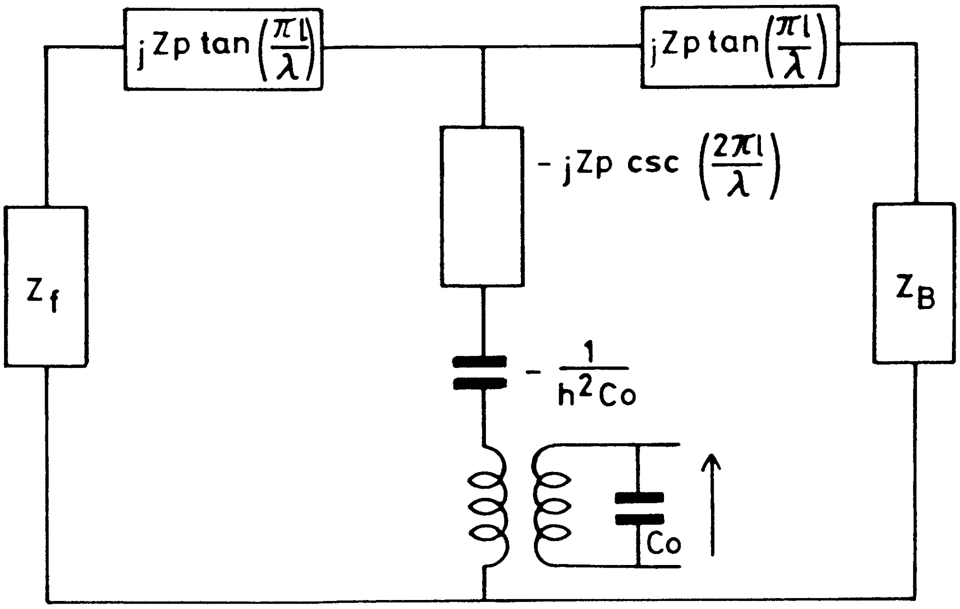

Figure 4.5 The lumped impedance equivalent circuit for a thickness mode transducer.

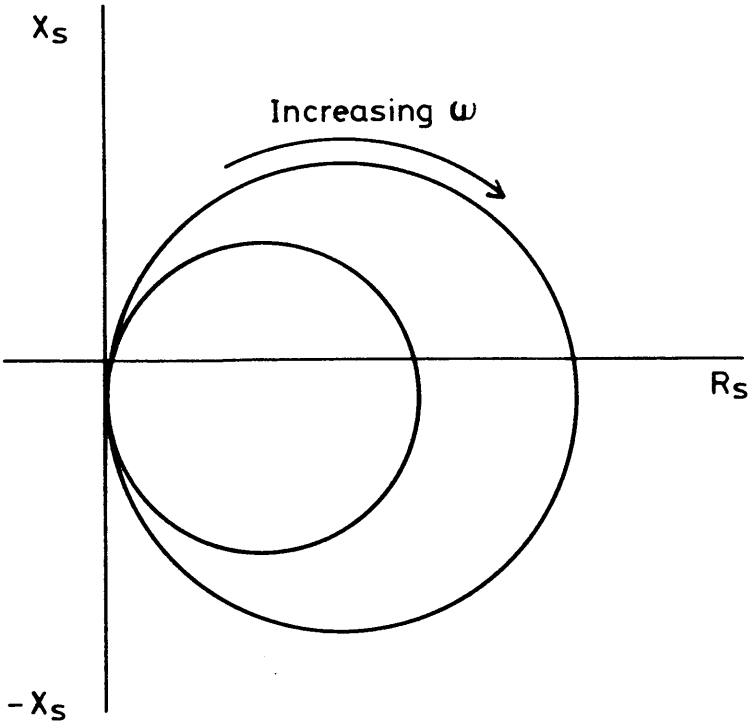

Figure 4.6 The idealised Argand diagram for the electrical driving impedance.

The ultrasound transducer is often used to transfer broad bandwidth signals such as impulses or pulsed signals; the bandwidth of the transducer is therefore of interest. It is more convenient to express the quality factor, Q, of the transducer than the bandwidth, B.

$$Q = \frac{f_o}{B} = \frac{f_o}{f_1 - f_2} \tag{4.13}$$

where

f_o is the resonant frequency

f_1 and f_2 is the lower and upper 3 dB frequency respectively.

An expression between Q and the mechanical impedances might be obtained by noting that at resonance the equivalent series resistance, R_s, is infinite or the denominator of equation (4.11) becomes zero.

$$\cot\left(\frac{\pi \ell}{\lambda}\right) = \frac{Z_b + Z_f}{2 Z_p} \tag{4.14}$$

Using this equation together with equation (4.13) gives

$$Q = \frac{\pi}{2}\left(\frac{Z_p}{Z_b + Z_f}\right)$$

This equation is strictly only valid near to the resonance frequency, but it shows that Q is decreasing when the loading of the transducer is increased.

By increasing the loadings the simple half wave resonant transducer is made more like a quarter wave resonator. The transfer function for the loaded transducer will therefore be expected to have two small resonant tops, one near to the half wave resonance the other near to the quarter wave resonance. It can therefore be assumed that a heavy loaded transducer can have a Q in the order of $f_o/\frac{1}{2}f_o = 2$, or a bandwidth, $B = \frac{1}{2}f_o$.

CHAPTER FIVE

SIGNAL PROCESSING, ANALOGIES WITH SONAR AND RADAR

5.1 THE BASIS OF SONAR

ASDIC (Allied Submarine Detection Investigation Committee) or SONAR (Sound Navigation and Ranging) as it is now widely called, is the name of a technique for detecting objects in water by the use of elastic waves. During World War I the early development of this technique took place.(1,2,3) First came the passive SONAR listening for the sound emitted from submarines and ships. At the end of the War the active SONAR was operational, enabling submarines to be detected even when the engines were shut down.

The basic active SONAR consists of a sender and a receiver with one common transducer. During the sending period the transducer emits a short gated sinusoidal wave within the frequency range 3-300 kHz. With a mean velocity of the elastic wave in seawater of 1500 m/s this corresponds to a wavelength in the range 5-500 mm. Due to the low shear modulus of water only the longitudinal wave is of any importance. This means that no polarisation of the wave is possible. The longitudinal wave is reflected from any areas of a different elastic impedance than the surrounding media; a part of this reflected energy is returned in the direction of the transducer which now is acting as a receiving transducer. The signal generated in the transducer by this reflected wave is amplified , processed and displayed.

The display can then give information of the distance to the object and the strength of the reflected wave. With prior knowledge of the direction and the shape of the object, its size might be estimated.

5 .2 THE BASIS OF RADAR

The development of RADAR (Radio Direction and Ranging) started prior to the World War II.$^{(4)}$ RADAR is used mainly for the detection and ranging of objects such as boats and aeroplanes by electromagnetic radiation. It is based on the same principles as SONAR, but uses electromagnetic waves instead of elastic waves. The electromagnetic wave is transversal in nature so polarisation of this wave is possible. The frequency of the wave sent is in the range 1-35 GHz. This gives a wavelength in the range 8-300 mm. Both passive and active RADAR are used, however, the passive RADAR is mainly found in astronomy where interest is in the detection of distant stars sending out electromagnetic waves.

5.3 ANALOGIES BETWEEN SONAR/RADAR AND ULTRASONIC NDT

Ultrasonic NDT applies the same principles as RADAR and SONAR. These techniques send out a wave and detect part of the reflected wave, which indicates the position of the reflecting object.

Differences do however exist in the wavelengths used in ultrasonic NDT. The elastic wave sent into the material is usually in the frequency range 0.5-20 MHz. Both longitudinal and transversal waves are supported by solids, and polarisation of the transversal wave is possible. The different velocities encountered, depending both on the propagating wave as well as the material under investigation, give a wide range of wavelengths. For steel with a longitudinal wave velocity of approximately 6000 m/s the longitudinal wavelength is in the range 0.3-12 mm. The transversal wave velocity for steel is approximately 3100 m/s giving a transversal wavelength in the range 0.15-6 mm.

As mentioned the principles are the same for the three techniques even a counter part to passive RADAR and SONAR is found in ultrasonic NDT. This is known as acoustic emission, wide interest has recently been given to this subject.(5,6)

The three techniques use a transducer to generate a wave in the space to be investigated. This transducer has a limited size, in ultrasonic NDT it is usually made as a circular vibrating plate. The vibrating plate might be idealised as a piston moving backwards and forwards in harmony with the electric signal applied. Kinsler and Frey(7) give the pressure distribution from a piston source as:

$$p = \frac{j\rho_o ck}{2\pi r} Q_p \left| \frac{2J_1(ka \sin\theta)}{ka \sin\theta} \right| e^{j(\omega z - kr)} \tag{5.1}$$

Taking the intensity of an elastic wave as:

$$I = \left| \frac{p^2}{2\rho_o c} \right| \tag{5.2}$$

the intensity of the elastic wave becomes.

$$I = \frac{\rho_o ck^2}{8\pi^2 r^2} Q_p^2 \left| \frac{2J_1(ka \sin\theta)}{ka \sin\theta} \right|^2 \tag{5.3}$$

The beam pattern is obtained by the vector summation of the Huygens elements of the wavefront at the piston. Fig. 5.1 shows this beam pattern and the variation of the intensity of the wave along the normal axis of the transducer. The intensity varies between maximum and minimum as the distance from the transducer is increased. When $r > a^2/\lambda$ the intensity decreases inversely with the square of the distance and the wave front is spherically divergent. It is convenient to divide the intensity distribution into two regions; the near- and the far-field. The definition of the boundary between these two regions is not unique in the literature, but will be taken here as a^2/λ.

Due to the oscillatory nature of the intensity in the near field, it is advantageous to use the far-field for

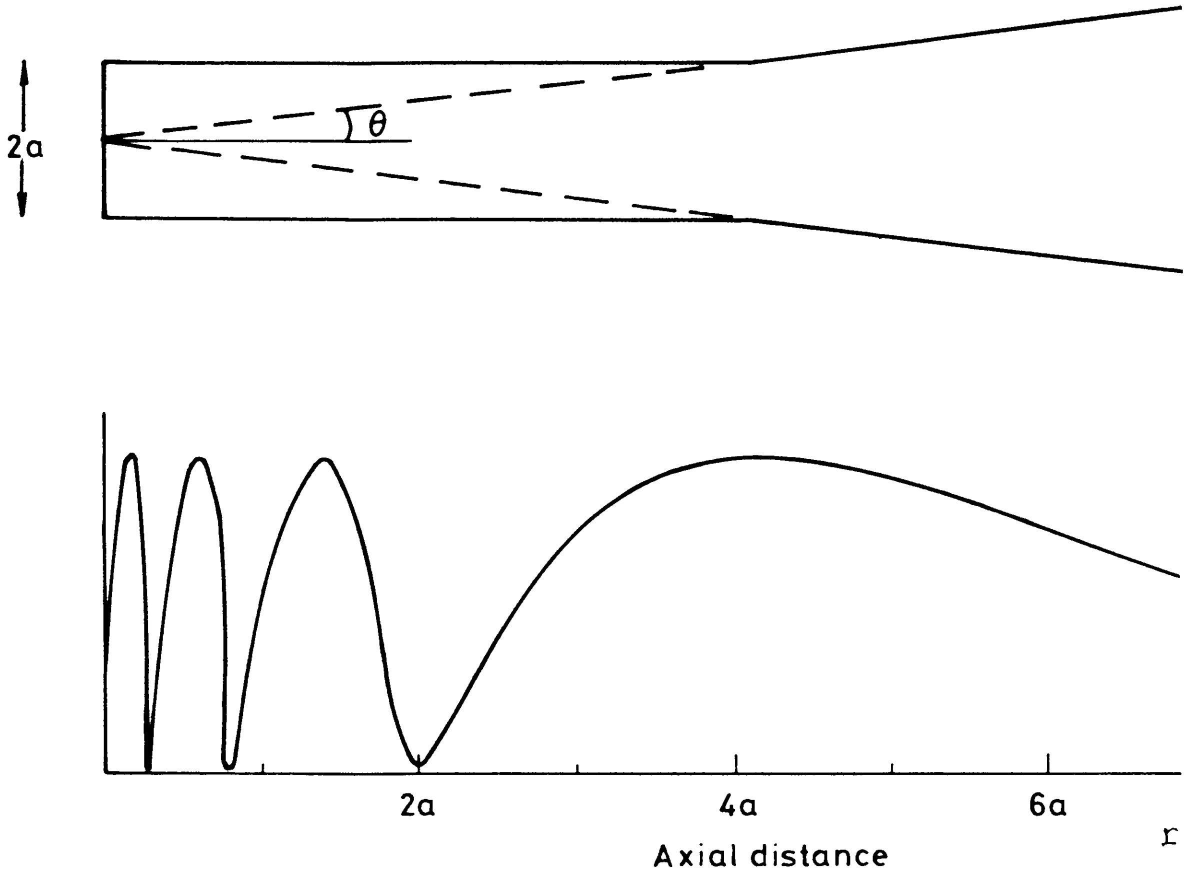

Figure 5.1 The idealised intensity distribution near a piston source for a= 4 wavelengths.

measurements, as interpretation of the returned echo signal is easier.

When the transducer is working as a receiver the spatial sensitivity pattern will be equal to the beam pattern for the sender transducer, assuming the transducer is electrically terminated as for the sender transducer. The sensitivity pattern for a pulse-echo system is therefore the square of the beam pattern for the sender transducer. The sensitivity pattern will hence be narrower than the simple beam pattern shown in Fig. 5.1, as the receiver has a finite sensitivity and small echo signals originating from the boundary of the beam will be below the detection threshold.

5.4 RANGE

The intensity of the wave sent depends on the distance from the transducer and the angular position of the point of interest with respect to the normal axis of the transducer. The wave is also attenuated in the material it propagates through. The maximum range for the detection of objects is reached when the object echo signal is below the noise caused by electronic noise and reflected waves from inhomogeneities in the material under investigation. These inhomogeneities are often referred to in Ultrasonic NDT as grass .

Attenuation in steel and many metals is a wavelength dependent phenomenon, the loss per wavelength being constant. The attenuation over a given distance is therefore proportional to frequency.

Scattering of the wave from inhomogeneities reduces the conveyed energy, as part of the wave is refracted from its normal path. The refracted energy is very dependent on the ratio of the size of the inhomogeneity to the wavelength and for most practical cases the refracted energy increases as this ratio increases.

A major problem in weld material is the inhomogeneity which gives it a complicated velocity structure. This distorts and refracts the ultrasonic wavefront producing shadows, and wave channelling (guiding) through the weld. Use of scanning arrays, sometimes using separate receivers and extremely sophisticated tomography type signal processing are used for these conditions.

The electronic noise present depends on the equipment used. Factors affecting this noise are mainly the self noise of the receiving transducer and the first stages of the receiver amplifier.

The maximum range obtainable depends also on the size and shape of the reflecting object. The energy of the reflected wave follows much the same laws as scattering of a wave by inhomogeneities and the reflected energy increases as the ratio of the scattering cross-section to wavelength increases.

5.5 RESOLUTION

Interest in Ultrasonic NDT is given to evaluating the severity of a defect in the construction material. This depends on the location, the shape and the size of the defect. Two different types of resolution might therefore be defined; location resolution and defect resolution.

5.5.1 Location Resolution

Location resolution might be subdivided into distance resolution and angular resolution.

5.5.2 Distance Resolution

Distance resolution determines with what accuracy the distance from a reference point to the object can be given. For a pulse-echo system this depends on the timing accuracy of the equipment and the velocity of the wave; as the distance to the object is given by:

$$R = \frac{c\ t_f}{2} \cos\left(\frac{\theta_{sep}}{2}\right)$$

where θ_{sep} is the separation angle of the transducers

c is the phase velocity

The time of flight, t_f, is the time taken by the wave to transverse the distance to the object twice.

The velocity, c, is usually assumed to be constant and for electromagnetic waves used in RADAR a large variation in the velocity is not observed. However, for SONAR and Ultrasonic NDT variations are often encountered.

The velocity of elastic waves in seawater depend on the temperature, the salinity and the pressure of the water.(7) For SONAR the temperature variations in the sea dominates the variations of the velocity. The temperature variation is most pronounced in the top layer where such factors as wind, sea state and the sea current cause irregular variations. The elastic wave velocity varies therefore in an unpredictable manner such that the range might be difficult to evaluate accurately. These velocity variations also cause the wave to bend away from its normal direction such that the distance travelled is to some extent unpredictable. Without a prior knowledge of the sea, no account of these variations can be made with single measurements.

The timing accuracy is given by the accuracy in both the sending and the receiving instant. The sending instant is usually well predictable as this is under operator control, however, the receiving instant is not so easy to estimate. The limited bandwidth of the inspection equipment in use causes an exponential increasing and decreasing envelope of the signal received. Figs 5.2 and 5.3 show the excitation and the received signal for a piezoelectric plate transducer.

5.5.3 Angular Resolution

Different inspection techniques must be applied in

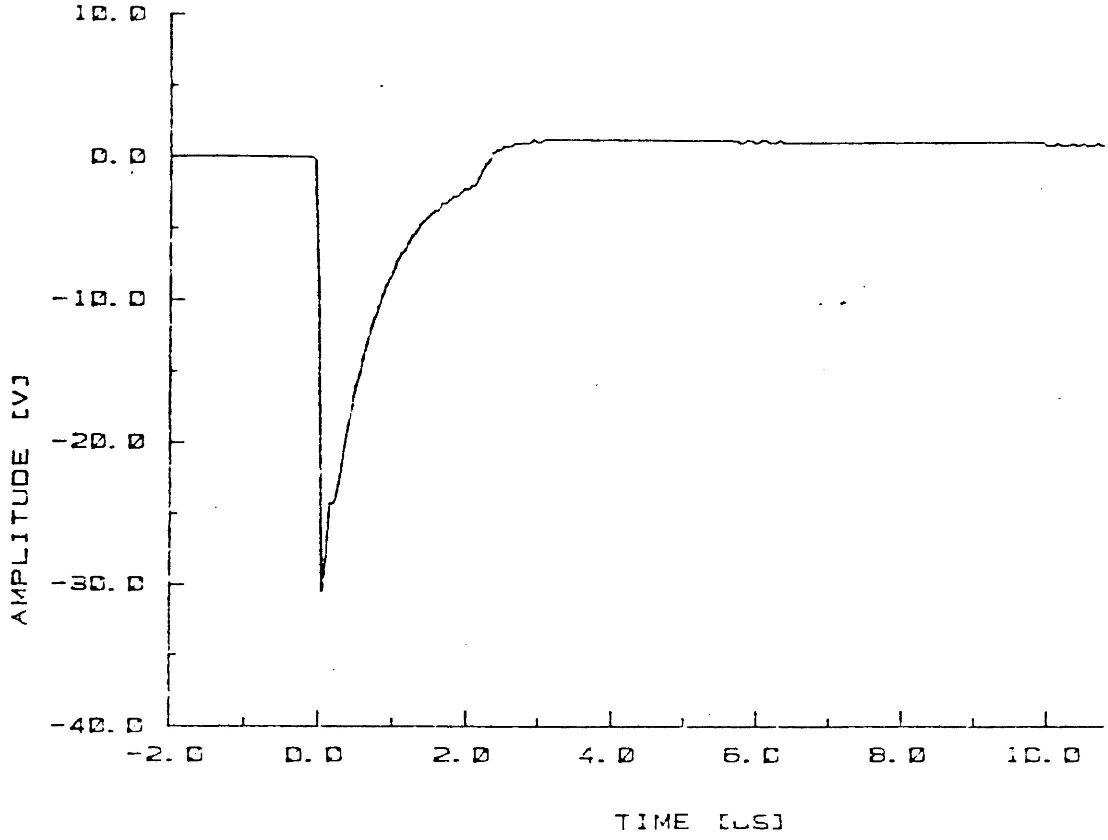

Figure 5.2. The electrical excitation signal used to obtain the received signal in figure 3.3.

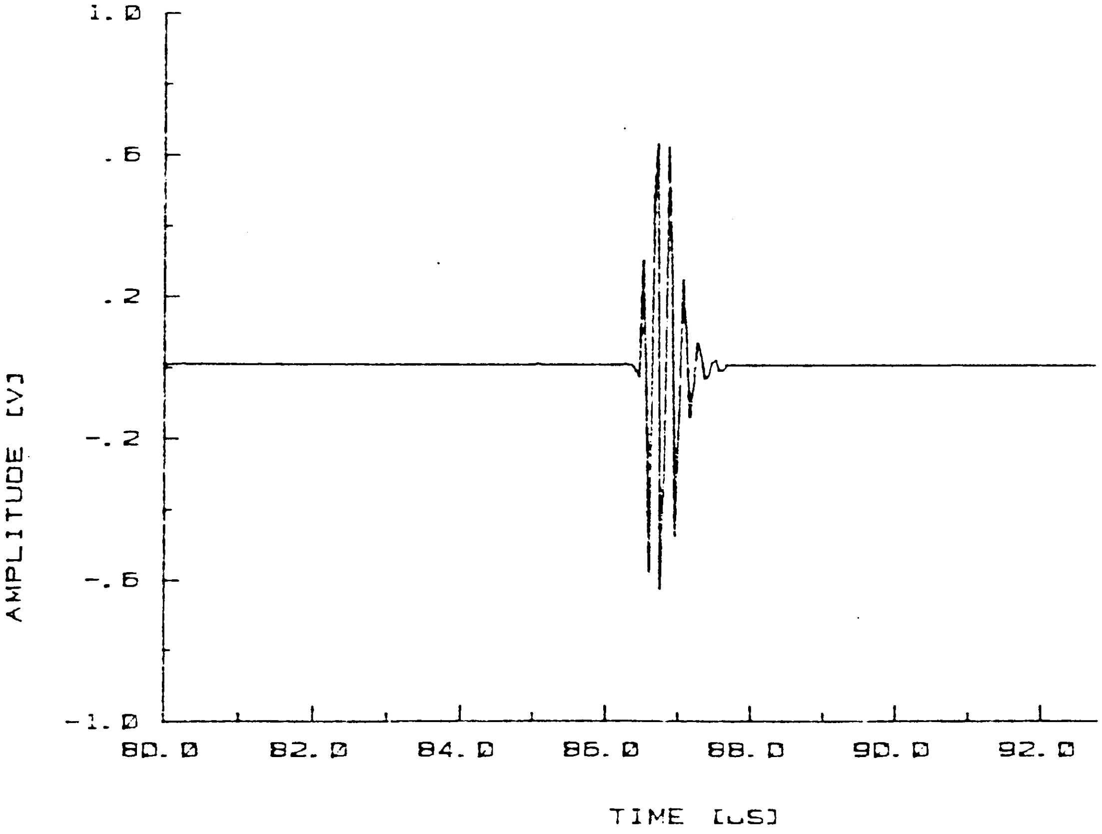

Figure 5.3. The received electrical signal from a 5 MHz piezoelectric plate transducer immersed in water and using a thick glass plate as the reflector.

SONAR, RADAR and Ultrasonic NDT. It is impractical to gain access to the whole perimeter of the space to be inspected for the SONAR and the RADAR case. The transducers are therefore placed at a few points along the perimeter and scanned along an arc so that the waves sent from the transducers cover the space of interest. The coordinates to the point of interest are then given in the cylindrical coordinate system. This inspection technique is possible since water and air can only support one mode of wave propagation and no mode conversion can therefore take place complicating the interpretation of the returned echo wave.

Solids can however support both transversal and longitudinal modes of wave propagation, and a conversion from one mode to the other is possible. This conversion takes place at the interface between materials having different elastic properties, such as at the surface of the solid. When the wave meets such an interface at an angle, mode conversion is accentuated. If the transducer is now scanned along an arc, mode conversion can be present, complicating the inspection problem. To avoid this complication in Ultrasonic NDT, the elastic wave is as far as possible kept perpendicular to the material to be investigated. As it is usually possible to gain access to the whole perimeter of the space to be investigated the transducer is scanned over the perimeter and any points of interest are given by their Cartesian coordinates.

Both inspection techniques required, however, that the wave sent out from the transducer has a well defined beam pattern. As it can be difficult to estimate the exact beam pattern in solids it is customary to try to achieve a narrow beam, enabling approximation to the "torch light" case.

The intensity of the wave sent, decreases when one is moving away from the normal axis of the transducer. From (5.3) the angle with which the beam diverges in the far-field for a circular transducer is given by:

$$\theta = \sin^{-1}(0.61\ \lambda/a)\ ,\ \text{at the 3 dB point.} \qquad (5.4)$$

also indicated in Fig. 5.1.

The beam spreading angle θ decreases as the radius of the transducer is increased, but the distance to the far-field increases with the radius of the transducer. Practical problems of making the transducer vibrate at a single mode become larger as the size of the transducer is increased. To reduce these problems SONARs have been built with a number of small transducers placed relatively close together to synthetise a larger transducer.(8) Certain restrictions have to be made to the spacing of the transducer elements. The far-field is the Fourier transform of the displacement on the surface of the transducer(9). Shannon's sampling theorem (see Chapter 7) might therefore be applied with its extension to spatial distributions. This states that the distribution of the field must be given at points not separated by more than one half-wavelength ($\lambda/2$). Due to the small wavelengths encountered in Ultrasonic NDT, difficult engineering problems arise in assembling and making these small transducer elements. Each transducer element should have an omnidirectional response, and a minimum amount of coupling between the individual elements of the array should be present. However, workers have tried to make ultrasonic array transducers for non-destructive testing.(10,11)

By processing the signals from each individual transducer element, the beam may be steered so that points outside the normal axis of the transducer may be investigated. This reduces the number of mechanical movements and as electronic processing is faster than mechanical movements the inspection time is reduced.

This processing method might also be extended to another method of obtaining a larger aperture. As the beam pattern for a small aperature transducer is wide, a single transducer may be moved a relatively short distance and thereby obtain more information about one point. The transducer is then moved mechanically and the signals from each individual transducer position are processed so that a larger aperture is synthetised. This technique is given the name synthetic aperature focussing. Synthetic aperture focussing does not encounter any problems with coupling between each individual transducer position and commercially available transducers can be applied. This focussing method is applied in RADAR(12) and workers in Ultrasonic NDT are applying the same idea.(13,14)

5.5.4 Defect Resolution

Distance resolution and angular resolution define with what accuracy the size and shape of a single defect can be given. It may happen that small defects are clustered together giving an overall large defect area. Each defect returns a small portion of the wave sent, and the total echo wave is a complex sum of a number of individual waves. The individual waves interface with each other forming an interference pattern. An analogy to this is found in optics where interest is in investigating distant stars.

Each star returns a part of the wave which when viewed through a finite aperture appears as having a number of fringes due to the diffraction at the aperture. This fringe pattern is known as an Airy disk.

Lord Rayleigh found that two adjacent and equally bright stars can just be resolved if the image of one star falls near to the innermost dark ring in the Airy disk from the other. For a circular aperture this corresponds to a separation angle of the two objects of(15):

$$\theta = \sin^{-1}(1.22\ \lambda/2a) \tag{5.5}$$

This can also be found from (5.3) as the mathematical analysis of a circular aperture in optics and a piston source in acoustics is the same.

The Rayleigh criterion (5.5) is almost impossible to achieve in RADAR, SONAR and Ultrasonic NDT, mainly for two reasons:(9)

(1) The wavelength of light is approximately four magnitudes shorter than the wavelengths encountered in Ultrasonic NDT. Objects will therefore appear to have a smooth surface for elastic waves while random scattering will be present for light. The elastic incoming wave will be reflected quasispecularly.

(2) The Rayleigh criterion assumes an arbitrarily large signal to noise ratio which is not the case for Ultrasonic NDT.

However, the Rayleigh criterion indicates the finite resolving power of RADAR, SONARs and Ultrasonic NDT equipment.

5.6 DIFFERENCES BETWEEN SONAR/RADAR AND ULTRASONIC NDT

Even if the basic principles of SONAR and RADAR are the same as applied in Ultrasonic NDT the cause for the limitations of the techniques are different. The limiting factors for all three techniques are electronic noise and inhomogeneities in the space to be investigated, causing scattering of the sent wave. The inhomogeneities for SONAR are time varying scatterers such as fish, zoo plankton, phytoplankton, inorganic particles and thermal inhomogeneities. For RADAR the scattering of the wave sent is caused by clouds, rain, snow and birds which also are time varying scatterers. The signal to noise ratio of the object signal will therefore vary with time and time averaging techniques might be applied to improve the signal to noise ratio.

5.7 SPATIAL AVERAGING

The grains in metals causing the scattering of the elastic wave are stationary with respect to the flaw. Simple time averaging can therefore not be applied to improve the ratio of signal to scattered noise.

Workers(16) have suggested a spatial averaging to improve the flaw signal to grain noise ratio. The flaw signal is kept relatively stationary while the signals from the smaller grains are randomizerd by a slight movement of the transducer.

The limitations of this 'signal enhancement' technique is the amount of movement of the transducer. Fig. 5.4 shows the normalised amplitude of a number of sinusoidal signals when each signal is moved with respect to each other. The figure is drawn for different numbers of signals

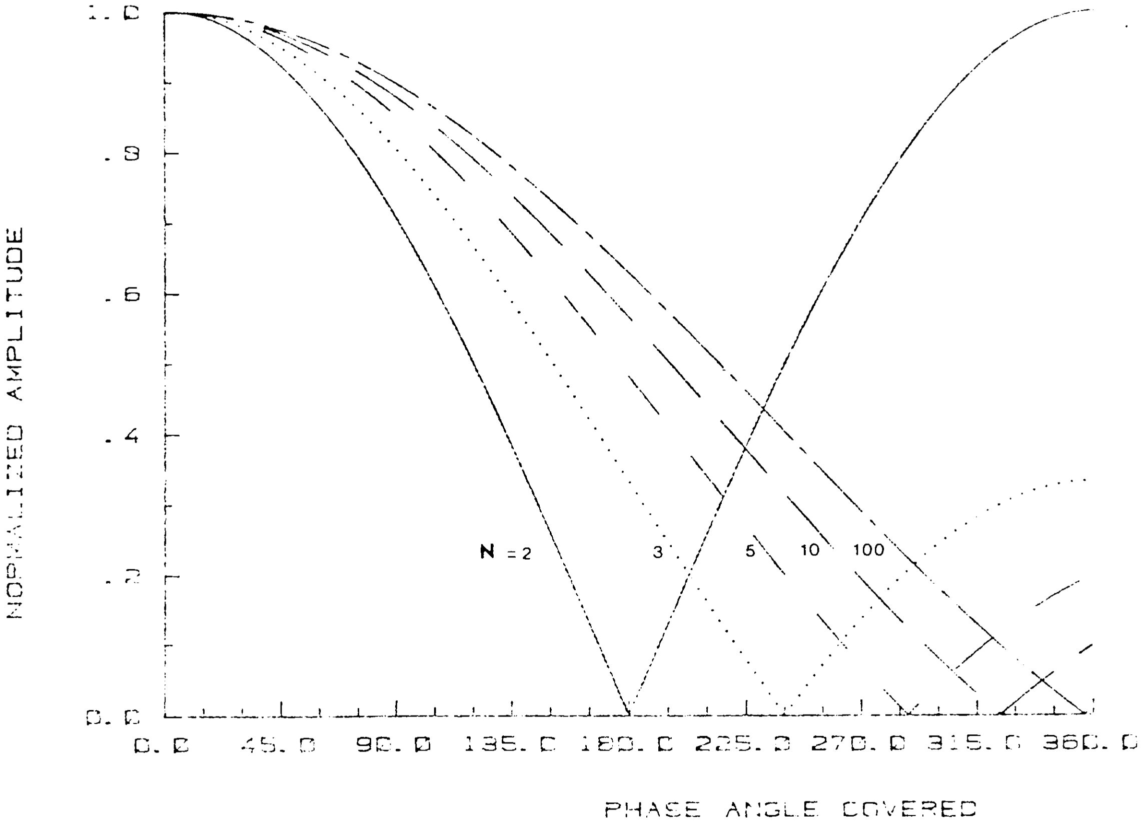

Figure 5.4. The sum of a number of sinusoidal signals, as a function of total phase angle covered.

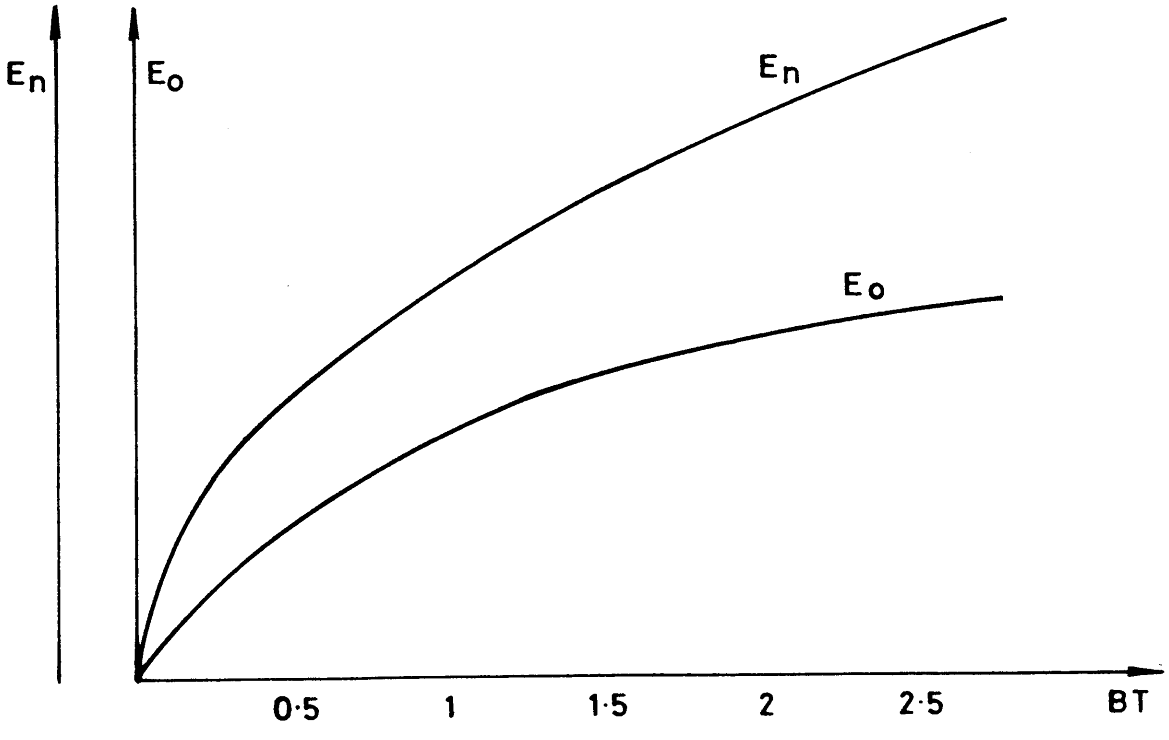

Figure 5.5 **Amplitude of pulse signal, Eo, and noise, En, versus bandwidth.**

(N = 2, 3, 5, 10 and 100), for each graph the probability distribution of the movement is rectilinear.

If resolution is neglected a movement corresponding to a total phase angle of 215 degrees might be accepted before the amplitude is reduced by 6 dB. This corresponds to a difference in distance travelled of:

$$\Delta d = \frac{C}{f} \frac{\phi}{360}$$

For a 5 MHz signal with a propagation velocity of 6000 m/s this gives a differential distance of 0.36 mm.

When resolution is incorporated the effect of blurring has to be considered. The amount of blurring will be equal to the differential distance. For the example above, the amount of blurring will be 0.36 mm.

To overcome this limitation of spatial averaging the difference in propagation distance has to be included. This is in practice the same technique used in synthetic aperture focussing. This technique is described in more detail in other places(9, 13).

5.8 REDUCTION OF INSPECTION VOLUME

The wavelength to grain diameter ratio used in ultrasonic nondestructive testing is usually chosen to be in the Rayleigh scattering region. This gives an approximate uniform volume distribution of the elastic wave. The received noise signal due to grains can therefore be reduced by reducing the volume of the ultrasonic beam volume.

This method can be implemented by using two ultrasonic transducers, one sender and one receiver. The transducers are placed so that the two beams are perpendicular to each other forming a small common inspection volume.

A practical disadvantage with this method is that only a small volume is inspected at the time; giving a large total inspection time for the structure.

5.9 BANDWIDTH CONSIDERATIONS

Considering an electronic amplifier and detector, the main component of the noise present on the output is due to Johnson noise. The mean square value of the noise voltage is given by:

$E_n^2 = 4kTRB$ Where k is the Boltzmans constant
T is temperature
R is source resistance
B is bandwidth

The noise voltage is proportional to the square root of the bandwidth of the amplifier and the detector.

$E_n \approx \sqrt{B}$

The amplitude of a pulse signal after passing through a bandlimited amplifier and detector will depend on the bandwidth of the combination. Assuming a pulse of duration T passing through the amplifier/detector then the amplitude of the output pulse will be given by

$$E_{out} \simeq (1-e^{-BT})\ E_{in}$$

Fig. 5.5 shows the amplitude of the noise and the signal as a function of bandwidth. The duration of the pulse is set constant for this figure.

The signal to noise ratio will be

$$\frac{E_{out}}{E_n} \simeq \frac{(1-e^{-BT})}{\sqrt{B}}$$

The maximum signal to noise ratio is given by

$$\frac{d\,\frac{E_{out}}{E_n}}{dB} = \frac{1}{B^{\frac{3}{2}}}\left(\left(\frac{1}{2}+BT\right)e^{-BT} - \frac{1}{2}\right) = 0$$

This gives $BT \simeq 1.26$ by numerical solution.

The optimum bandwidth for maximum signal to noise ratio will hence be:

$$B = 1.3\ \frac{1}{T}$$

5.10 CORRELATION DETECTION

If the signal sent is known it is possible to use cross-correlation detection. The cross-correlation function of signal x(t) and y(t) is defined:-

$$R\,xy(\tau) = \lim_{T\to\infty} \frac{1}{T} \int_{-\infty}^{\infty} x(t)\; y(t+\tau)\; dt$$

For a signal of duration T, the cross-correlation function can be written as:

$$R\,xy(\tau) = \frac{1}{T} \int_{0}^{T-\tau} x(t)\; y(t+\tau)\; dt$$

A cross-correlation detector will remove any white noise present in the signal. This can be shown by assuming that a sinusoidal sent $x(t)$ is corrupted by additive white noise $n(t)$. The received signal can then be symbolised by:

$$y(t) = x(t) + n(t)$$

When the received signal is correlated with the sent signal, the cross-correlation function becomes:

$$Rxy(\tau) = \lim_{T\to\infty} \frac{1}{T} \int_{-\infty}^{\infty} x(t)\; y(t+\tau)\; dt$$

$$= \lim_{T\to\infty} \frac{1}{T} (\int_{-\infty}^{\infty} x(t)x(t+\tau)dt + \int_{-\infty}^{\infty} x(t)n(t+\tau)dt$$

$$= Rxx(\tau) + Rxn(\tau)$$

$Rxn(\tau)$ is equal to zero as the additive noise is white.

$Rxx(\tau)$ remains and depends only on the signal sent.

The longitudinal range resolution, i.e. the accuracy with which the distance from the transducer to the defect can be given, depends on the width of the correlation peak.

The auto-correlation function is the Fourier transform of the power density spectrum of the signal. This is shown by the Wiener-Khinchin relation (Appendix I).

To obtain a sharp correlation function it is required that the signals have a broad bandwidth. (Ref. the Fourier transform of a Dirac delta function).

Correlation detectors have been applied to ultrasonic nondestructive testing previously. Newhouse et al.(17) have used a band limited noise signal with a simple polarity coincident correlator.

CHAPTER SIX

CHOICE OF DRIVE WAVEFORM FOR A CROSS-CORRELATION, ULTRASONIC FLAW DETECTOR

To obtain a well-defined correlation function the signals being correlated have to have a broad bandwidth shown by the Wiener-Khinchin relation described in Chapter Five. Different signals have a broad bandwidth such as frequency modulated sinusoidal signals and white noise signals. Ultrasonic NDT requires a limited duration of the signal as reverberation increases with the length of the signal. Suitable signals for ultrasonic NDT equipment employing a correlating detector are therefore of a relatively short duration, i.e. broad bandwidth.

The first type of signal to be investigated is the linear frequency modulated sinusoidal signal. The received signal will be of the same nature as the signal sent and it is therefore of interest to investigate the auto-correlation function of this type of signal.

6.1 THE AUTO-CORRELATION FUNCTION OF A LINEAR FREQUENCY MODULATED SINUSOIDAL SIGNAL

The angle θ traversed by a sinusoidal signal is the integral of the frequency with respect to time i.e.

$$\theta = \int_0^t \omega dt \qquad \text{where } \omega \text{ is the angular frequency}$$

From Fig. 6.1 the instantaneous frequency of a linear frequency modulated sinusoidal (LFMS) signal is

$$\omega = \omega_1 + Mt$$

The LFMS signal is then expressed by

$$x(t) = \sin\theta = \sin \int_0^t \omega dt = \sin \int_0^t (\omega_1 + Mt)dt$$

$$= \sin (\omega_1 t + \frac{M}{2}t^2) \qquad (6.1)$$

For a pulsed LFMS signal of duration T equation (6.1) becomes

$$\begin{aligned} x(t) &= \sin(\omega_1 t + \frac{M}{2}t^2) && 0 < t < T \\ &= 0 && \text{elsewhere} \end{aligned} \qquad (6.2)$$

The starting frequency is ω_1 and the end frequency $\omega_1 + MT$.

The auto-correlation function of the LFMS signal can be found by evaluating the following integral:

$$R_{xx}(\tau) = \frac{1}{T}\int_0^{T-\tau} x(t)x(t+\tau)\, dt \qquad (6.3)$$

$$= \frac{1}{T}\int_0^{T-\tau} \sin(\omega_1 t + \frac{M}{2}t^2)\sin(\omega_1(t+\tau) + \frac{M}{2}(t+\tau)^2)dt$$

$$R_{xx}(\tau) = \frac{1}{2T}(\int_0^{T-\tau} (\cos(\omega_1\tau + \frac{M}{2}(2t\tau+\tau^2))dt$$

$$(6.4)$$

$$- \int_0^{T-\tau} \cos(\omega_1(2t+\tau) + \frac{M}{2}(t^2+(t+\tau)^2))dt)$$

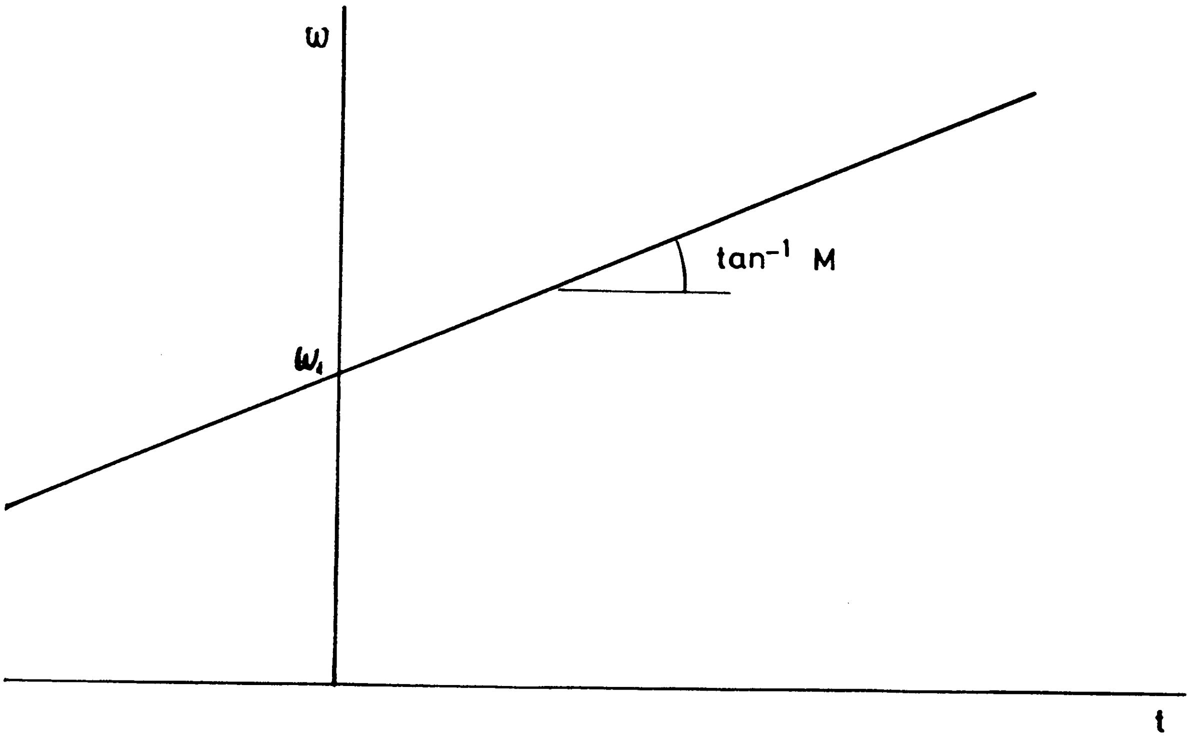

Figure 6.1 The instantaneous frequency of a linear frequency modulated sinusoidal signal as a function of time.

The first integral can be expressed as:

$$R_{xx}1(\tau) = \frac{1}{2T}\int_0^{T-\tau} \cos(\omega_1\tau + \frac{M}{2}(2t\tau+\tau^2))\,dt$$

$$= \frac{1}{2T}\left[\frac{1}{M\tau}\sin(\omega_1\tau + \frac{M}{2}(2t\tau+\tau^2))\right]\Bigg|_{0}^{T-\tau}$$

$$= \frac{1}{2MT\tau}(\sin(\omega_1\tau + \frac{M}{2}(2\tau(T-\tau)+\tau^2)) - \sin(\omega_1\tau + \frac{M}{2}\tau^2))$$

$$= \frac{1}{2MT\tau}(\sin(\omega_1\tau + \frac{M}{2}\tau(2T-\tau)) - \sin\tau(\omega_1 + \frac{M}{2}\tau))$$

$$= \frac{1}{MT\tau}\ (\cos\frac{1}{2}(\omega_1\tau + MT\tau - \frac{M}{2}\tau^2 + \omega_1\tau + \frac{M}{2}\tau^2).\sin\frac{1}{2}(\omega_1\tau + MT\tau - \frac{M}{2}\tau^2 - \omega_1\tau - \frac{M}{2}\tau^2))$$

$$= \frac{1}{MT\tau}\ (\cos(\omega_1\tau + \frac{M}{2}T\tau).\sin(\frac{M}{2}\tau(T-\tau)))$$

The second integral becomes:

$$R_{xx}2(\tau) = \frac{1}{2T}\int_0^{T-\tau} \cos(\omega_1(2t+\tau) + \frac{M}{2}(t^2+(t+\tau)^2))\,dt$$

$$= \frac{1}{2T}\int_0^{T-\tau} \cos(Mt^2 + 2(\omega_1 + \tau\frac{M}{2})t + \tau(\omega_1 + \tau\frac{M}{2}))\,dt \tag{6.5}$$

From Abramowitz and Stegun$^{(1)}$ $R_{xx}2(\tau)$ is:

$$R_{xx}2(\tau) = \frac{1}{2T}\sqrt{\frac{\pi}{2M}}\ \Big|\cos\Big(\frac{(\omega_1+\tau\frac{M}{2})^2 - M\tau(\omega_1+\tau\frac{M}{2})}{M}\Big)C\Big|\sqrt{\frac{2}{M\pi}}(MT+\omega_1+\tau\frac{M}{2})\Big|$$

$$+ \sin\Big(\frac{(\omega_1+\tau\frac{M}{2})^2 - M\tau(\omega_1+\tau\frac{M}{2})}{M}\Big)S\Big|\sqrt{\frac{2}{M\pi}}\ (Mt+\omega_1+\tau\frac{M}{2})\Big|\ \Bigg|_{0}^{T-\tau}$$

$$= \frac{1}{2T}\sqrt{\frac{\pi}{2M}}\ \Big|\cos(\frac{1}{M}(\omega_1^2 - (\frac{\tau M}{2})^2))C\Big|\sqrt{\frac{2}{\pi M}}(\omega_1 + \frac{M}{2}(2t+\tau))\Big|$$

$$+ \sin(\frac{1}{M}(\omega_1^2 - (\frac{\tau M}{2})^2))S\Big|\sqrt{\frac{2}{\pi M}}(\omega_1 + \frac{M}{2}(2t+\tau))\Big|\ \ \Bigg|_{0}^{T-\tau}$$

$$
\begin{aligned}
&= \frac{1}{2T}\sqrt{\frac{\pi}{2M}}\,\Big|\cos\Big(\frac{1}{M}\Big(\omega_1^2-\Big(\frac{\tau M}{2}\Big)^2\Big)\Big)\Big(C\Big|\sqrt{\frac{2}{\pi M}}\Big(\omega_1+\frac{M}{2}(2T-\tau)\Big)\Big| \\
&\quad - C\Big|\sqrt{\frac{2}{\pi M}}\Big(\omega_1+\frac{M}{2}\tau\Big)\Big|\Big) \\
&\quad + \sin\Big(\frac{1}{2M}\Big(\omega_1^2-\Big(\frac{\tau M}{2}\Big)^2\Big)\Big)\Big(S\Big|\sqrt{\frac{2}{\pi M}}\Big(\omega_1+\frac{M}{2}(2T-\tau)\Big)\Big| \\
&\quad - S\Big|\sqrt{\frac{2}{\pi M}}\,\Big(\omega_1+\frac{M}{2}\tau\Big)\Big|\Big)\Big|
\end{aligned}
\tag{6.6}
$$

The auto-correlation function of the LFMS signal is the sum of these two integrals. This is plotted for Bandwidth-Time products (MT.T) of 5 and 40 in Figs. 6.2 and 6.3. These signals are plotted with a signal duration of 10 μs and a starting frequency of 1 MHz. The width of the lobe (the central peak) is inversely proportional to the bandwidth of the LFMS signal and the height of the sidelobes (the local peaks away from the centre) are reduced with an increase in the Bandwidth-Time product. Fig. 6.4 shows the effect of the Bandwidth-Time product on the ratio of the maximum sidelobe to the lobe height. This figure was obtained by plotting a number of auto-correlation functions and measuring the maximum sidelobe/lobe ratio.

The detection of signals separated by less than the duration of the correlation function requires that the sidelobe-lobe ratio should be as small as possible. This ratio can be decreased by increasing the Bandwidth-Time product as shown in Fig. 6.4. The transducers used in ultrasonic NDT have a limited bandwidth and the duration of

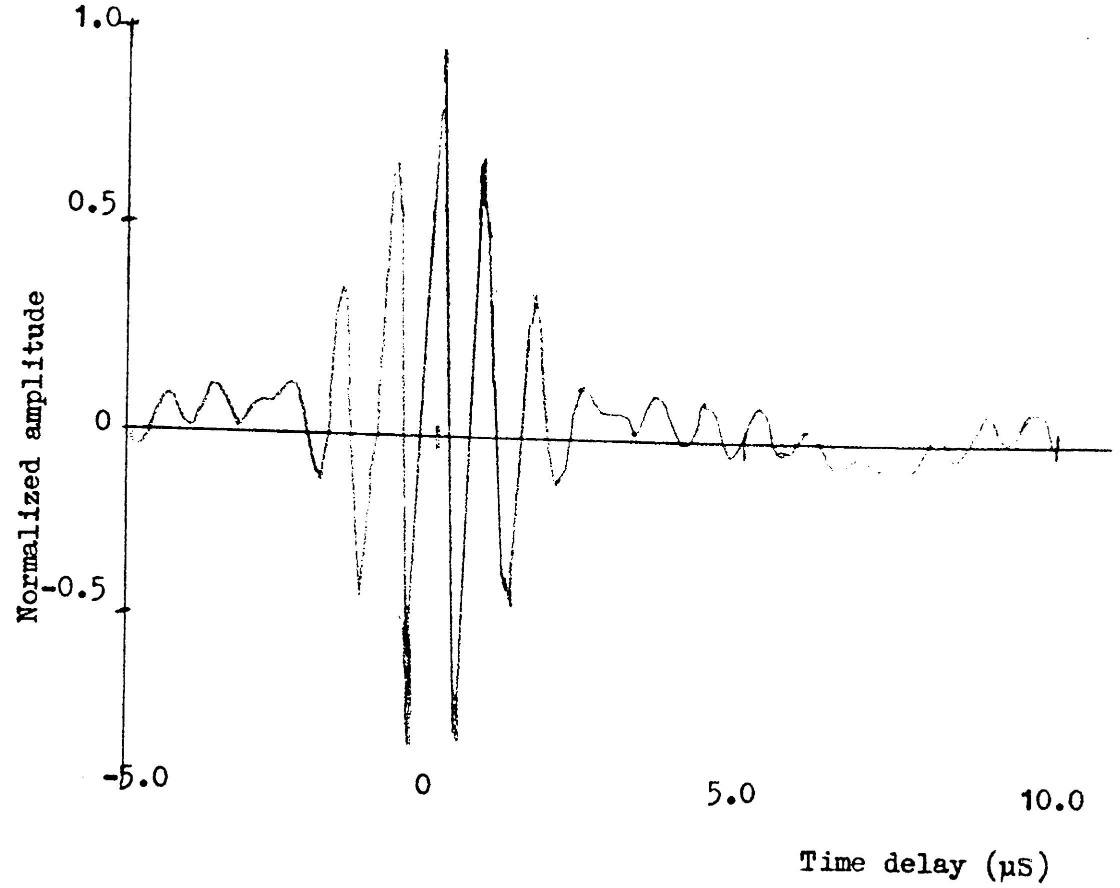

Figure 6.2 The autocorrelation function for the LFMS signal with duration T=10 µS and bandwidth*time=5.

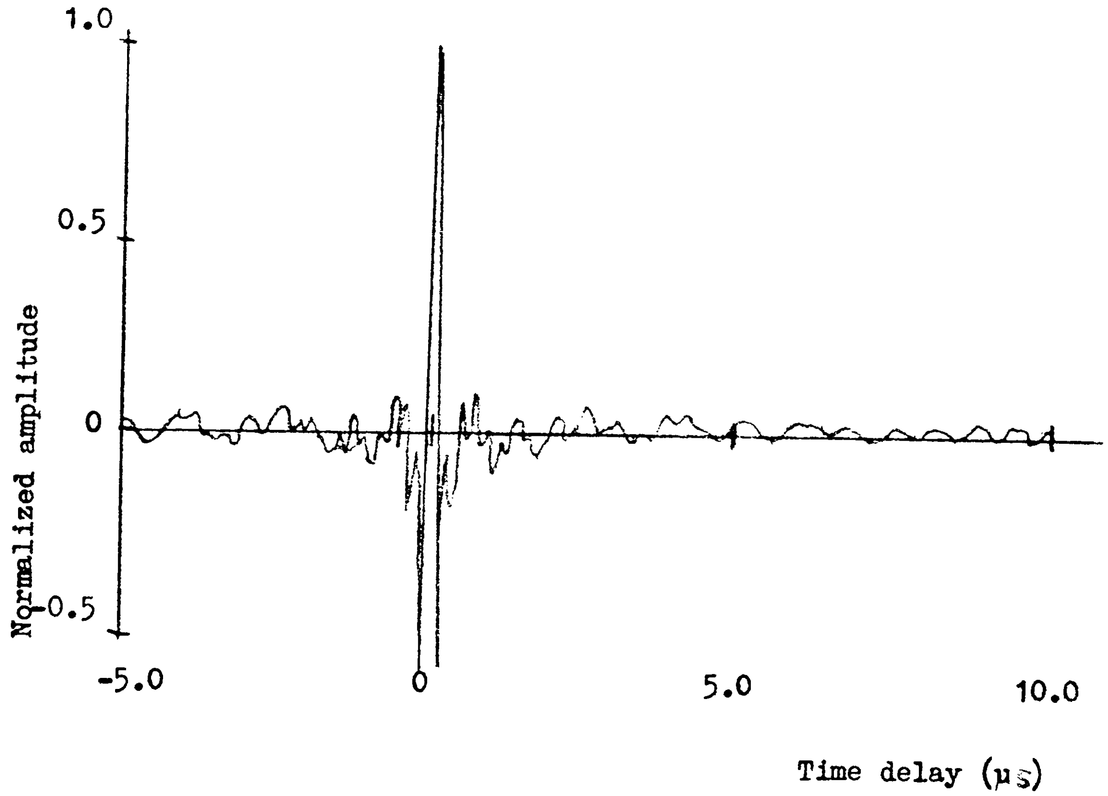

Figure 6.3 The autocorrelation function for the LFMS signal with duration T=10 µs and bandwidth*time=40.

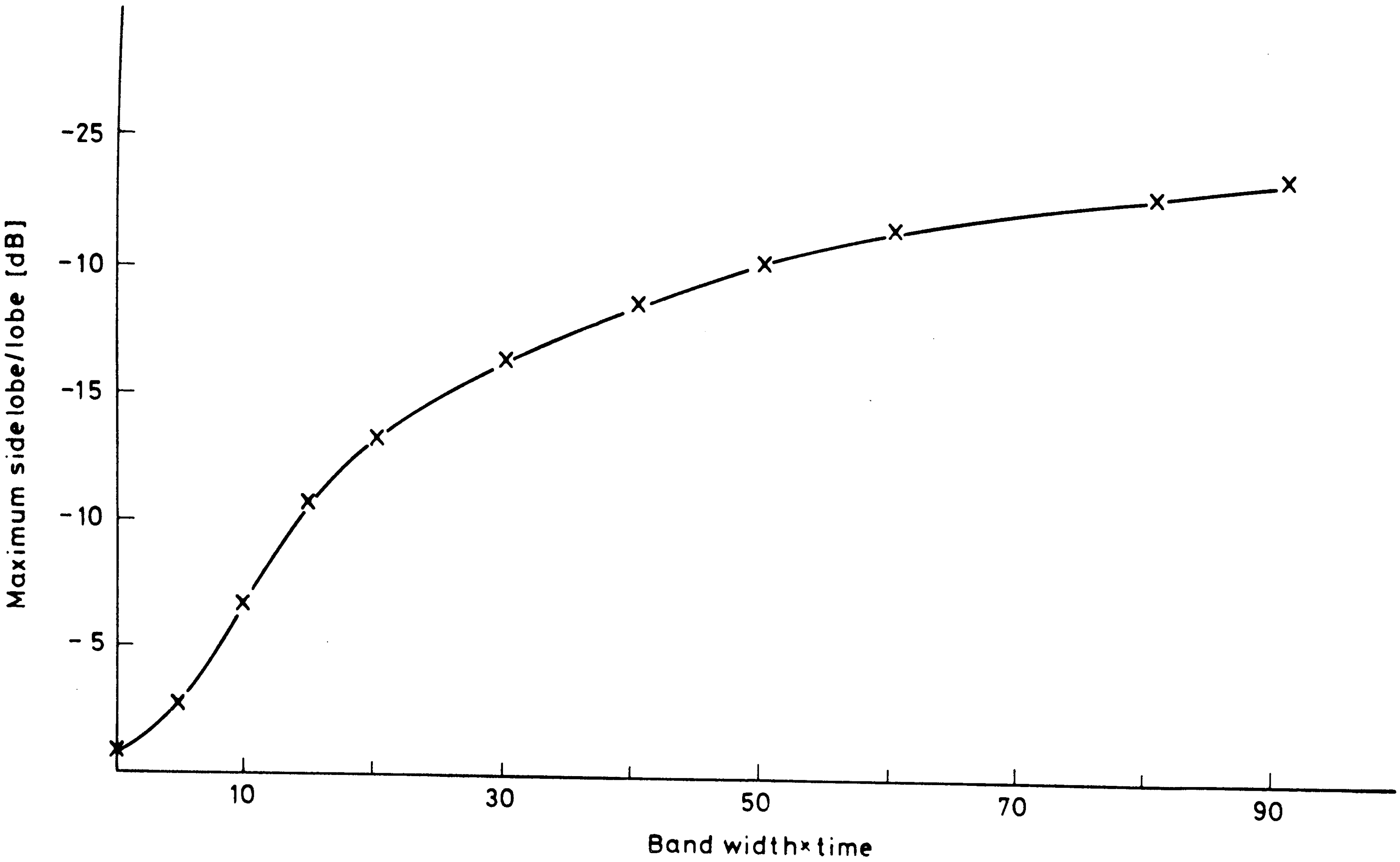

Figure 6.4 The sidelobe-mainlobe amplitude ratio for a LFMS signal as a function of bandwith*time.

the signal sent is limited by reverberations as previously mentioned. The total sending time can however be increased by synthesizing it with a number of short signals. These transmissions are then separated by the time required for the reverberation due to the previous transmission to be attenuated below a detectable level. This can be illustrated with correlating a number of pulsed sinusoidal waves of different frequencies and then average these correlation functions to obtain a final broad bandwidth correlation function.

6.2 THE AUTOCORRELATION FUNCTION OF A PULSED SINUSOIDAL SIGNAL

The auto-correlation function of a pulsed sinusoidal signal of duration T is

$$R_{xx}(\tau) = \frac{1}{T}\int_0^{T-\tau} \sin \omega t \, \sin \omega(t+\tau) \, dt \qquad (6.7)$$

$$= \frac{1}{2T}\int_0^{T-\tau} (\cos(\omega t) - \cos(2\omega t+\omega\tau))\,dt$$

$$= \frac{1}{2T}\left(t\cos(\omega t) - \frac{1}{2\omega}\sin(2\omega t+\omega\tau)\right\Big|_0^{T-\tau}$$

$$= \frac{1}{2T}\left((T-\tau)\cos(\omega\tau) - \frac{1}{2\omega}(\sin(2\omega T-\omega\tau)+\sin(\omega\tau))\right)$$

$$R_{xx}(\tau) = \frac{1}{2T}\left((T-\tau)\cos(\omega\tau) - \frac{1}{\omega}\sin(\omega T)\cos(\omega T-\omega\tau)\right)$$

but $\omega T = 2\pi n$, n is the number of cycles and an integer larger than 0 hence,

$$\sin(\omega T) = \sin(2\pi n) = 0$$

and

$$R_{xx}(\tau) = \frac{T-\tau}{2T} \cos \omega\tau$$

Since the signal duration $T = \frac{2\pi n}{\omega}$, the auto-correlation of a pulsed sinusoidal signal can be written as:

$$R_{xx}(\tau) = \frac{2\pi n-\omega\tau}{4\pi n} \cos\omega\tau \qquad (6.8)$$

For a number of pulsed sinusoidal signals with different frequencies the sum of the auto-correlation functions will be

$$R_{\Sigma xx}(\tau) = \sum_{k=1}^{N} \frac{n-f_k\tau}{nN} \cos(2\pi f_k\tau) \qquad (6.9)$$

This function is plotted in Fig. 6.5 for five pulsed sinusoidal signals with 10 cycles each. The instantaneous frequency of the sinusoidal signals are divided linearly over a frequency range of 1:5. The sidelobe/lobe ratio is however unacceptably high. To improve this ratio smaller steps between each frequency gives Fig. 6.6. This function is the sum of 17 sinusoidal auto-correlations each of 10 cycles and a linear frequency separation over a frequency range of 1:5.

However, this frequency division is not making optimal use of the available bandwidth. The frequency spectrum of a pulsed sinusoidal signal has an envelope of the form

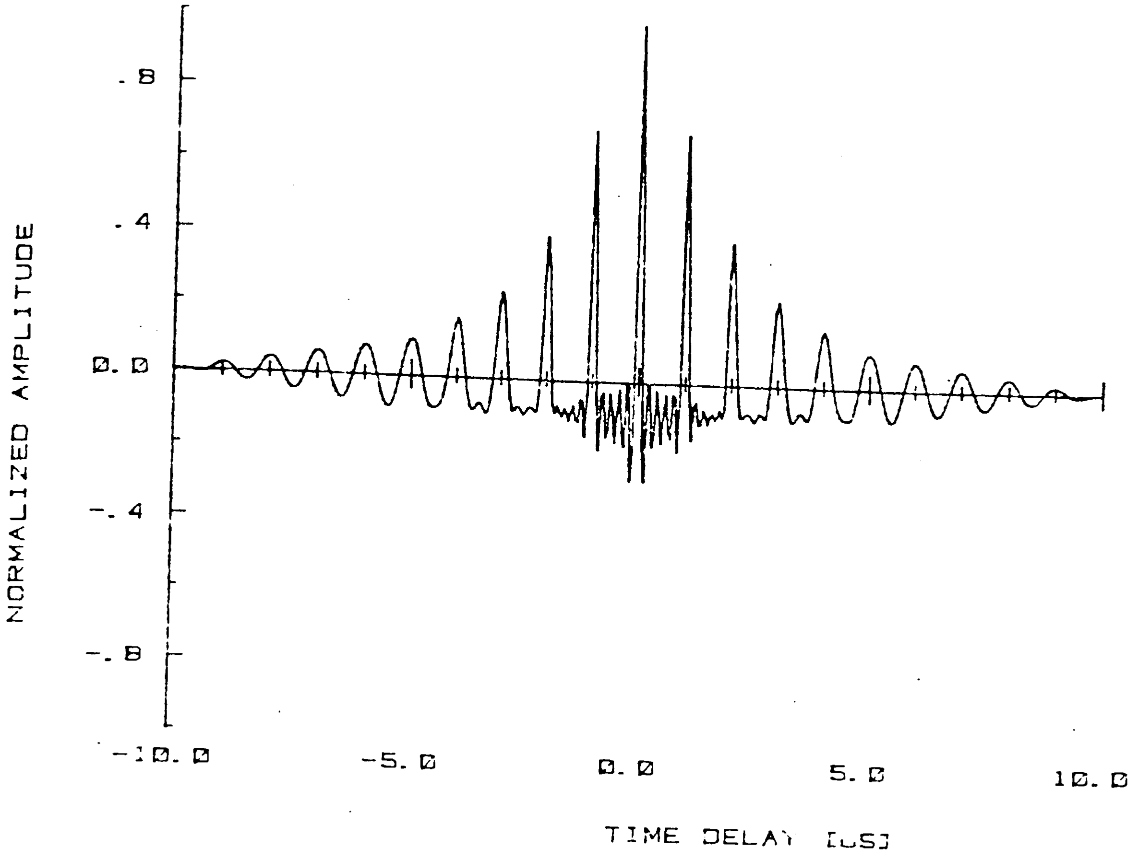

Figure 6.5. The sum of five auto-correlation functions obtained from pulsed sinusoidal signals with 10 cycles each and a frequency difference of 1 MHz.

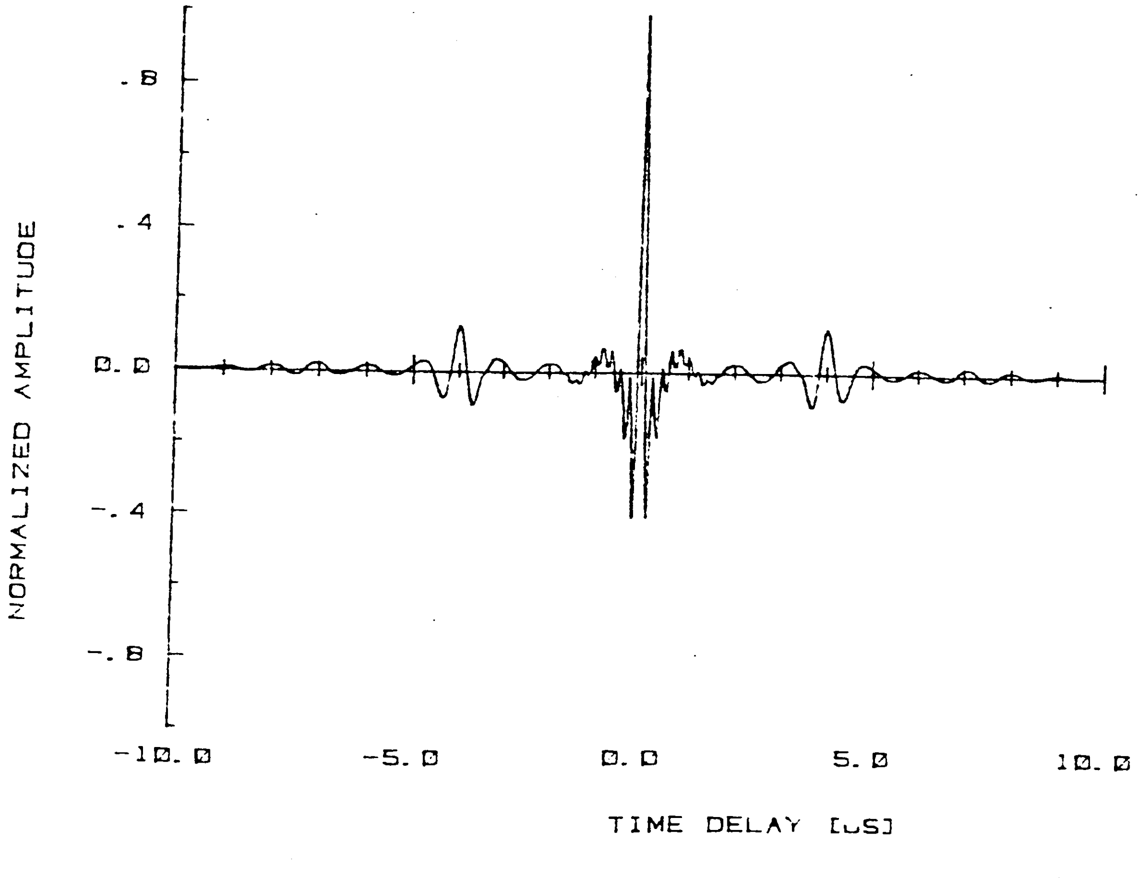

Figure 6.6. The sum of seventeen auto-correlation functions obtained from pulsed sinusoidal signals with 10 cycles each on a frequency difference of 0.25 MHz.

$|\sin x/x|$ as shown in Fig. 6.7. This spectrum might be approximated by a rectangular function centred at f_o:

$$G(f) = 1 \qquad f_o - \frac{f_o}{n} < f < f_o + \frac{f_o}{n}$$

$$= 0 \qquad \text{elsewhere}$$

To fill the available bandwidth with these rectangular spectra, their central frequencies can be found from the following equation:

$$f_k + \frac{f_k}{n} = f_{k+1} - \frac{f_{k+1}}{n}$$

$f_k + \frac{f_k}{n}$ is the upper frequency of the kth spectrum centred at f_k and $f_{k+1} - \frac{f_{k+1}}{n}$ is the lower frequency of the (k+1)th spectrum centred at f_{k+1}, hence,

$$f_{k+1} = f_k\left(\frac{1 + \frac{1}{n}}{1 - \frac{1}{n}}\right) \qquad (6.10)$$

When the same bandwidth as in ~~the previous~~ examples is used i.e. 1:5 the starting frequency becomes 1.1. A total number of 8 sinusoidal signals are required to fill this bandwidth, when each sinusoidal signal contains 10 cycles. The frequencies of these pulsed sinusoids form a geometric series with the following centre frequencies: 1.10, 1.34, 1.64, 2.01, 2.45, 3.00, 3.67 and 4.48.

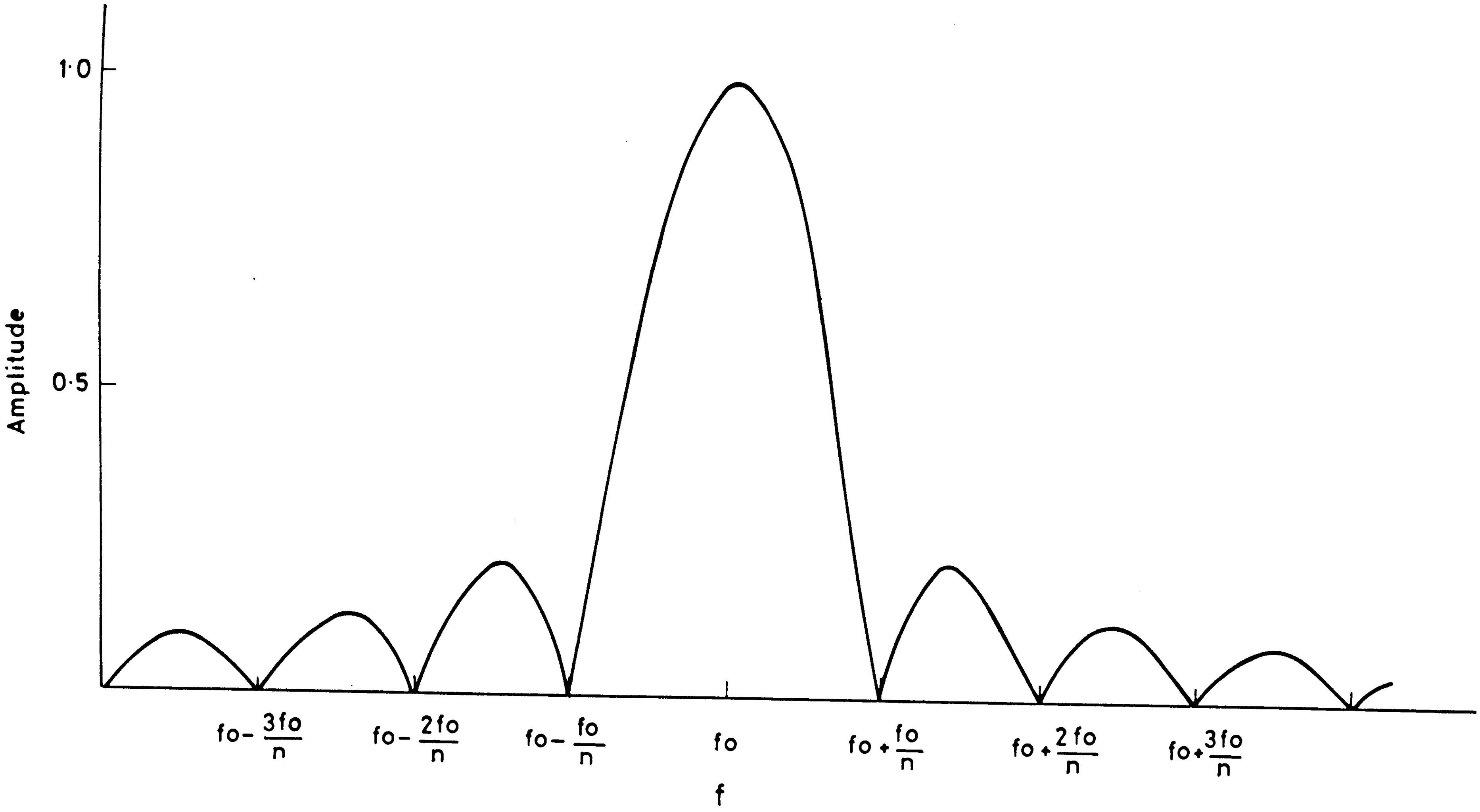

Figure 6.7 The frequency spectrum of a pulsed sinusoidal signal of frequency fo and n cycles.

The spectrum of this frequency distribution is shown in Fig. 6.8 with the corresponding summed auto-correlation function in Fig. 6.9.

The regularity in the sidelobe structure observed for the linear frequency separation has been removed by a geometric progression of the frequencies. The sidelobe level is however constant over a much wider range than for the linear separation. By increasing the number of sinusoidal signals in the auto-correlation function the sidelobe level is reduced as seen in Fig. 6.10. This figure shows the maximum sidelobe/lobe ratio as a function of the number of sinusoidal signals used to obtain the summed auto-correlation function. The frequency of each sinusoidal signal is following the geometrical progression of equation (6.10). Fig. 6.10 was obtained by finding the auto-correlation function for each number of sinewaves and a search for the maximum sidelobe/lobe ratio was performed. As can be seen a general reduction in the sidelobe level is achieved by increasing the number of sinusoidal signals, but the sidelobe level is still high.

To reduce the sidelobe level further the full available bandwidth can be used for each transmission, but changing the structure of the signal for each repeated transmission. This will enable a reduction in the sidelobe level as the sidelobes will average each other out with repeated transmissions. Signals exhibiting this property are usually referred to as random noise signals.

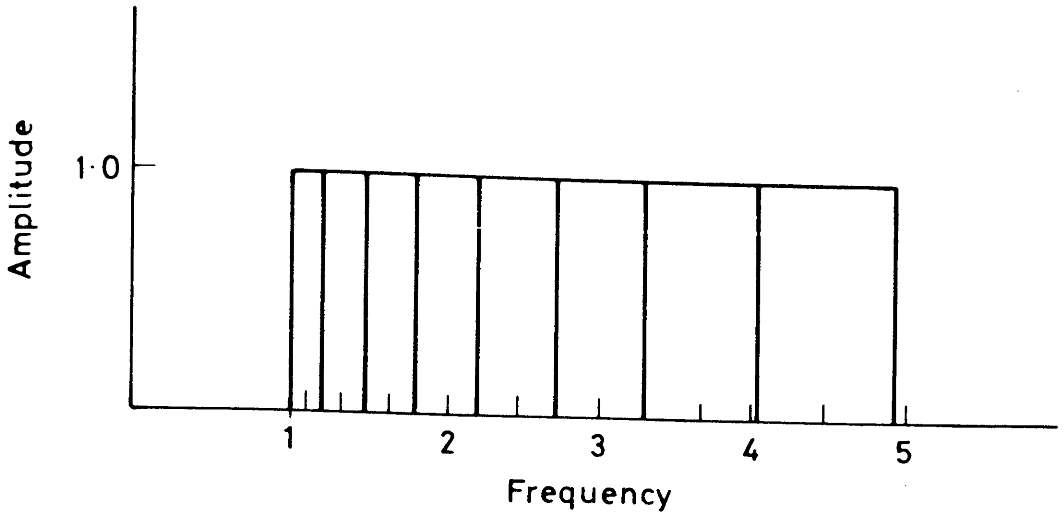

Figure 6.8 The spectrum of pulsed sinusoidal signals with a geometrical progressing centre frequency.

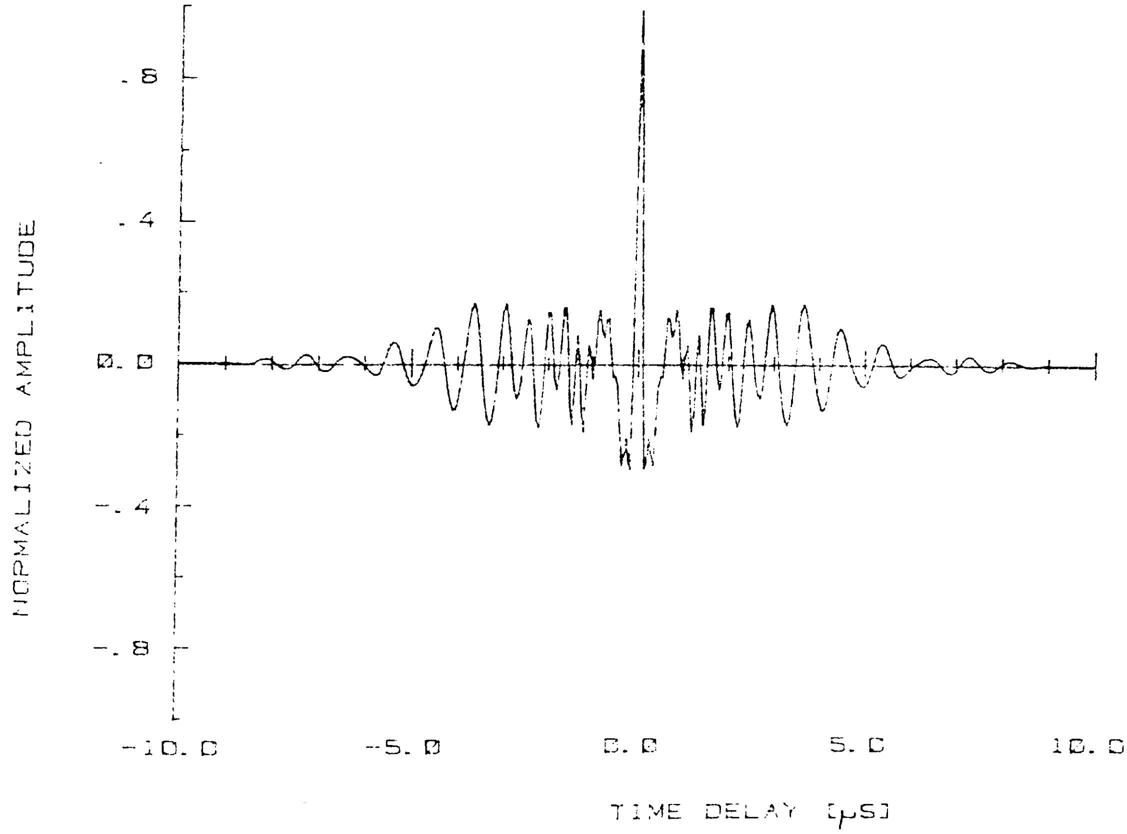

Figure 6.9. The sum of eight auto-correlation functions obtained from pulsed sinusoidal signals with 10 cycles each and with the frequencies shown in figure 6.8.

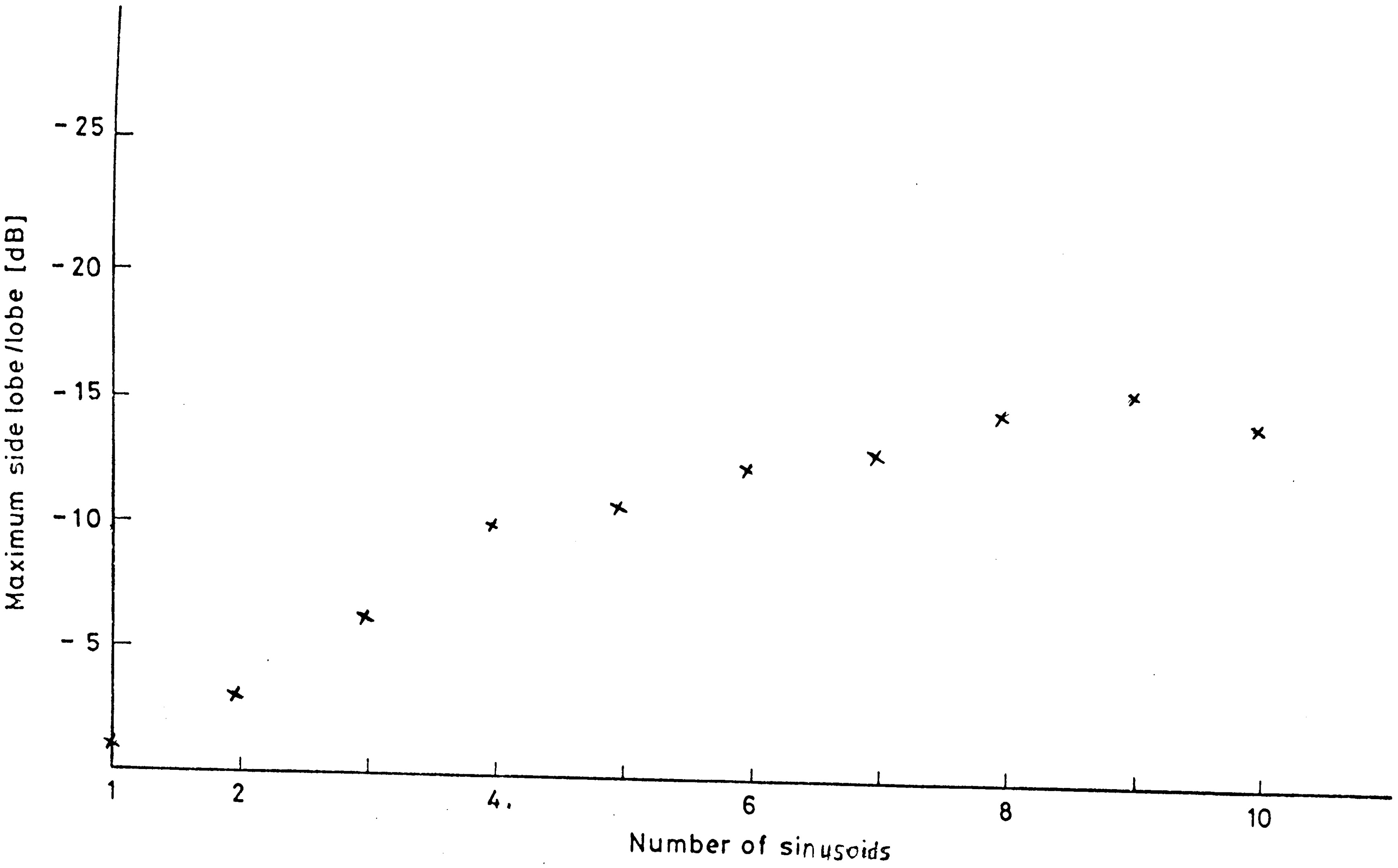

Figure 6.10 The maximum sidelobe-mainlobe amplitude ratio for the frequency stepped sinusoidal autocorrelation function as a function of the number of steps.

6.3 THE AUTO-CORRELATION FUNCTION OF BANDLIMITED RANDOM NOISE

A bandlimited random noise signal has a rectangular spectrum centred at f_o and with a bandwidth of B i.e.

$$G(f) = 1 \qquad \text{for } f_o - \frac{B}{2} < f < f + \frac{B}{2}$$

$$= 0 \qquad \text{elsewhere}$$

Applying Wiener-Kinchins equation[2].

$$R_{xx}(\tau) = \int_{-\infty}^{\infty} G(\omega)\, e^{j\omega\tau}\, d\omega \tag{6.11}$$

and introducing the angular frequency

$$\omega_o = 2\pi f_o \qquad \text{and} \qquad \omega_B = 2\pi B$$

The auto-correlation function for a bandlimited random noise signal with a one sided spectrum can be written as:

$$R_{xx}(\tau) = \mathrm{Re}\Big(\int_{\omega_o - \omega B/2}^{\omega_o + \omega B/2} e^{j\omega\tau}\, d\omega \Big)$$

$$= \mathrm{Re}\Big(\frac{1}{j\tau} \Big|\, e^{j\omega\tau} \Big|_{\omega_o - \omega B/2}^{\omega_o + \omega B/2} \Big)$$

$$= \mathrm{Re}\Big(\frac{2}{\tau}\, e^{j\omega_o} \Big(\frac{e^{j\frac{\omega B}{2}\tau} - e^{-j\frac{\omega B}{2}\tau}}{2j} \Big) \Big)$$

$$= \mathrm{Re}\Big(\frac{2}{\tau}\, e^{j\omega_o\tau}\, \sin\big(\frac{\omega B}{2}\tau\big) \Big)$$

$$R_{xx}(\tau) = 2B\pi\, \frac{\sin(\pi B\tau)}{\pi B\tau}\, \cos(2\pi f_o\tau) \tag{6.12}$$

This function is plotted in Fig. 6.11. However, this is for an infinite duration signal which can not be obtained in practice. To simulate a more practical case, random numbers were generated by a digital computer to synthesize a random noise signal. This string of random numbers was then correlated against itself giving one auto-correlation function. Repeating this with different random numbers gave a different sidelobe structure for each individual auto-correlation function. Fig. 6.12 shows the sum of eight auto-correlation functions. Each individual signal making up the auto-correlation functions consists of 40 numbers with a change of the numbers occurring every 1/40 of the duration. This can be taken to simulate a random signal of 10 μs duration with a change in the signal occurring every 0.25 μs, hence corresponding to a signal bandwidth of 4 MHz. This correlates with the Bandwidth-Time products in Fig. 6.9.

Fig. 6.13 shows the maximum sidelobe/lobe ratio for the random signal auto-correlation function versus the number of signals averaged. Comparing this with Fig. 6.10 the random signal gives a lower level of the sidelobes than the sinusoidal signals.

Fig. 6.13 also indicates the variations in the sidelobe level for different runs of the computer program, this is due to the variable nature of the random signal.

Figs. 6.14 and 6.15 show the output from a correlating

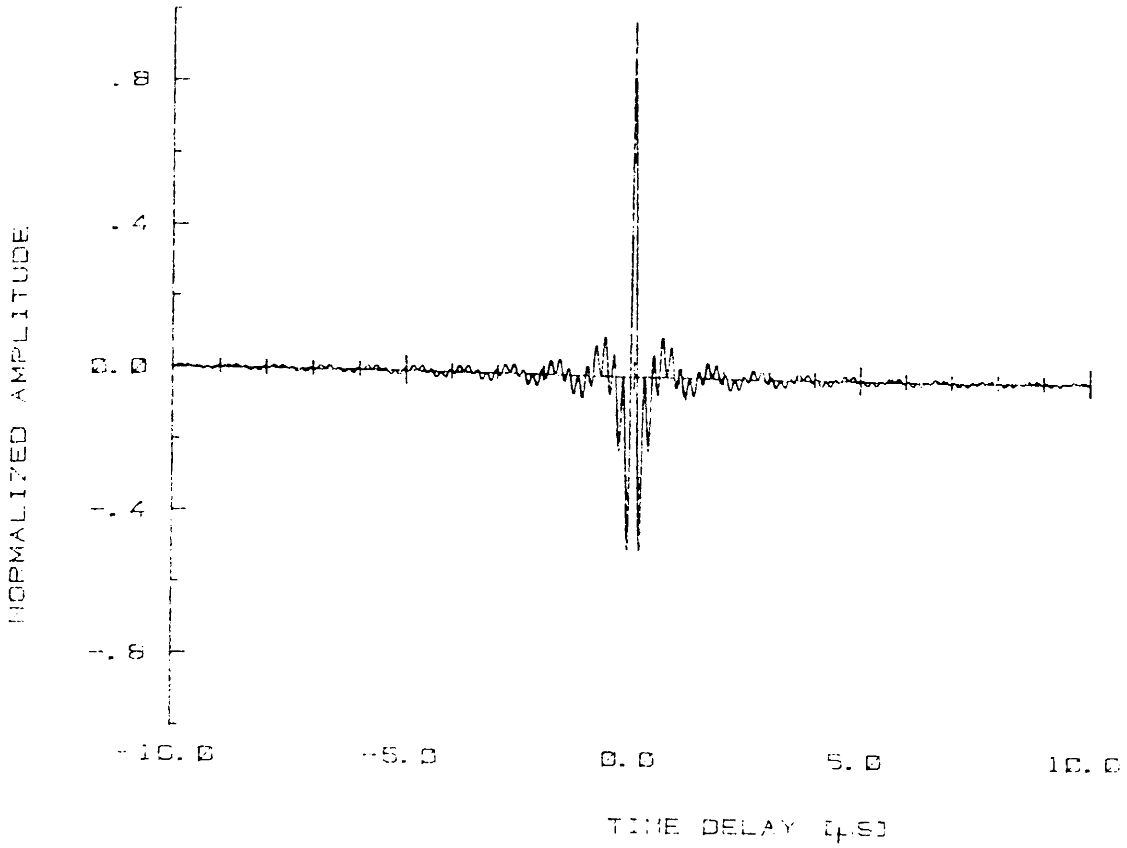

Figure 6.11. The auto-correlation function of a random noise signal with 4 MHz bandwidth and a centre frequency of 3 MHz.

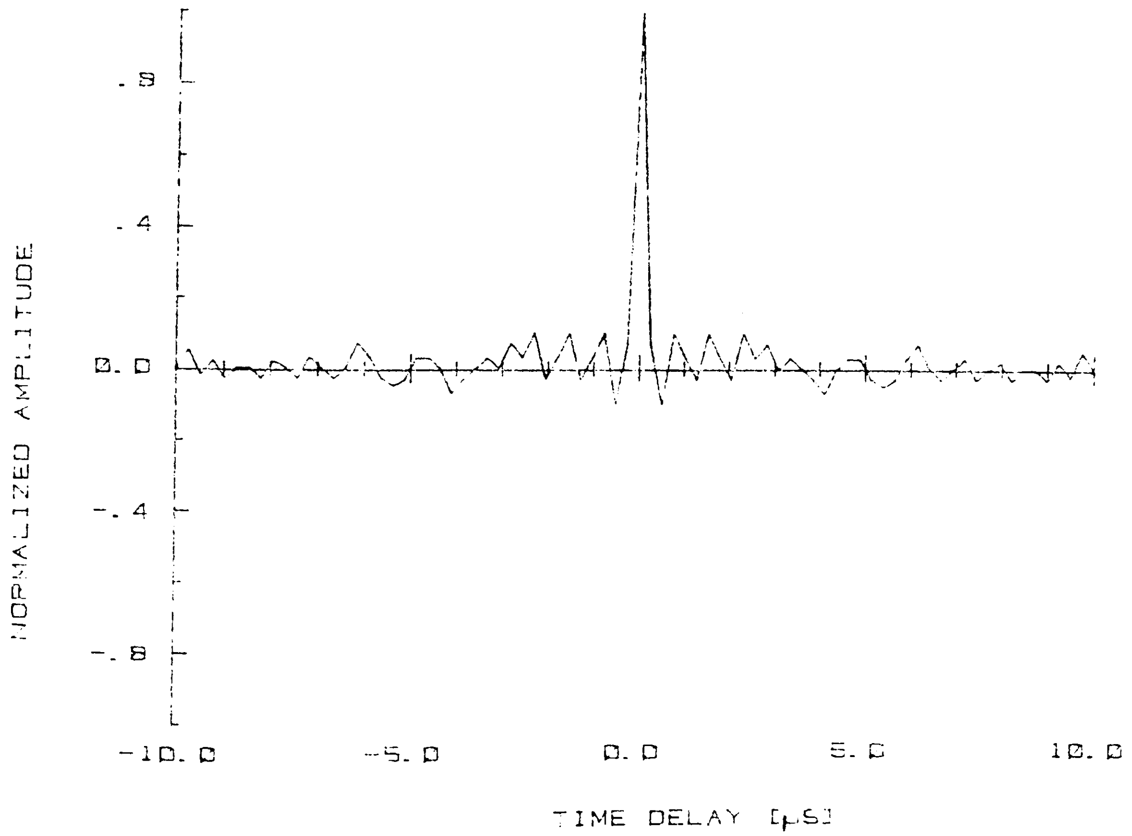

Figure 6.12. The sum of eight autocorrelation functions obtained from synthesised random noise signals.

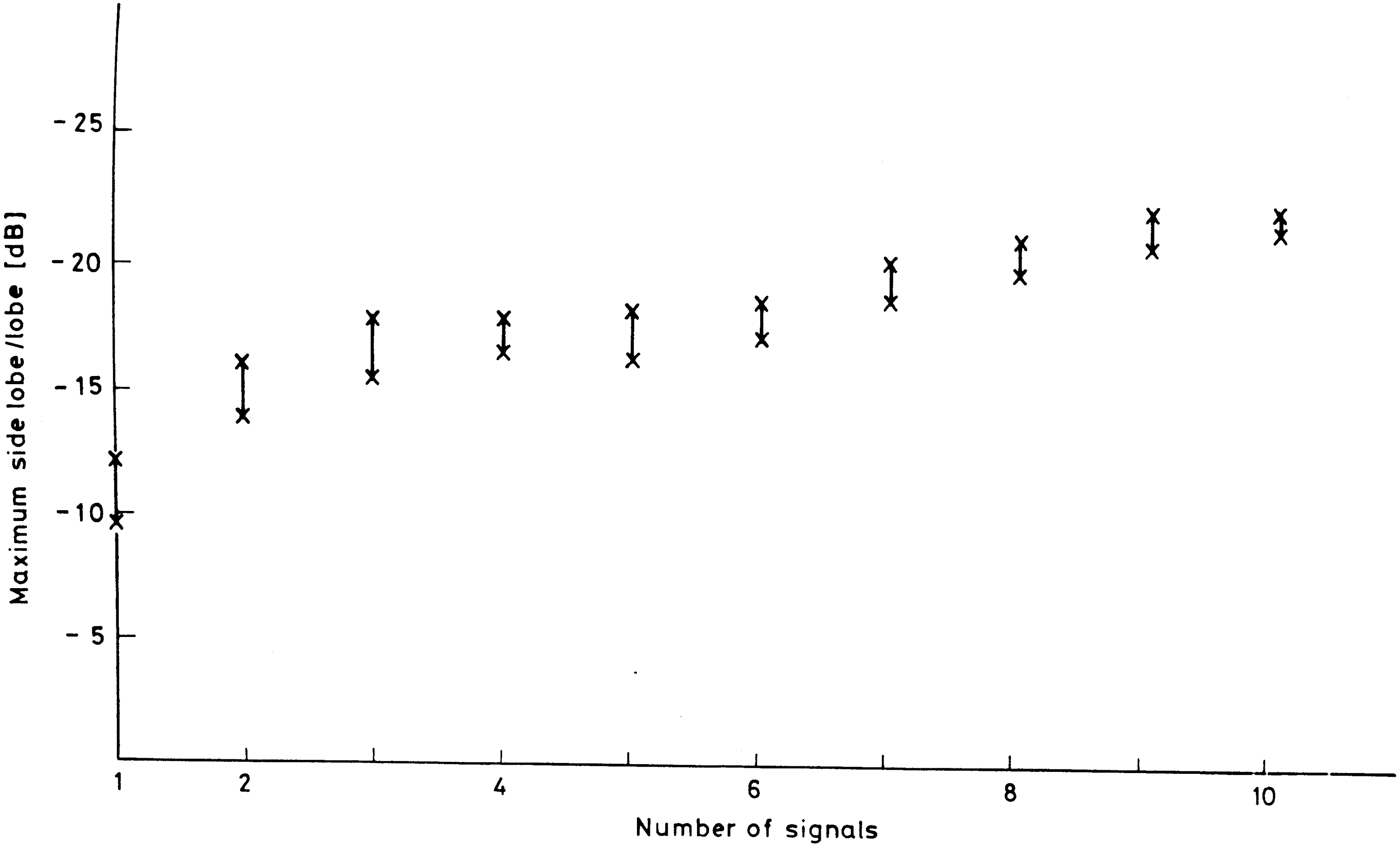

Figure 6.13 The maximum sidelobe-mainlobe amplitude ratio for the averaged random noise autocorrelation function.

detector for two simulated defects separated in time by 5 μs. The amplitude ratio of the two reflected signals is 1:5. Fig. 6 .14 shows the output for the sinusoidal excitation described by Fig. 6 .8. The smallest echo at -5 μs is below the sidelobe structure due to the largest signal and hence below the detectable level. The same defect configuration is simulated in Fig. 6 .15 using a random noise signal. The smallest echo signal is for this excitation well above the larger signal's sidelobe structure.

The random noise signal excitation gives the smallest sidelobe level of these two signals, however the signal energy is lower for the random signal excitation than the sinusoidal signal.

6.4 THE ENERGY OF THE SIGNAL SENT

The energy of a signal is the time integral of the power of the signal. If one assumes a unit loading of the signal generator the signal energy of a pulsed sinusoidal signal with an amplitude A is:

$$E_{signal} = \frac{\omega}{2\pi} A^2 \int_0^{2\pi} \sin^2 \omega t \, dt$$

$$= \frac{1}{2} A^2 \qquad (6.13)$$

The total energy sent by m excitations of n cycles each is hence:

$$E_{total} = \frac{1}{2} A^2 . n . m$$

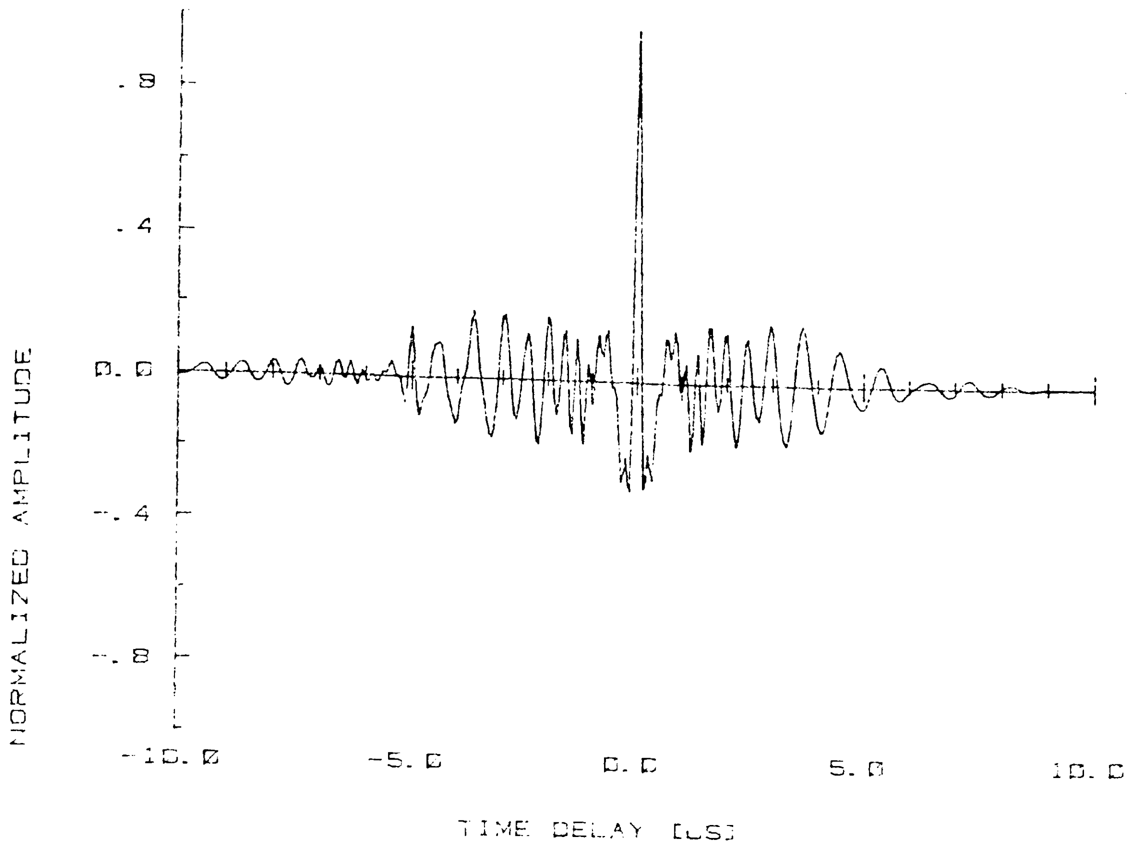

Figure 6.14. Two auto-correlation functions obtained from pulsed sinusoidal signals superimposed

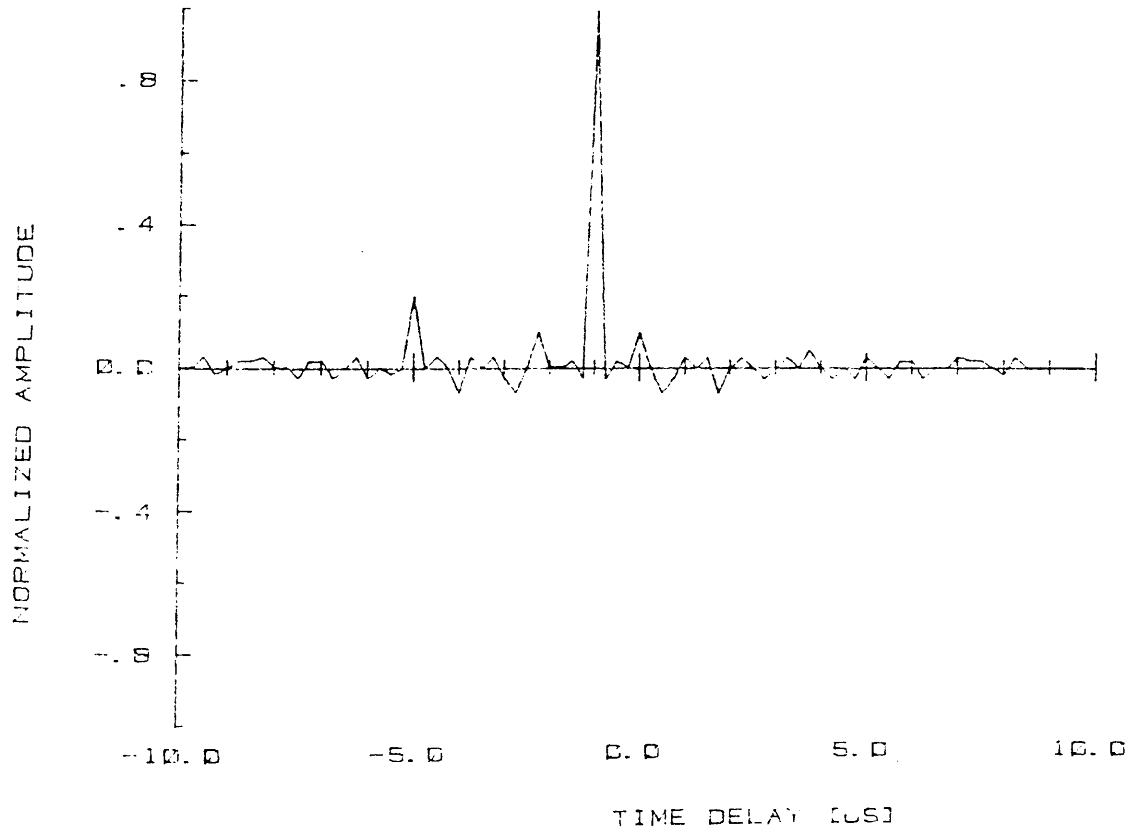

Figure 6.15. Two auto-correlation functions, obtained from random noise signals superimposed

The energy of a random noise signal varies from excitation to excitation. However, a mean signal energy can be estimated.

At a time delay of zero the auto-correlation function is:

$$R_{xx}(0) = \frac{1}{T}\int_0^T x^2(t)\,dt$$

This is the same as the power of the signal into a unit load. Hence the height of the central peak in the auto-correlation function is equal to the power of the signal.

The signal power can also be found from the amplitude distribution of the signal. The variance of the signal is equal to the power of the signal, when a unit loading is applied to the signal generator. The random noise used for the plotting of the auto-correlation function in Fig. 6.12 has a uniform amplitude distribution. The variance of this signal with an amplitude between -A and A is:

$$\sigma^2 = P = \frac{1}{2A}\int_{-A}^{A} x^2 dx = \frac{1}{3}A^2$$

The computer program used to plot the auto-correlation functions for the random noise was used to find the power of the signal as a function of the number of the samples in the signal. The result is shown in Fig. 6.16. The

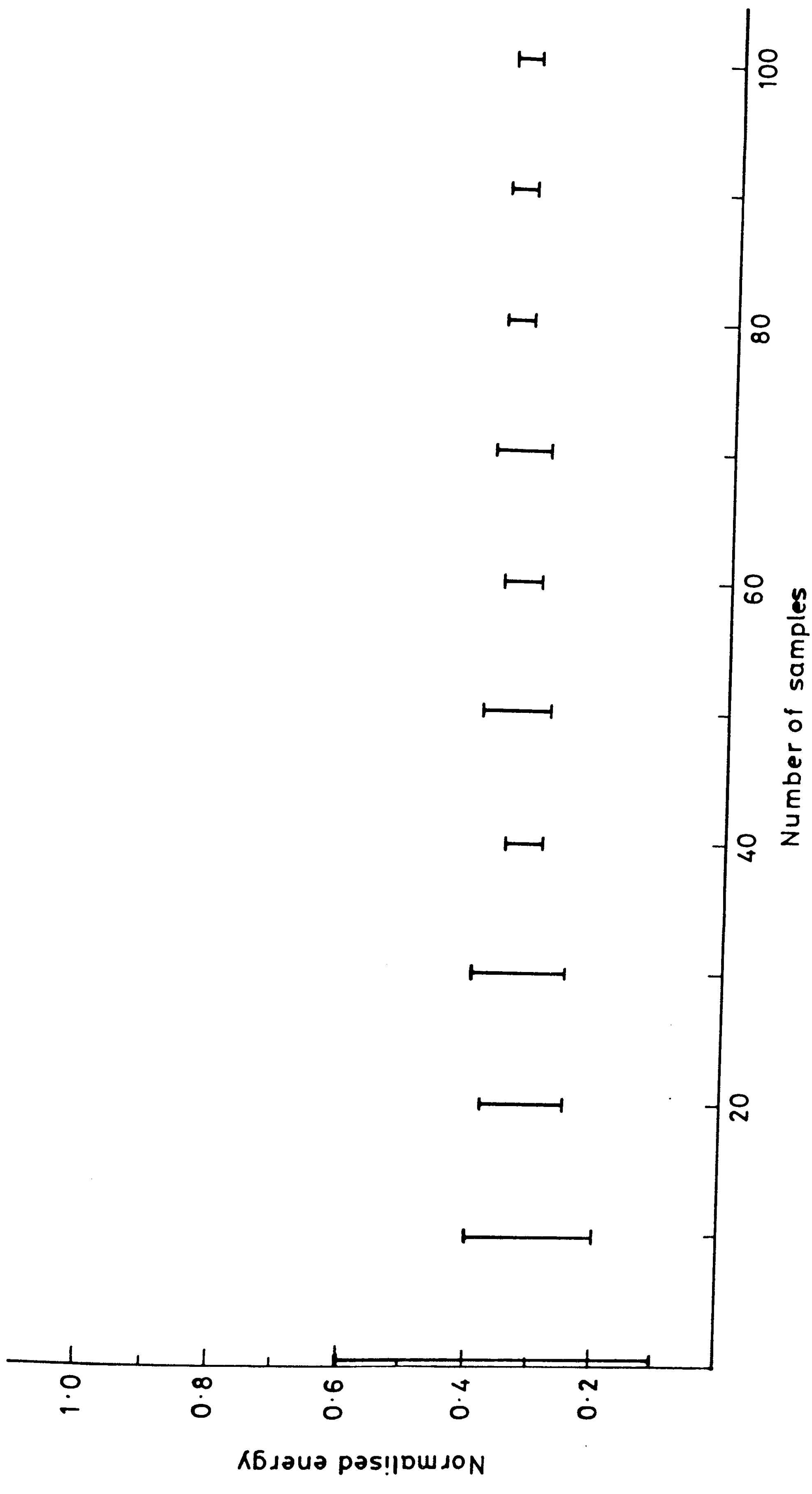

Figure 6.16 The energy of a random noise signal versus the number of samples in the signal.

computer program was run six times and the maximum and minimum power for each number of samples was plotted. As the number of samples increases the variation in the signal power is reduced. For 30 samples and more the signal power approaches the theoretical value of $\frac{1}{3}A^2$. The energy of this random noise signal of duration T and with m repeated excitation is hence:

$$E_{noise} = \frac{1}{3} A^2.T.m \tag{6.14}$$

The ratio of the excitation energy for these two signals can then be found. For random noise signals and pulsed sinusoidal signals with equal durations and amplitude, the ratio of the signal energy is the same as the ratio of the mean signal power for the two signals:

$$\frac{E_{noise}}{E_{sinusoid}} = \frac{\frac{1}{3} A^2}{\frac{1}{2} A^2} = \frac{2}{3} \tag{6.15}$$

The corresponding range reductions can then be found by assuming a homogeneous attenuation coefficient. The energy received, E_r is given by

$$E_r = E_s e^{-\alpha x}$$

where

E_r is the received energy

E_s is the energy of the source wave

α is the attenuation coefficient

x is the distance travelled by the wave.

When detectors of equal sensitivity are applied to both types of signals, the required received energy is the same:

$$E_r = E_{sn} e^{-\alpha x_n} = E_{ss} e^{-\alpha x_s}$$

$$\frac{E_{ss}}{E_{sn}} = e^{\alpha(x_s - x_n)}$$

$$x_s - x_n = \frac{1}{\alpha} \text{ Ln } \frac{E_{ss}}{E_{sn}}$$

$$= \frac{1}{\alpha} \text{ Ln } \frac{3}{2} = \frac{1}{\alpha} 0.41 \qquad (6.16)$$

where

x_s and x_n is the distance travelled by the sinusoidal and noise wave respectively.

E_{ss} and E_{sn} is the energy of the source wave for sinusoidal and noise signals respectively.

The signal source energy is the product of the signal power and the pulse length. To obtain an equal source energy for the two signals, the pulse length of the noise signal can merely be extended. The pulse length cannot however be extended using conventional amplitude height detectors as resolution restricts the pulse length, but if cross-correlation processing is used there is no need to restrict the pulse length. In a random noise flaw detector the source pulse can be so long that pulses from neighbouring flaws overlay considerably, it is the cross-correlation processing procedure which yields the desired resolution of the flaws. Immediately the duration of the noise pulse is allowed to exceed 1.5 times the maximum allowable conventional pulse length, the noise based flaw detector becomes a more powerful device.

6.5 A SUMMARY OF SIGNAL DETECTION FOR ULTRASONIC FLAW DETECTION USING CROSS-CORRELATION

In contrast to conventional flaw detectors, cross-correlation detectors offer an optimal use of the waveform of the received echo signal. This is demonstrated in optimal time delay resolution and sensitivity of pulse detection. These are usually conflicting parameters with normal edge excitations, where the pulse length is made as short as possible to obtain good resolution while the sensitivity of pulse detection decreases with decreasing pulse length. In cross-correlation detectors increasing the pulse length can however be used to obtain an improvement in both sensitivity and resolution. The resolution of the cross-correlation detector is proportional to the bandwidth of the signal sent. When the signal sent is a long pulse, (the exact nature of the signals is discussed previously in this chapter) its bandwidth can be increased by increasing the length of the pulse. This is because more variation in the signal is produced (Ref. the autocorrelation function of a linear frequency modulated sinusoidal signal). The sensitivity of pulse detection is also increased by increasing the pulse length, since the energy of the signal is proportional to the duration of the signal.

Cross-correlation detection offers also other advantages. Firstly, additive white noise corrupting the signal is effectively removed (see Chapter 5). The amplitude detector used in normal ultrasonic flaw detectors requires, however, that the signal amplitude exceeds the additive noise amplitudes for detection. Secondly, with normal amplitude detection the instant of sending has to be accurately defined to give the time of flight for the echo. The time of flight is given by the difference between the reception and sending instant. As only the absolute time of reception is known the absolute time of sending has also to be given **to obtain accurate time of flight measurements.** This is of great importance when averaging techniques are applied in conjunction with amplitude detectors to reduce any additive noise present (see Chapter 5). Cross-correlation detectors do however always use both the sending instant and the reception instant to find the time of flight for the echo. Variations in the absolute time of sending and reception are therefore of no importance, but only the relative difference. Cross-correlation detection is hence a more direct method of measuring the time of flight in ultrasonic flaw detectors. (The time of flight is of utmost importance in ultrasonic flaw detectors. Engineering structures often have maximum stress perpendicular to the thickness of the material, the longitudinal position of the flaw is therefore of great importance (Ref. pressure vessels and discussion in Chapter 2)).

Signals corrupted by noise, similar in nature to the signal, are also enhanced by the cross-correlation detector. The degree of improvement depends on the degree of similarity between the noise and the signal. For ultrasonic flaw detectors one of the noise sources is the small echoes of the signal from grain boundaries in the metal to be investigated (see Chapter 3). The size of the grains determines the degree of similarity between the signal and interfering grain noise. When the grains are small compared to the flaw, a change in the shape as well as amplitude of the reflected waveform is observed, yielding a reduction in the correlation with the signal sent. A cross-correlation detector should therefore offer an improvement to interfering noise caused by reflections from small grains.

An ultrasonic flaw detector based upon a cross-correlation using random noise signals should hence give an improvement with respect to use of a conventional amplitude detection in the following ways:

1. Smaller flaws should be detected.

2. A better estimate of the longitudinal position of the flaw should be obtained.

3. Averaging techniques can be applied without dependence on precise reproducibility of the sending instant.

4. White noise introduced by the amplifiers should be reduced.

5. Partially coherent noise caused by small grain echoes should be reduced.

Implementation of an ultrasonic flaw detector based on the principle of cross-correlation with random noise as the signal source will then be considered in the next two chapters. By using a digital computer as the basis of the experiments an easilty adaptable flaw detector can be built. The use of digital techniques require some considerations however and these are discussed in the next chapter.

CHAPTER SEVEN

CONSIDERATION FOR IMPLEMENTATION OF AN EXPERIMENTAL ULTRASONIC FLAW DETECTOR BY DIGITAL TECHNIQUES

The interpretation of ultrasonic signals requires that the signals are processed and presented in a form understood by the operator. Signal processing techniques can be divided into two main classes; analogue and digital signal processing.

Instruments used for analogue signal processing have an instability to temperature and ageing even when ingenious compensation techniques are applied. This instability together with the inherent self noise of the instrument limits the processing techniques available. These limitations together with the need for fast numerical calculations led to the development of the electronic digital computer. Being arithmetical, digital processing is not subject to saturation effects as are methods based on analogue devices. This means that, once a signal is in digital form the dynamic range is virtually unlimited and there is no fall off in accuracy at the lower end of the range. These machines compute sums and differences of numbers usually represented in the binary number system. From these basic operations of addition and subtraction other mathematical operations can be performed. By using the binary number system the full static range of the electronic devices are used for the representation of the two states needed. This gives an excellent noise immunity as well as a high stability to temperature and ageing. This superior performance of the digital electronic computer has given impetus to workers in a number of divergent fields. With the opportunity of programming these computers, a number of application based algorithms have been written which can be transported with ease among the different computers in use.

Ultrasonic signals are represented as a continuous voltage after reception by a displacement transducer and amplification. These continuous signals have to be converted to a series of numbers suitable for the electronic computer. The sequence of the operations associated with this conversion is illustrated in Fig. 7.1.

7.1 SAMPLING

The sampler and the quantizer are commonly referred to as one unit and given the name analogue to digital converter. Depending on the construction of the analogue to digital converter the sampler and quantizer can be one physical unit or they may be separate as in Fig. 7.1. In the latter case the sampler is often referred to as a sample and hold unit. Another name for a sample and hold unit is zero order hold unit which originates from the ideal behaviour of such a unit. This takes a sample of the incoming signal in zero time and then holds the value of the sample for a predetermined time with perfect accuracy. The effect of this on a continuous analogue signal can be determined by finding the transfer function of a sample and hold unit. By use of the

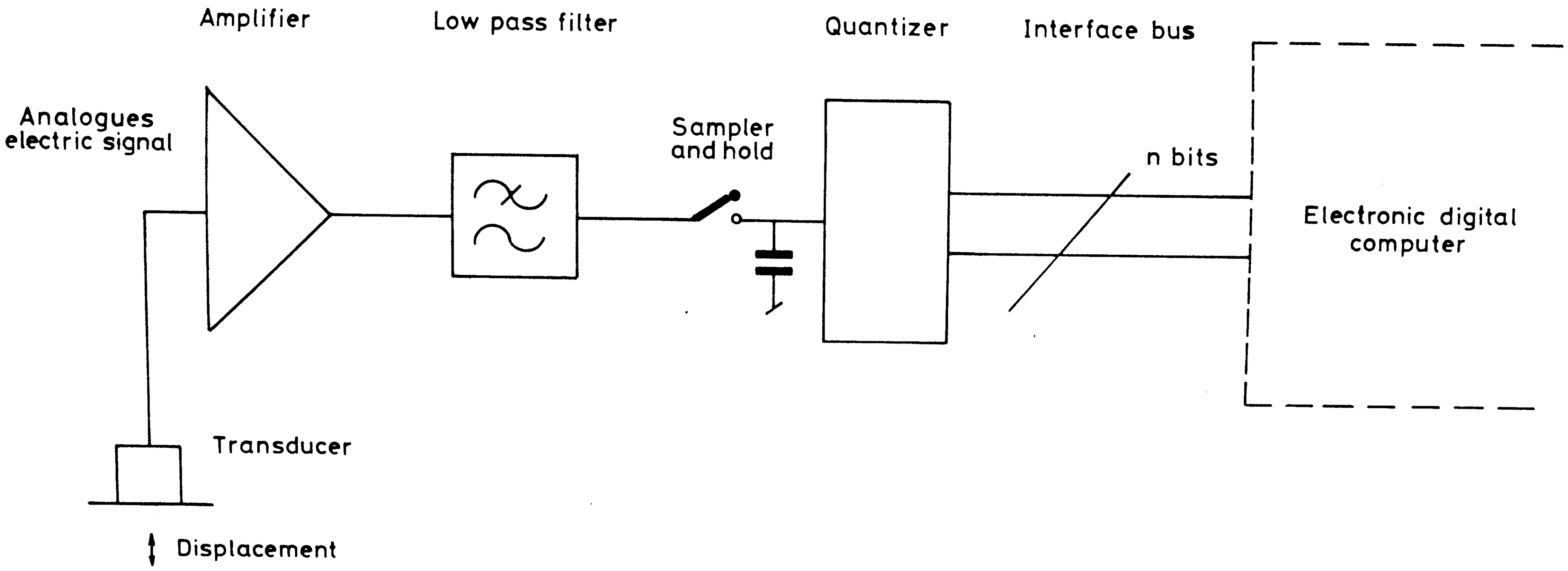

Figure 7.1 The sequence of operations for the conversion of acoustic **wave displacement** to a digital signal suitable for analysis by electronic digital computer.

impulse response and the Laplace transform the transfer function is found to be:

$$G(j\omega) = \frac{1-e^{-j\omega T_s}}{j\omega} = T_s \frac{\sin\omega T_s/2}{\omega T_s/2} e^{-j(\omega T_s/2)} \qquad (7.1)$$

where T_s is the sampling period.

The magnitude and phase of this function is plotted in Fig. 7.2 which shows that a sample and hold unit behaves similarly to a low-pass filter with a cut-off frequency of approximately 0.443 × sampling frequency and a constant time delay of $T_s/2$ or half the sampling period.

However a practical sample and hold unit does not operate perfectly, a more realistic behaviour is illustrated in Fig. 7.3, which also gives some of the parameters describing the operation of this unit.

Aperture Time, Δt:

The time the input signal is allowed to appear at the input of the sample and hold unit.

Aperture Uncertainty Time, $\Delta' t$:

The uncertainty in the aperture time. This is usually variation both in positive and negative direction, here it is treated as a positive number without loosing generality.

The Maximum Amplitude, A:

The maximum amplitude of the input signal. When this

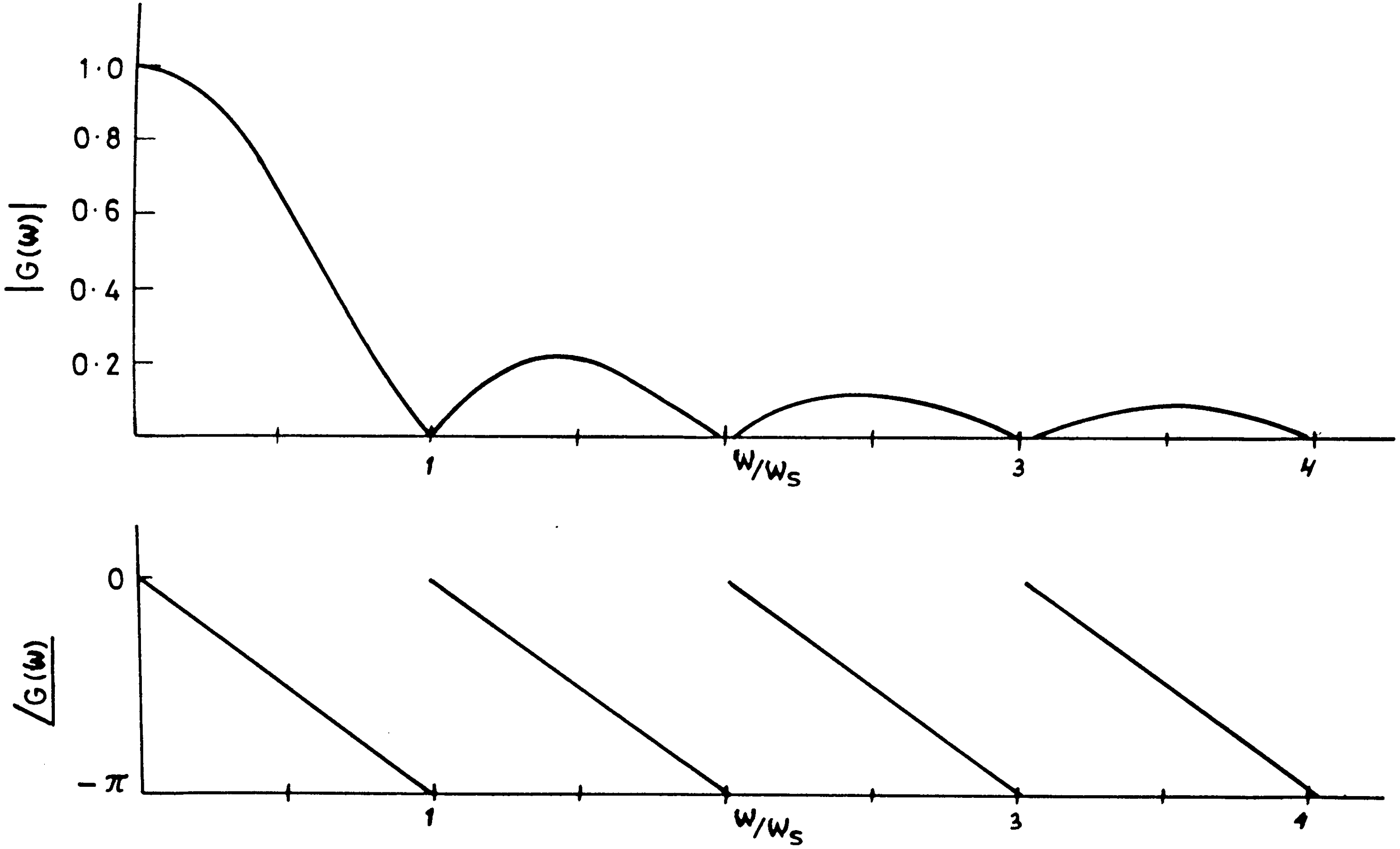

Figure 7.2 The magnitude and phase of the transfer function of a zero order hold unit.

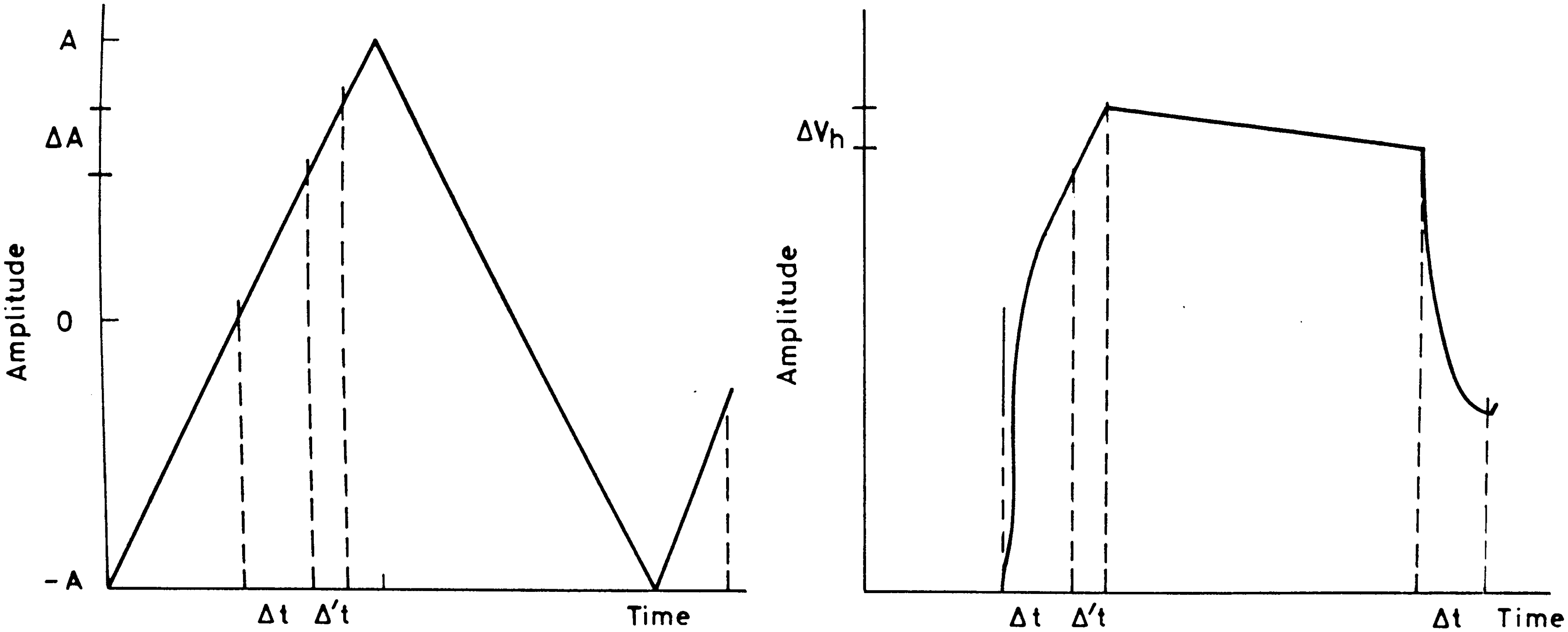

The input signal

The signal appearing on the hold capacitance

Figure 7.3 The effect of a finite sampling time for a sample and hold unit.

amplitude is exceeded, clipping of the input signal will occur.

The Amplitude Step Size, ΔA:

The amplitude step size is the maximum amplitude divided by the number of steps.

The Drooping Voltage, ΔV_n:

The drooping voltage is the decrease in the voltage across the hold capacitor between each sample command. This decides the speed of operation at which the analogue-to-digital converter has to work.

Other parameters describing the sample and hold unit are:

Acquisition Time:

The time elapsed from when the sample command is given, to the point when the output enters and remains within a specific error band around the input value. At the end of the acquisition time the output is tracking the input. The acquisition time must be less than the aperture time.

Feed Through:

The amount of input signal appearing at the output when the unit is in the hold mode.

7.2 QUANTIZATION

After the input analogue signal has been sampled at pre-determined times, each sample is converted to its equivalent number by the quantizer. The operation of a linear quantizer is illustrated in Fig. 7.4 which also indicates the type of error in an ideal linear quantizer. To obtain a higher dynamic range, the quantization levels might be distributed on a hyperbola or other suitable function but the main operation and errors introduced will still be of a similar nature. The most common law of quantization is linear. The number of levels in the quantizer decides the accuracy with which the quantizer represents the input sample, this is determined by technological and financial constraints. The quantizing error might be represented as a wide bandwidth noise superimposed upon the signal(1) of mean squared amplitude:

$$\sigma^2 = \frac{(\Delta A)^2}{12} = \frac{1}{(n-1)^2} \cdot \frac{(2A)^2}{12} \qquad (7.2)$$

where

A is the amplitude of the input signal

ΔA is the amplitude step size

n is the number of steps.

The quantization noise power is reduced with the square of the number of levels in the quantizer. When expressed on a Logarithmic scale as in equation (7.3) it is clear that the signal-to-noise ratio increases approximately

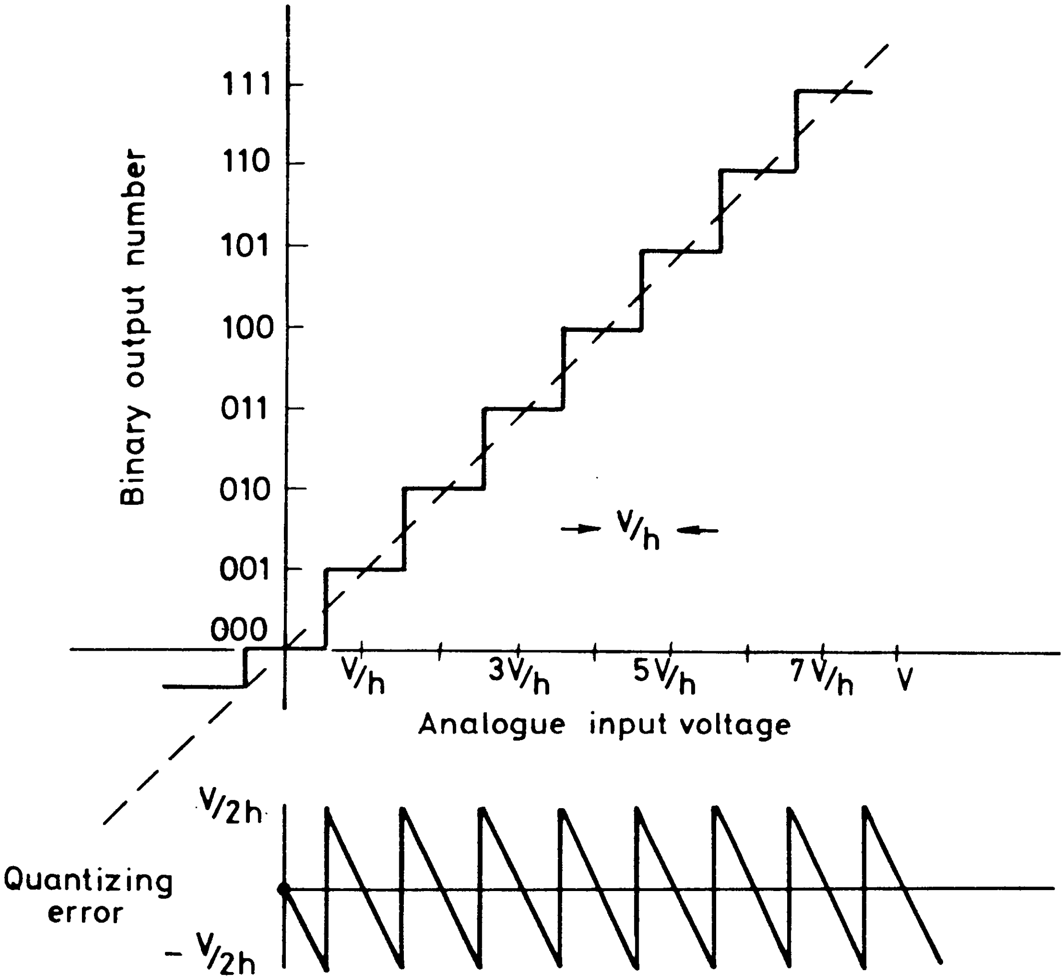

Figure 7.4 The transfer function for an ideal linear quantizer with truncation.

6 dB for each binary bit added.

$$SNR \approx 6.02b + 10.79 \quad |dB| \qquad (7.3)$$

where b is the number of binary bits.

This means that for an 8 bit quantizer as used in the Biomation 8100 transient recorder and also in the Lecroy 2256 waveform analyser, the expected best signal-to-noise ratio after quantizing is 50 dB. This then determines the dynamic range of the converter. As shall be shown later in this chapter the actual signal to noise ratio for these two analogue-to-digital recorders is less than this and the deviation depends on the rate of change of the input signal or slewrate as it will be referred to later.

Different types of errors might occur in a practical quantizer. Some of these are summarised in Fig. 7.5.

Offset Error: the error by which the transfer function fails to pass through the origin referred to the analogue axis.

Gain Error: the difference in slope between the actual transfer function and the ideal function.

Linearity Error: the maximum deviation from a straight line drawn between the end points of the actual transfer function.

When the analogue-to-digital converter is applied to an actual continuous signal, care must be exercised so

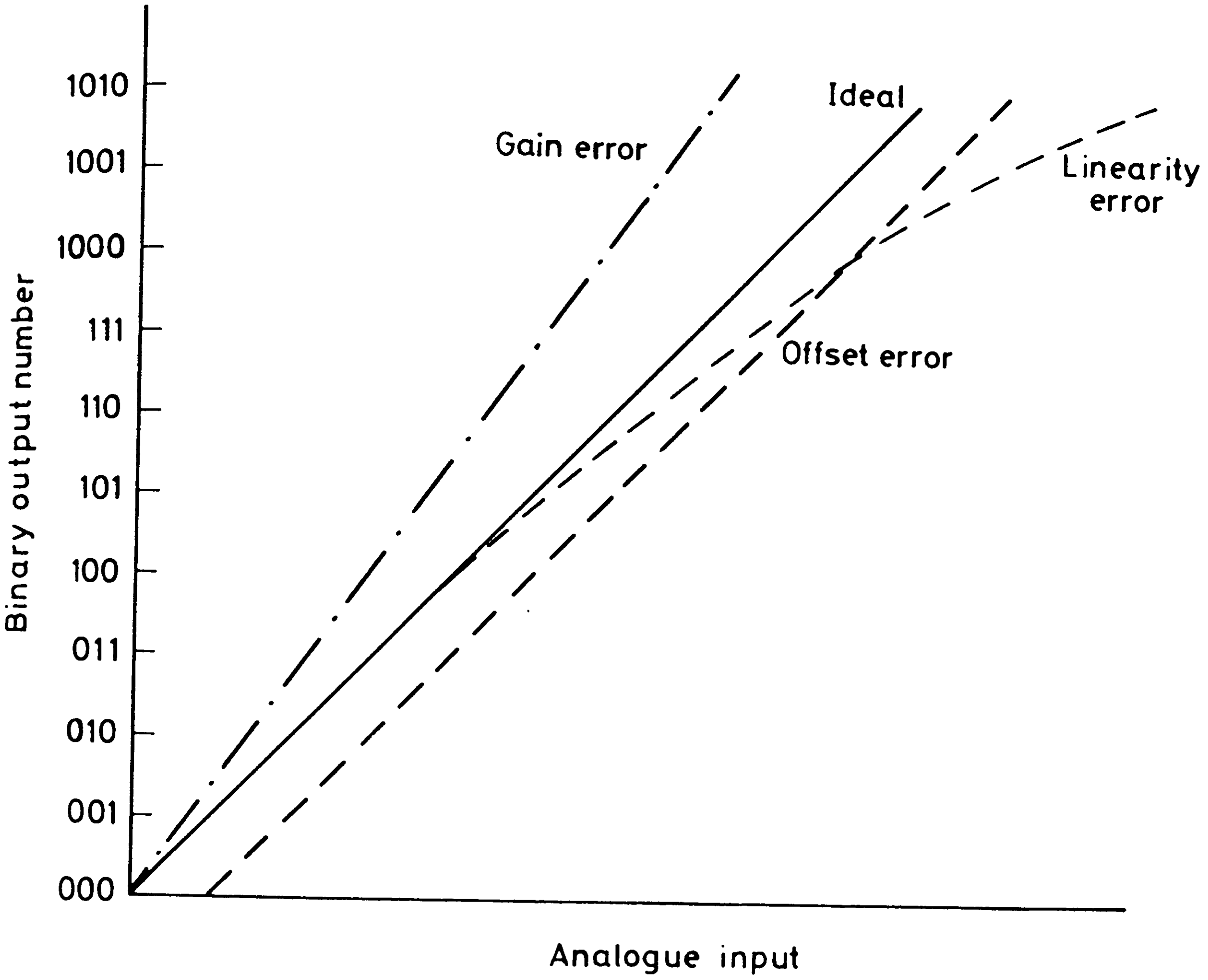

Figure 7.5 Some of the common errors which can occur in a practical quantizer.

that the errors introduced by the sampling and quantizing do not make the recorded signal useless.

One of the basic criteria for sampling a continuous waveform is that the sampling period does not violate the Shannon sampling theorem(2) which states:

> 'If a function f(t) contains no frequencies higher than W Hz it is completely determined by giving it ordinates at a series of points (1/2W) seconds apart'.

When the input waveform contains components of a higher frequency than 1/2 Ts, aliasing will occur and the original signal can not be recovered from the sampled waveform. The input signal is therefore filtered with a low pass filter to restrict the bandwidth of the input signal and noise, so that aliasing does not occur. It is however, impossible to make a low pass filter with an ideal rectangular transfer function so some aliasing will always take place. However, as the sampled waveform is quantised after the sampling and the quantization inherently introduces noise, aliasing errors not exceeding the quantization noise might be accepted. This is illustrated in Fig. 7.6. Most filters introduce dispersion or nonlinear phase delay, the only type of non-dispersion filter is the finite impulse response filter and as this is itself a sampled data filter it is not usual to use this as an anti-aliasing filter.

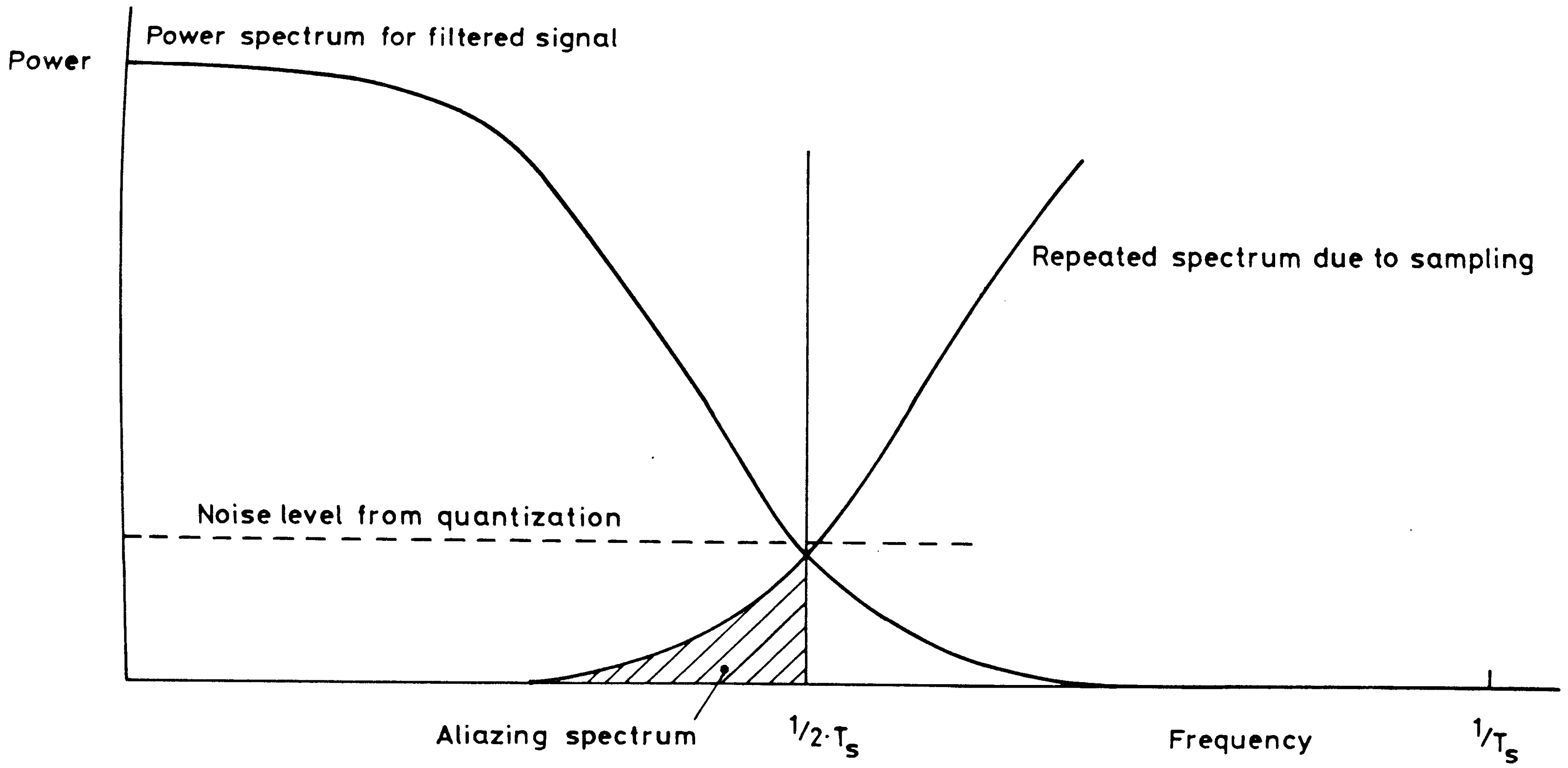

Figure 7.6 The requirement of the anti-aliasing filter.

To reproduce a broad bandwidth signal without introducing dispersion, the cut-off frequency of the filter must be higher than the roll-off frequency of the signal. Therefore the sampling period is made shorter than it would appear from the frequency content of the original signals. The anti-aliasing filter should be placed as physically close to the sampler as possible to reduce the probability of electro-magnetic noise introducing frequency components above the aliasing frequency.

As mentioned earlier the sample and hold unit never samples the input signal in zero time but has a finite aperture time, this introduces a low pass filter effect on the signal leading to constraints on the maximum slew-rate of the input signal.

7.3 APERTURE TIME

During the aperture time the sample-and-hold unit acquires the input voltage; this time is called the acquisition time. The acquisition time depends on the change required of the sample-and-hold unit to acquire the input voltage. After the elapse of the acquisition time the output tracks the input voltage. There is always some uncertainty in the aperture time and this will introduce errors as irregular sampling can occur. This is illustrated in Fig. 7.3. The errors introduced by the irregular sampling must be less than the errors introduced by the quantization, if they are to be neglected.

The change in the amplitude of the triangular wave during the aperture uncertianty time, $\Delta t'$, is

$$\Delta A = 4.f.A.\Delta t' \tag{7.4}$$

where

f is the frequency of the triangular wave

$\Delta t'$ is the aperture uncertainty time

The quantization error is from equation (7.2)

$$\Delta A = \frac{2A}{(n-1)} \tag{7.5}$$

The maximum aperture uncertainty time can hence be found. Since;

$$4.f.A.\Delta t' = \frac{2A}{(n-1)} \tag{7.6}$$

the maximum aperture uncertainty time is:

$$\Delta t' = \frac{1}{2f(n-1)} \tag{7.7}$$

Fig. (7.7) gives a nomogram for the maximum aperture uncertainty time for a given frequency of a triangular wave. A sinusoidal wave is more complex as the slewrate changes as a function of time. For the worst case with a single accession at the point of maximum slewrate, which occurs at the zero crossing of the wave; the maximum aperture uncertainty time might be found from Fig. 7.7

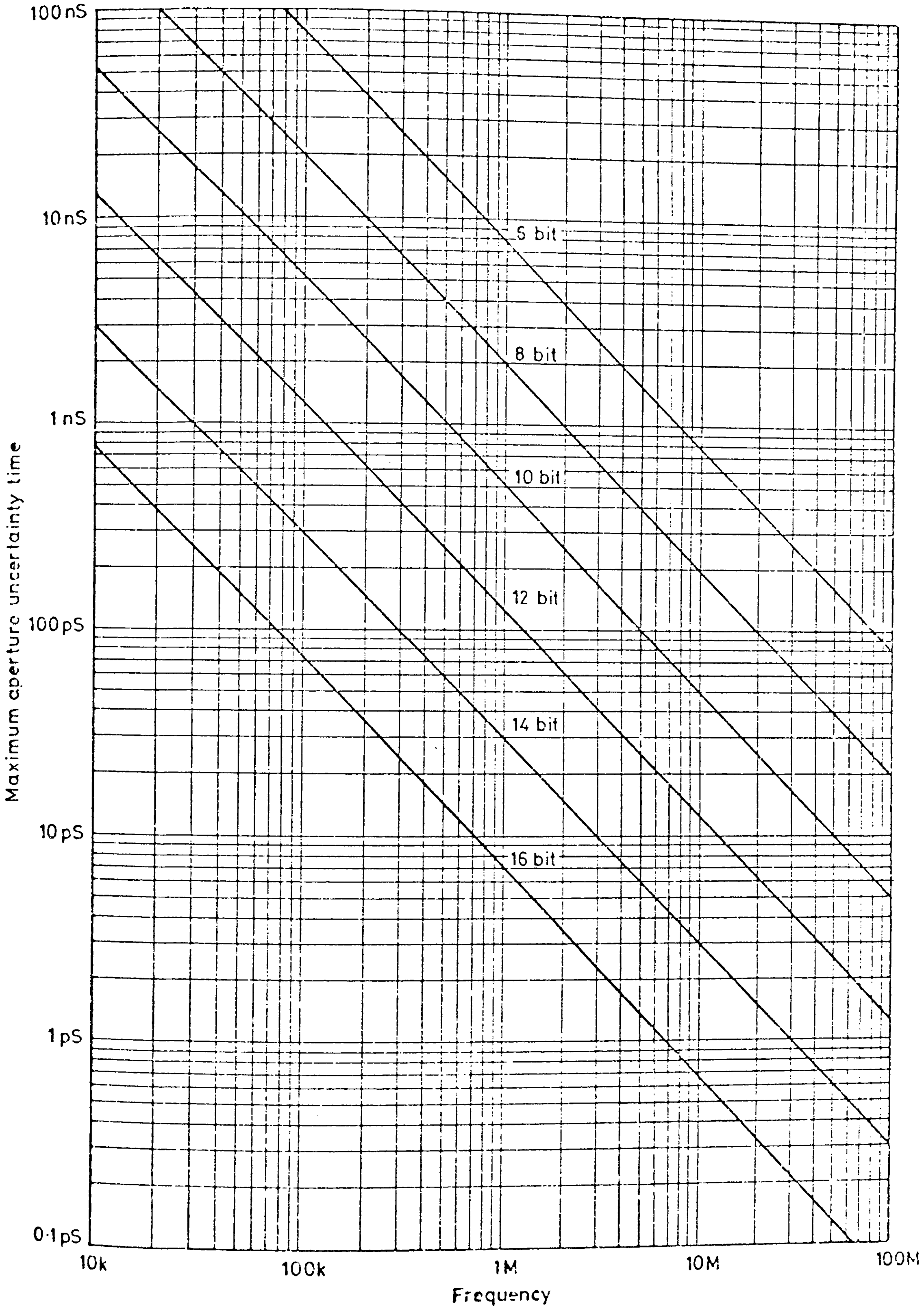

Figure 7.7 The maximum aperture uncertainty time versus frequency for a triangular signal.

by dividing the frequency for the triangular wave by $\pi/2$ to obtain the equivalent frequency for a sinusoidal wave. For more than one accession from a sinusoidal wave the distribution of sampling points along the wave needs to be known to assess the average error introduced by the aperture uncertainty time. Present day technology limits the accuracy with which a high frequency signal might be digitized, at present this limit is approximately 8 bit accuracy with a sampling rate of 100 MHz. This is mainly due to the short aperture uncertainty time required.

7.4 FINITE RECORDING LENGTH

Financial constraints set a limit to the length of the records one may obtain. As memory for electronic digital computers is relatively slow (access time in the order of 150 ns), normal practice is to make a separate buffer store for the recorded waveform. During non-recording periods the content of this buffer store is transferred to the main computer store. For continuous waveforms this finite recording length introduces rapid changes at the beginning and at the end of the digitized waveform, not present in the original waveform. Care must be exercised in the interpretation of these finite records. This is of special importance when exponential transforms are applied to the record, such as the Fourier transforms and related estimates of the power spectrum, correlation functions and convolutions.

The finite record length may be interpreted as a multiplication of the original continuous waveform with a rectangular window of amplitude 1 for $0<t<T_R$ (where T_R is the duration of the record) and zero elsewhere. By applying the Fourier transform to the window, which gives a sin x/x function, and the convolution theorem one may see that the Fourier transform of the finite length records broadens the peaks of the transform and introduces side lobes not present in the original signal. Many workers have given much effort to methods for the improvement of power spectrum estimates (3,4,5) and one of these technqiues is to change the amplitude of the samples in a recorded waveform (windowing), an excellent review of windowing techniques has been given by Harris (6).

In ultrasonic nondestructive testing the normal signals encountered are usually short compared with the length of the record so those signals may be treated as transient in nature, hence there is no need for the application of special techniques to the estimation of the exponential transforms.

7.5 ELECTRONIC DIGITAL COMPUTER INTERFACING

With the diversity of electronic digital computers and instruments to be interfaced to them, a need arose for standardization in the techniques used to interconnect these instruments. Two standards are at present in wide use, each providing for slightly different users.

The simplest of these standards is the IEEE 488-1975 digital interface for programmable instruments(7). This is intended for the small user interested in interconnection of bench-top laboratory instrumentation for measurement, parameter control and computation in automated testing. The dataway and protocol organisation of the IEEE 488-1975 interface is illustrated in Fig. 7.8. The basic system is limited to a maximum length of the interconnecting cables of 20 m and a maximum transfer rate of 1 Mbyte /s.

The other standard is called CAMAC(8). This standard is more rigidly specified in terms of hardware and is intended for the relatively larger computer user. It consists of a 19" crate with power supplies and room for 25 modules. At least two of the modules are computer interface/crate controllers or branch highway modules. The dataway and protocol organisation for CAMAC is shown in Fig. 7.9. The CAMAC standard can trasfer data at a maximum data rate of 1 Mwords/s and with the use of multiple crates an interconnection distance of 50 m may be achieved.

Due to the physical layout of the laboratory there arose a need for having two fast analogue-to-digital converters, one handling the signals for the active ultrasonic non-destructive testing and another for more

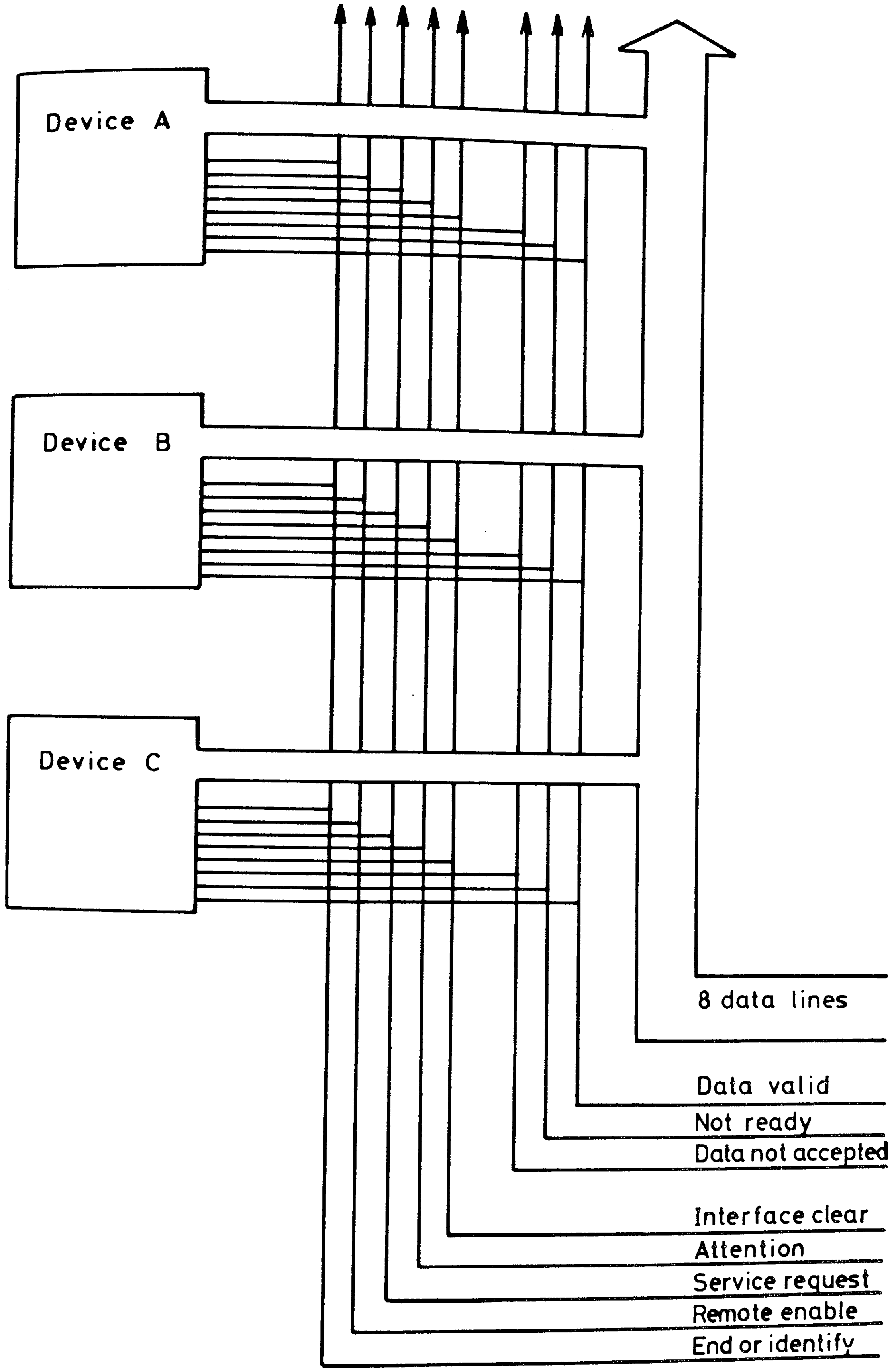

Figure 7.8 The organization of the dataway and control lines for the interface standard IEEE-488-1975.

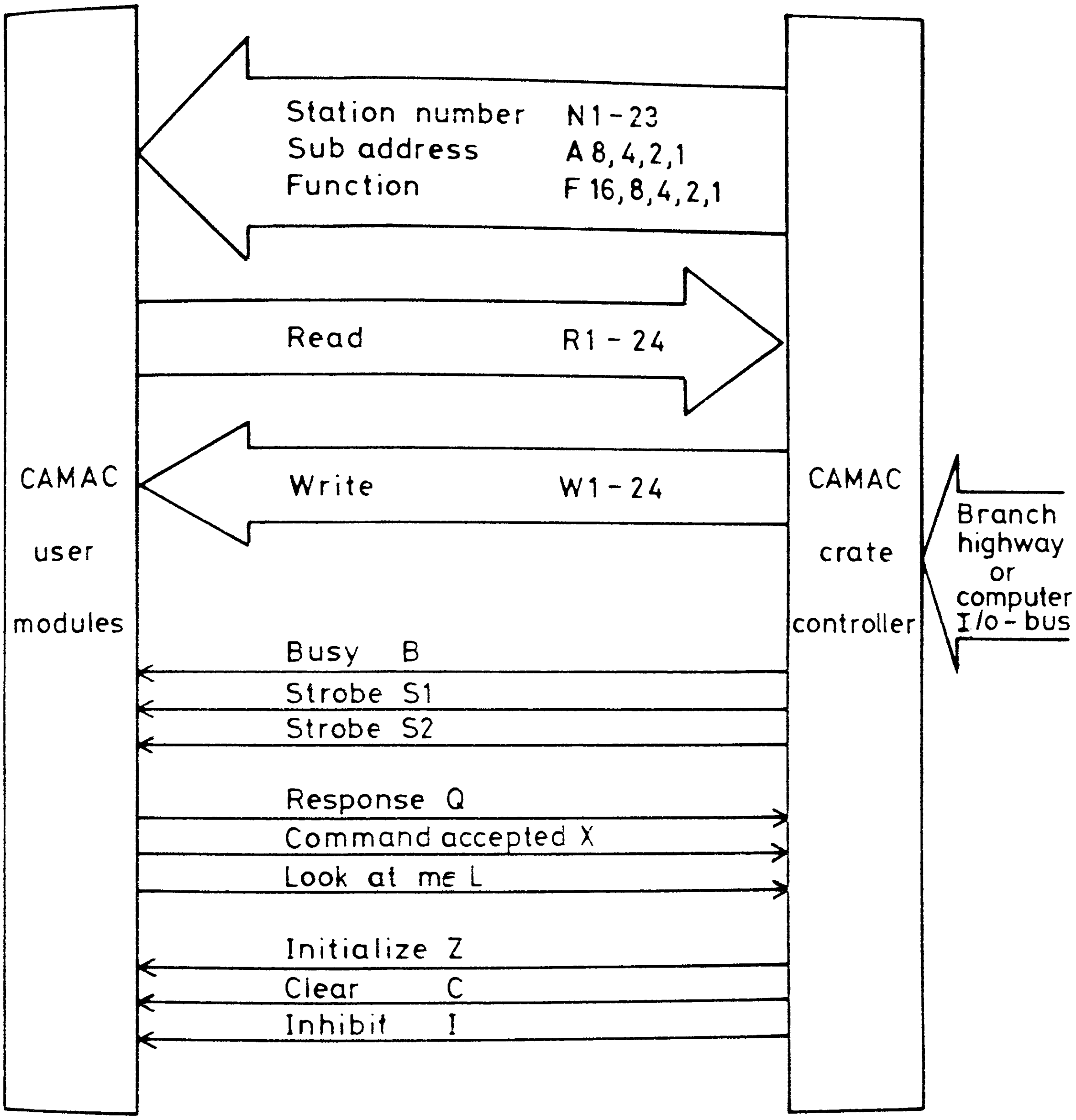

Figure 7.9 The organization of the dataway and control lines for the interface standard CAMAC.

general use such as acoustic emission. Analogue-to-digital converter modules available in the CAMAC standard were financially advantageous compared to other stand alone instruments. As the present computer system, Hewlett-Packard series 1000, had an IEEE-488-1975 interface it was decided to connect the CAMAC standard to this interface. A commercially available unit would provide for this and was adopted. Programs had however to be written to enable such an interconnection and a sample program for the accession of 1024 data bytes from the Lecroy research systems model 2256 waveform analyser is shown in Fig. 7.10. This program is written in the Hewlett-Packard adapted version of FORTRAN.

7.6 QUANTIZATION ACCURACY

To test for accuracy of this analogue-to-digital converter an experiment was conducted, as illustrated in Fig. 7.11. This experiment consisted of applying a gated triangular wave with equal number of positive and negative slopes.

The number of times each level was recorded was counted and a histogram of these counts versus amplitude levels plotted. The expected histogram would be a rectangular distribution of height N_{lev}/N where N is the number of samples taken and N_{lev} is the number of available levels. Expressing this in terms of relative frequency

```
      SUBROUTINE [illegible]
C
C SUBROUTINE TO READ IN LECROY 2256 WAVEFORM ANALYSER
C IN CAMAC STATION NUMBER 1.
C TRANSFER IS WITH ONE WORD AT THE TIME AND
C THE DATA IS RETURNED IN INTEGER FORMAT IN THE ARRAY IDAT
C D.MUIR ATTACHED TO THE NDT CENTRE,AERE,HARWELL,1979
C THIS IS WRITTEN ON A HEWLETT PACKARD 1000 COMPUTER WITH A
C RTE-4 OPERATING SYSTEM.
C
      DIMENSION IDAT(1),IOUT(2)
      LU=32
C ENABLE HP INTERFACE BUS.
      CALL [illegible](LU)
C ASK FOR 1 WORD RETURN FROM THE CAMAC-HPIB INTERFACE UNIT.
      CALL EXEC(2,LU,[illegible]B,1)
      CALL EXEC(1,LU,IA,1)
C SEND OUT F=9,A=0,N=1
      IOUT(1)=[illegible]B
      IOUT(2)=400B
      CALL EXEC(2,LU,IOUT,2)
      CALL EXEC(1,LU,IA,1)
C SEND OUT F=26,A=0,N=1
      IOUT(1)=[illegible]B
      CALL EXEC(2,LU,IOUT,2)
      CALL EXEC(1,LU,IA,1)
C TEST LAM BY SENDING OUT F8.
      IOUT(1)=4100B
      CALL EXEC(2,LU,IOUT,2)
10    CALL EXEC(1,LU,IA,1)
C READ Q AND TEST IT SET.
      CALL EXEC(1,LU,IB,1)
      IB=IAND(IB,3B)
      IF(IB.NE.3) GOTO 10
C SEND OUT F=2,A=0,N=1
      IOUT(1)=1000B
      CALL EXEC(2,LU,IOUT,2)
C READ THE DATA.
      DO 20 I=1,1024
      CALL EXEC(1,LU,IDAT(I),1)
      IDAT(I)=IAND(IDAT(I),177400B)
      IDAT(I)=IDAT(I)/256
C MASK OUT THE MOST SIGNIFICANT BYTE.
      IDAT(I)=IAND(IDAT(I),377B)
20    CONTINUE
      RETURN
      END
```

Figure 7.10 An accession subroutine for the LeCROY waveform analyser.

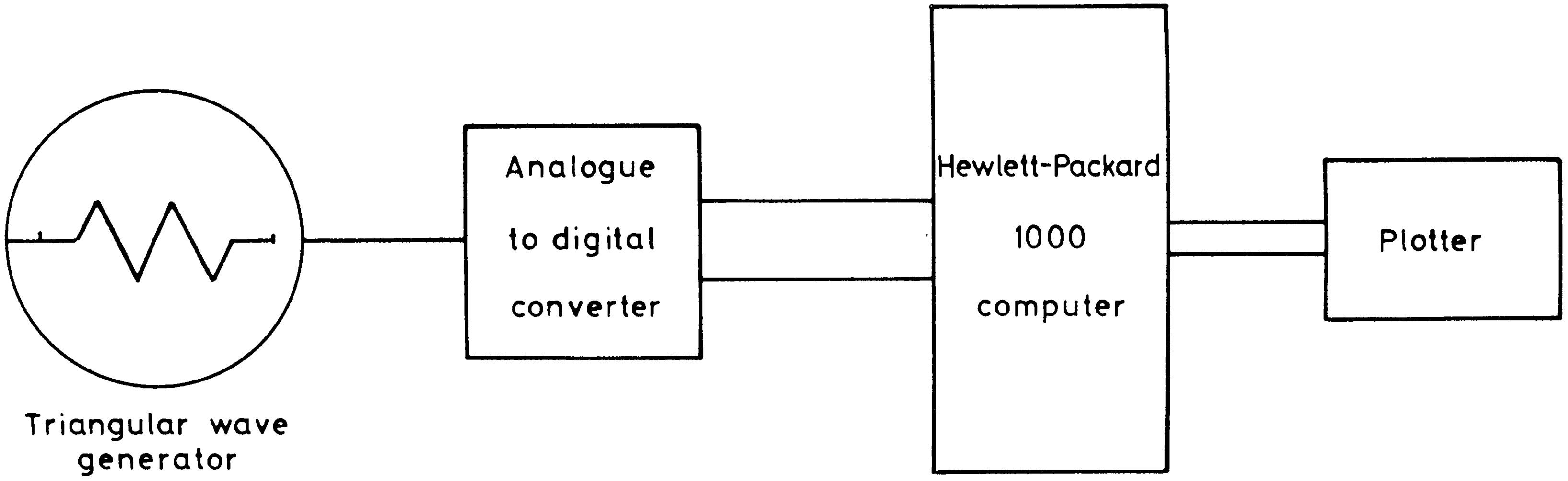

Figure 7.11 Experimental equipment to test for equal probability of occupancy in analogue to digital converters.

and using the above mentioned transient recorder the expected height of the histogram would be: $1024/(1024\times240) = 4.17\ 10^{-3}$ which approximates 0.42%. It is then assumed that no overload of the converter takes place and to secure this, the amplitude of the input triangular wave was adjusted so that only approximately 240 of the 256 available levels were in use. Figs. 7.12 to 7.14 show the obtained histogram as the slewrate of the triangular signal was increased from 24 levels/ms to 5 levels/ns. To increase the probability of equal occupancy of each level and reduce any random noise present, the average of 100 separate accessions is shown. At higher slewrates it is a marked reduction in the accuracy of the analogue-to-digital converter. At the highest slewrate it appears to be only 14 dominant levels. If the top and bottom levels are included the stated 8 bit converter appears to give only 4 bit accuracy. To simulate a more realistic signal encountered in signal processing, a random noise generator replaced the triangular signal generator. This reduces the change of continuous charging of storage elements, such as stray capacitances and inductors, contributing errors. A histogram of a 5 MHz bandlimited noise signal is shown in Fig. 7.15. The same spiky pattern is observed for this input signal as for the triangular signal. Four converters of the same model were tested with this method. All the converters showed the same distribution of the preferred quantization levels. The construction of this analogue-to-

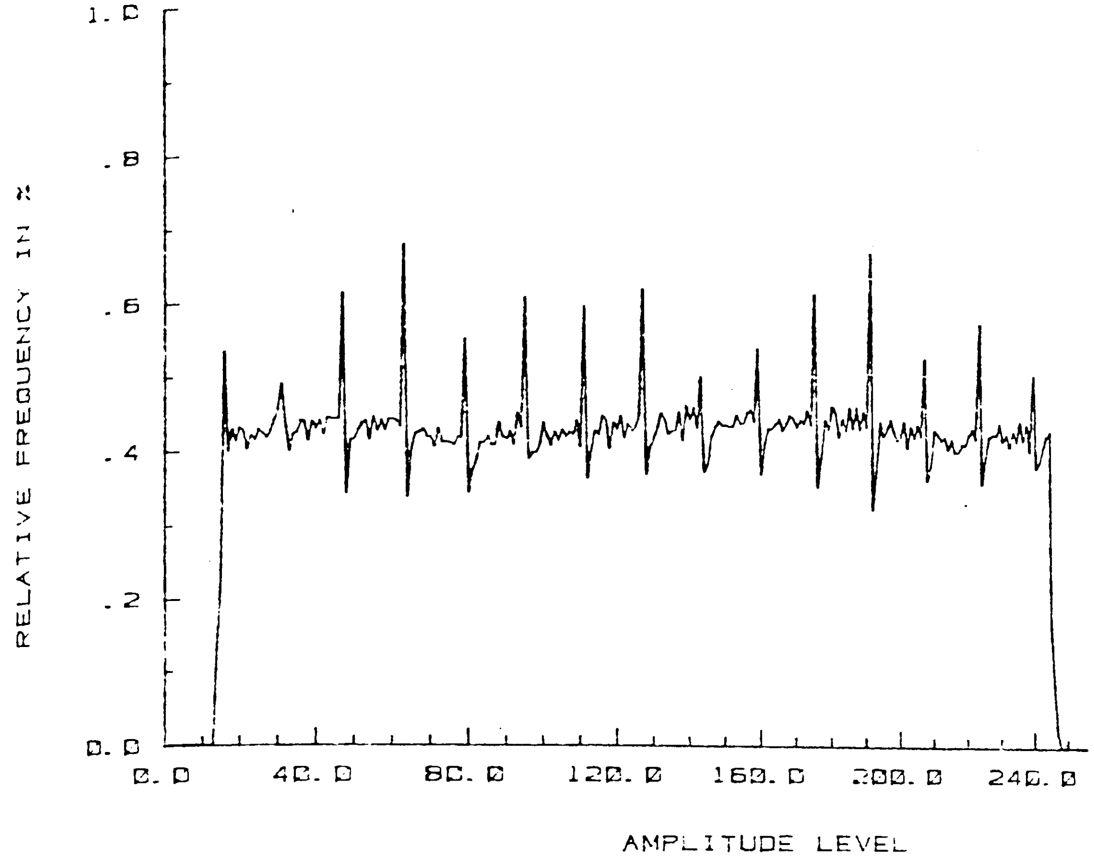

Figure 7.12. A histogram of the occupied amplitude levels for the LECROY 2256 waveform analyser, with a triangular signal of frequency 50 Hz (or a slewrate of 24 levels/ms).

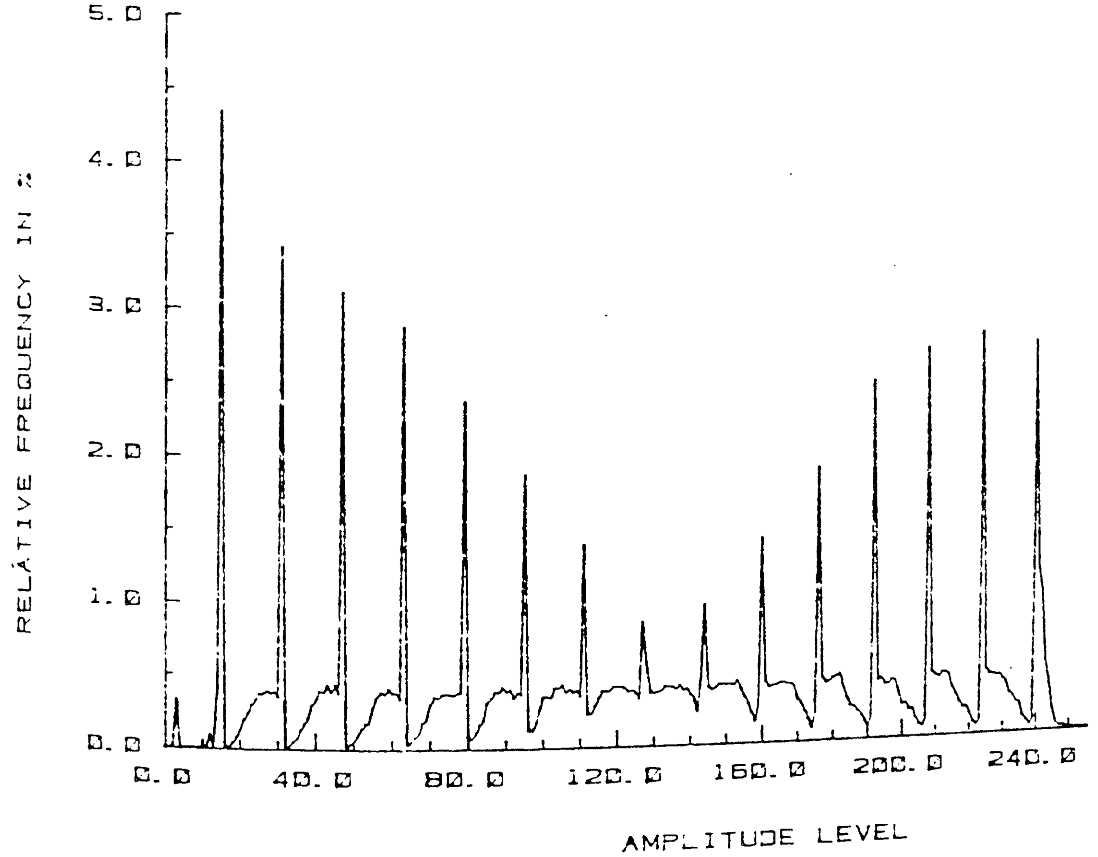

Figure 7.13. A histogram of the occupied amplitude levels for the LECROY 2256 waveform analyser, with a triangular signal of frequency 2.5 MHz (or a slewrate of 1.25 levels/ns).

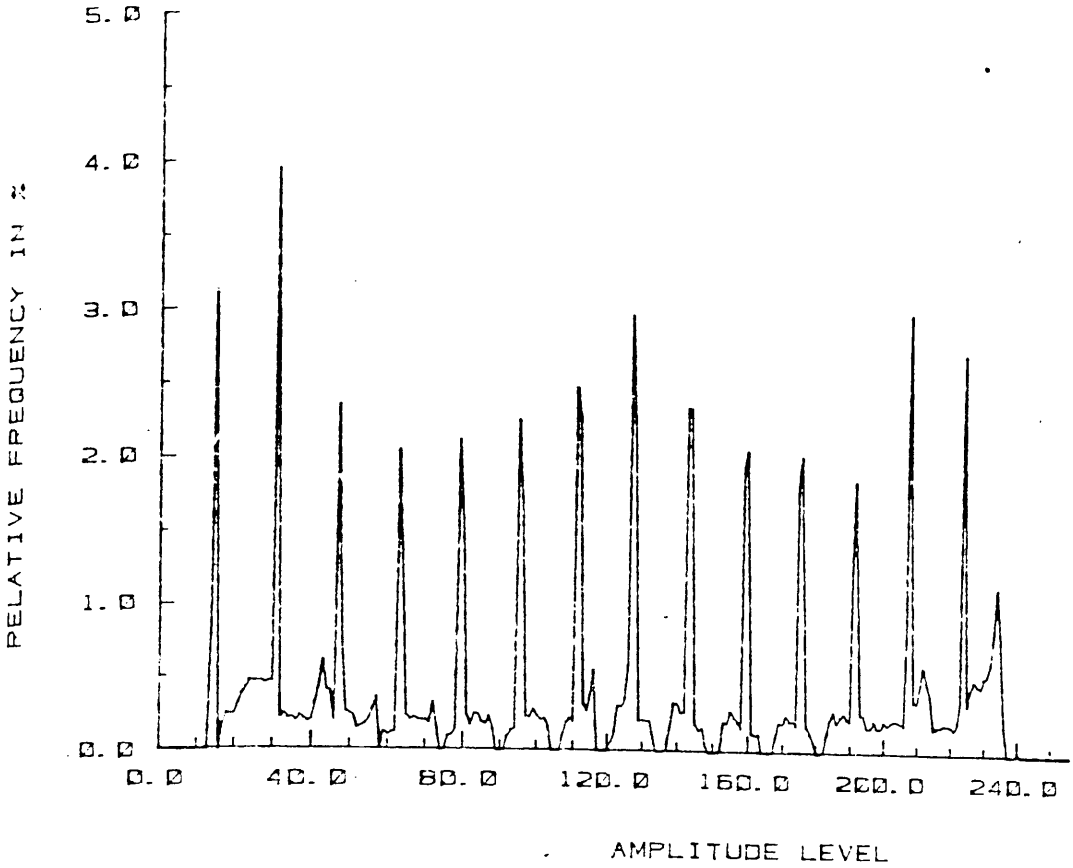

Figure 7.14. A histogram of the occupied amplitude levels for the LECROY 2256 waveform analyser, with a triangular signal of frequency 5.0 MHz (or a slewrate of 2.5 levels/ns).

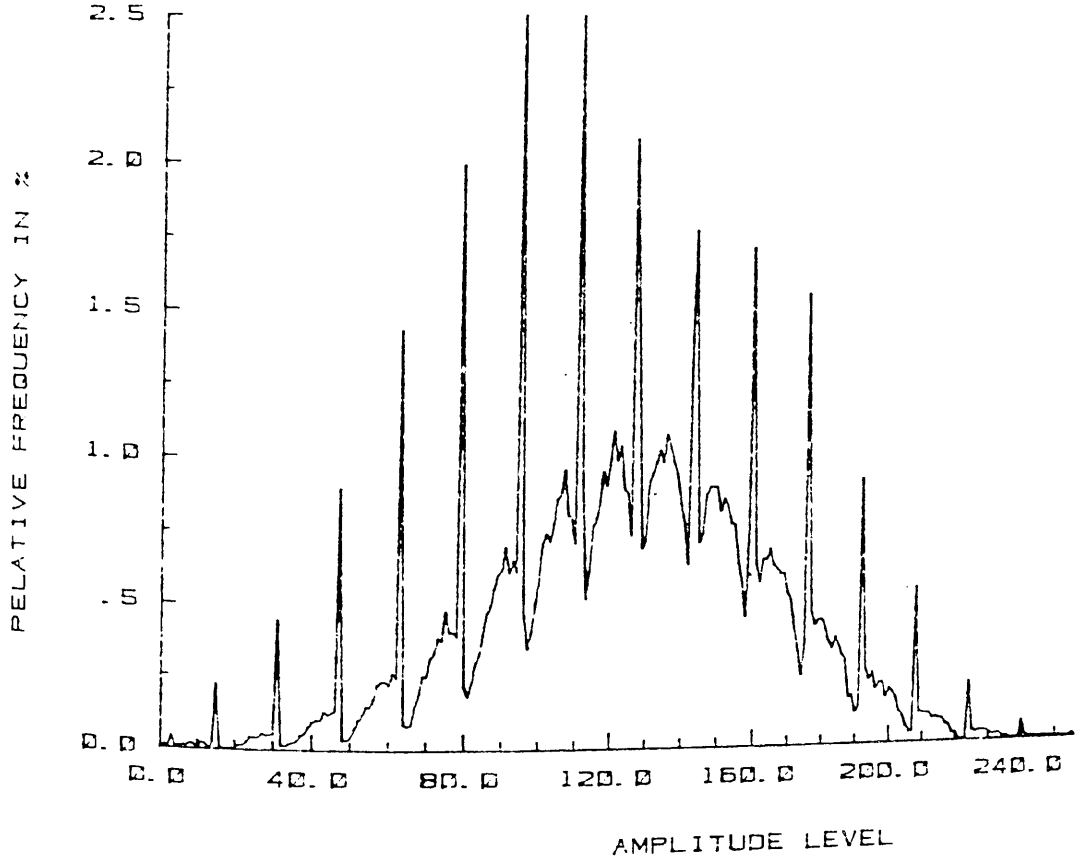

Figure 7.15. A histogram of the occupied amplitude levels for the LECROY 2256 waveform analyser, with a Gaussian noise signal with a -3 dB bandwidth of 5.0 MHz.

digital converter may indicate the cause of these errors. The converter consists of 2 batteries of 15 discriminators each. The first battery quantizes to the first 4 bits of accuracy and the last battery interpolates between these bits to the last 4 bits accuracy. It appears that only the first 15 discriminators work satisfactorily.

To make an estimate of the actual accuracy of the converter, the number of levels exceeding an occupation frequency of 0.2% were counted. The resulting graph is shown in Fig. 7.16 as a percentage of the total number of levels activated during the recording. At the highest slewrate of the input signal i.e. 5 levels/ns only half the number of levels are exceeding an occupation frequency of 0.2%. This corresponds to a quantization accuracy of 7 bits. For a comparison with other analogue-to-digital converters quantization accuracy, Elsleys(10) findings for the Biomations 8100 transient recorder are shown in Fig. 7.17. When comparing Figs. 7.16 and 7.17 it is clear that the Lecroy digitizes more accurately at higher frequencies.

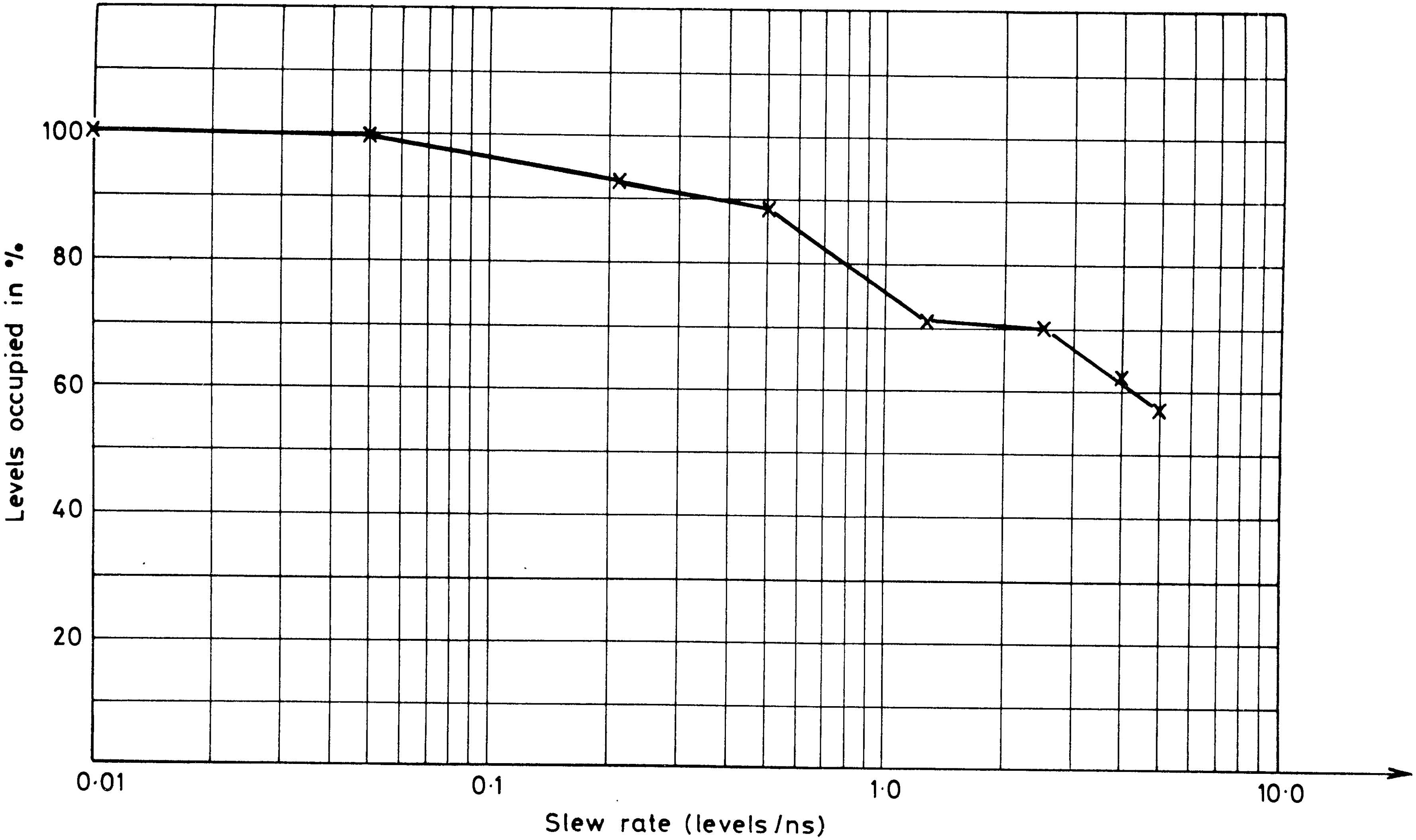

Figure 7.16 The fraction of occupied amplitude levels versus the slew rate of the input signal for the Lecroy 2256 waveform analyser.

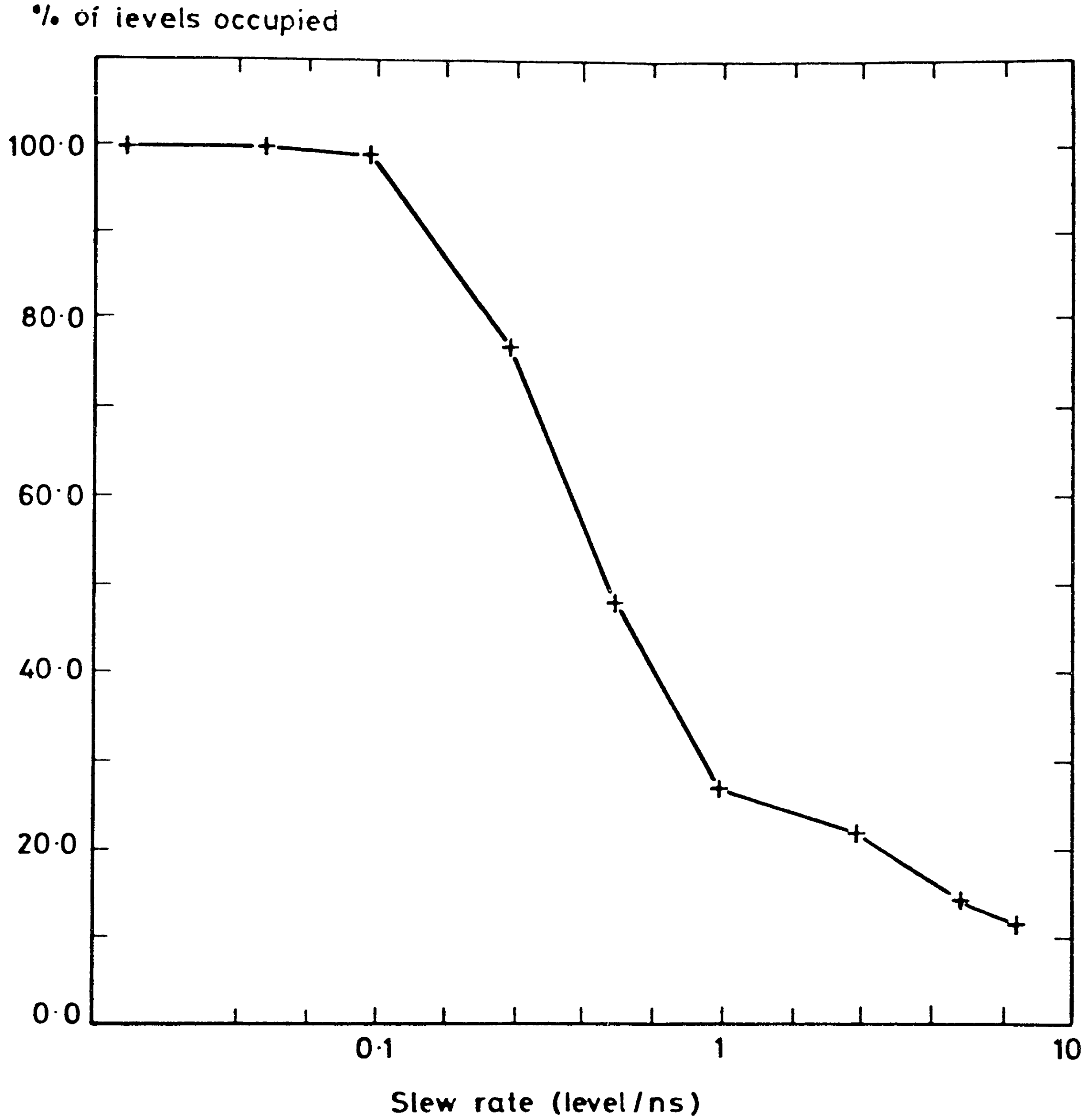

Figure 7.17 The fraction of occupied amplitude levels ~~versus~~ the slew rate of the input signal for ~~the Biomation~~ 8100 transient recorder(after Elsley).

CHAPTER EIGHT

A CRITICAL PRACTICAL COMPARISON OF CROSS-CORRELATION METHOD USING RANDOM NOISE SIGNALS WITH THE CONVENTIONAL EDGE EXCITATION TECHNIQUE

An experimental ultrasonic flaw detector based on a cross-correlation detector and using random noise as the signal source was built to investigate this detection principle applied to ultrasonic nondestructive testing. The main advantage to be expected of applying cross-correlation detection instead of conventional amplitude detection is in sensitivity of detection and ability to separate pulses close to each other. This stems from cross-correlation processing of long echo pulses derived from increased energy of the signal sent. This naturally gives an improvement in detecting and resolving small flaws. To obtain a comparison between conventional ultrasonic flaw detectors and the cross-correlation based detector, conventional techniques are used in the same experiments; but it must be expected that the amplitude of the source signal used with conventional techniques has to be increased considerably compared to the amplitude used with the cross-correlation detector.

The experimental flaw detector has been built around a digital computer to make the experiment easy to adapt to new processing techniques during the development of the equipment. However, considerations had to be given to the special restrictions applicable to digital techniques discussed in Chapter 7. The selection of the analogue to digital converter is of highest importance as it's accuracy is the basis for consequent computer processing. At the commencement of this research the state-of-the-art ADC for work in the low MHz region was the Biomation 8100. It was soon followed by the LeCroy 2256. Some time was spent determining the relative performance of these devices and for reasons detailed in Chapter 7 the LeCroy was chosen to be the digitizer in the Harwell-Aston Cross-Correlation Flaw Detector. This chapter will deal with the other elements of the Flaw Detector and indicate its performance.

8.1 THE HARWELL-ASTON EXPERIMENTAL FLAW DETECTOR

The experimental ultrasonic flaw detector was assembled according to the block diagram shown in Fig. 8.1(a). Fig. 8.1(b) shows a photograph of it. (The HP-1000 mini computer used is not shown as this was installed in an adjacent room).

The signal sent was produced with a noise generator modulated with a sinusoidal carrier. The random noise generator will be discussed in Section 8.1.5 together with a final test of the equipment. The pulse length was determined by the length of a gate pulse applied to the carrier generator. This was obtained by triggering-on a

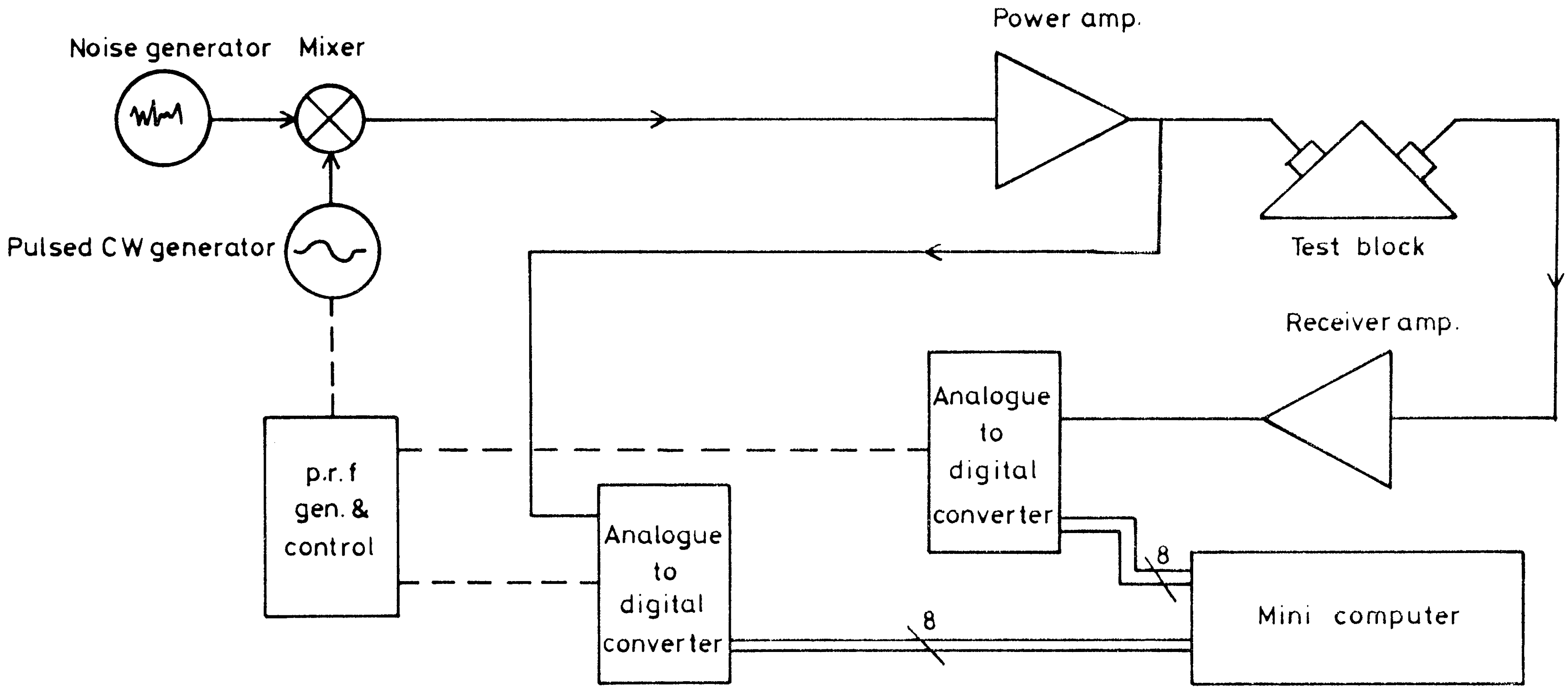

Figure 8.1A Diagram of experimental equipment.

Figure 8.1(b) Photograph of experimental cross-correlation equipment.

(The HP-1000 mini computer used is not shown as this was installed in an adjacent room.)

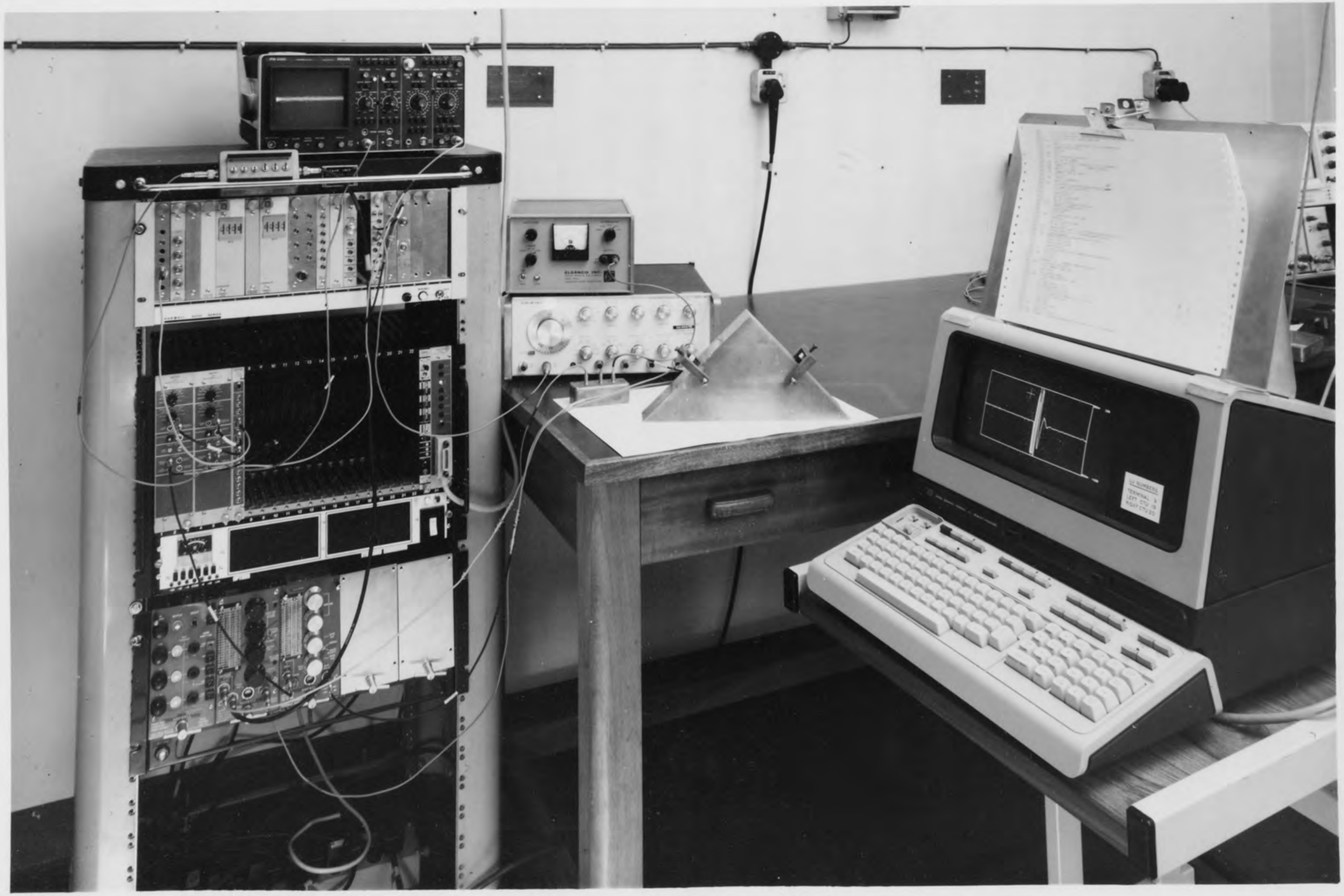

bistable multivibrator at the start of the send sequence and using a delayed pulse to trigger the bistable multivibrator to switch off. The delayed pulse was obtained by dividing the pulse rate from the master clock generator. Different durations of the gating pulse were obtained by changing the dividing ratio.

The gating pulse was then fed to the carrier generator which generates a pulsed sinusoidal signal of the same duration as the gating pulse. At the start of the gating pulse the carrier generator sends out a sinusoid, starting at a zero crossing having a positive slope. It was found to be of importance that the carrier wave started with exactly the same phase for every excitation. At the end of the gating pulse the carrier generator was gated-off. However, if the gating-off edge appeared before a complete cycle of the carrier was finished, the carrier generator continued until the signal crossed the zero line with a positive slope. By making sure that the sinusoidal signal generated always started and finished with a zero crossing and a positive slope, a whole number of cycles was always used for the modulating signal. The stability of the carrier generator was found to be well within the variations of other experimental parameters so the pulse length for each excitation remained constant.

The mixer used to modulate the random noise signal was of the balanced modulator type usually found in radio communication equipment. The modulator efficiently stopped the random noise passing to the excitation amplifier during the silent periods. A rejection ratio exceeding 60 dB was measured.

8.1.1 The Sender and the Receiver Amplifiers

The modulated and pulsed noise from the mixer is ready to be amplified and used for excitation of the sending transducer. After detailed study of ways of isolating amplifiers used with a combined sending/receiving transducer, it was decided to use a separate sender and receiver. The difficulty with using a combined sender and receiver was in rejecting the sending signal at the receiver. The sending signal passed through the receiver and caused spurious echoes at the detector. To overcome this difficulty an attempt was made to inhibit this signal with an analogue gate. This was partially successful, but difficulties in obtaining a rejection ratio exceeding an acceptable level (~50-60 dB) was experienced at the high frequencies used (~5-10 MHz). An equally serious problem with the combined sender/receiver was the recovery of the receiver amplifier after the sending period. The application of the high voltage excitation from the sender to the sensitive receiver amplifier paralysed it for hundreds of microseconds after the sending period, making the receiver useless for reception of the first and more informative echo from any flaw. By applying more and more limiting diodes, which were carefully selected for a low conduction voltage, the recovery time was reduced to under 100 microseconds. (Achieved with the Harwell designed charge amplifier 95/0613-2). The number of limiting diodes used was finally limited to six, three with the cathode to the signal conductor and three with the anode to the signal. A resistor network separated each diode pair.

The two diodes nearest to the sender were silicon diodes to withstand the excitation voltage, the other diodes were germanium diodes which have a lower conduction voltage than silicon diodes (0.2V against 0.7 for silicon), but do not withstand high voltages so well as silicon diodes. The recovery time was still not satisfactory and as the experiment was intended to show the usefulness of cross-correlation processing principle, using random noise, it was decided to abandon a combined sender/receiver and instead use separate amplifiers. This restricted the choice of test specimens as the standard test specimens used with ultrasonic nondestructive testing are usually made for use with one transducer. It was considered economical and instructive to make one special test specimen for this experiment, as discussed later.

After selecting different types of amplifiers according to bandwidth requirements (~5 MHz) and easiness of operation (giving the possiblity of controlling both bandwidth and amplifications), two Harwell designed amplifiers were selected for the work. Data for the receiver amplifier 95/0187-1 and the sender amplifier 95/2153-1 are given in Appendix V. When extra high excitation was desired an ENI high frequency power amplifier was used for the sending amplifier.

8.1.2 The Analogue-to-Digital Converters

After the signal has passed through the sender amplifier, the sender transducer, the specimen, the receiver transducer (the ultrasonic transducers will be described in Setion 8.2) and the receiver amplifier, it is converted by an analogue-to-digital converter so that it can be processed by the computer. As random signals were used, a replica of the sent signal had also to be digitized and fed to the computer; this was achieved by a second analogue-to-digital converter.

The use of the second analogue-to-digital converter makes the experiment more expensive. Other methods were therefore investigated to exclude this. One way is to make the computer generate the random numbers. Firstly, this requires a digital buffer store for the generated numbers since the input/output bus of the computer is too slow to generate the required signal bandwidth. The maximum signal frequency required was in the order of 5 MHz.

This would require an output rate of $\frac{1}{2}\times 5.10^6$=100 ns between each number. (This assumes two numbers for each period of the output signal, Shannon's sampling theorem criterion). An optimistic estimate of the maximum data rate from the output bus would be 1μs between each number (see Chapter 7, discussion of the CAMAC interface). Secondarily it requires a fast digital-to-analogue converter.

The expense of developing a programmable random noise signal generator would exceed the cost of the second analogue-to-digital converter, the solution using the second analogue-to-digital converter was therefore chosen. (Towards the end of the work a programmable signal generator was introduced by the signal generator manufacturers, Wavetek. This however did not cover the frequency range of interest, but it is to be hoped that such signal generators will appear in the future).

The analogue-to-digital converters converted to 8-bit accuracy with a recording length of 1024 samples each. (A description of performance for the analogue-to-digital converters is given in Chapter 7). The sampling rate of the converters was 20 MHz. The sampling rate was set by a separate clock pulse generator which was also used as a master clock for the rest of the equipment. It was found that this reduced variations of the sampling instants for successive accessions. The pulse repetition frequency for the ultrasonic driver was also derived from the master clock by a frequency divider.

The recording time of the analogue-to-digital converters is given by the product of the number of samples and the sampling time. For the analogue-to-digital converters used this gives a recording time of $1024 \times 1/20\ 10^6 = 51.2\ \mu s$. For experiments where the received signal is later than this a delayed trigger is generated by dividing the pulse rate from the master clock and using this pulse to trigger the analogue-to-digital converter used for the receiving signal.

Appendix V shows the circuit diagram for the ultrasonic flaw detector.

8.1.3 The Storage of the Signals

The reference and the received signals are stored on a magnetic fixed disc in the computer employing a program called RECST. RECST is an interactive program requesting control information from the operator through the terminal. Firstly, it requests if one or two analogue-to-digital converters should be used (the analogue-to-digital converters are called recorders in the program). The option of one recorder is useful when setting up the equipment and general inspection of either the received or sent signal. Then information is requested with respect to the number of recordings to be made and under which name the file containing these recordings is to be stored. The reading of the analogue-to-digital converters is performed by a subroutine which activates the CAMAC interface. A more detailed description of the interface is given in Chapter 7. When the requested number of recordings are made, the data file containing the signals is closed, ready for later inspection and processing. A listing of RECST, which is written in FORTRAN, is given in Appendix II.

Some difficulties could arise in reading the recorders during excitation or reception of the flaw echo. This was overcome by inhibiting reading the recorders until their store was full. The computer waited until the reception recorder told it that it was ready and then the computer read the store in both recorders. The recorders were then ready for the next operation. The pulse repetition frequency of the excitations was set sufficiently low that the computer had time to finish the reading of the recorders before a new excitation.

8.1.4 The Processing of the Signals

The recorded signals stored on the disk are now ready for processing. Finding the cross-correlation function of two time series consists mainly of shifting one of the series with respect to the other, forming the product of the time series and sum up the product at each point. This procedure is then repeated until all time series points are processed.

There are two different methods in which cross-correlation detectors can be implemented on a digital computer:

(i) By the direct evaluation of the cross-correlation function in its discrete form (i.e. for a time series)

$$R_{xy}|m| = \sum_{n=o}^{N-m-1} x|n|\ y|n+m| \qquad (8.1)$$

where R_{xy} is the cross-correlation function of time series x and y

m and n are counting variables

N is the number of points in the time series.

(ii) By the application of the Fast Fourier transform. Using a simple extension of the Wiener-Khinchin relations (see appendix I) it can be shown that the cross-correlation function is the inverse Fourier transform of the cross-power spectrum. The operation of obtaining the cross-correlation function can therefore be performed by first forming the cross-power spectrum and then merely finding the inverse Fourier transform. This operation can be summarised as:

$$R_{xy}\ |m| = IF(F(x|n|)F^*(y|n|)) \qquad (8.2)$$

where F( ) denotes the Fourier transform

IF( ) denotes the inverse Fourier transform.

The number of samples in x(n) and y(n) decides which method is the most economical to implement. The break even point between method (i) and (ii) is usually taken to be less than 100 sampling points(1) with method (ii) as the most economical for more sampling points. The period over which correlation is carried out decides the available range of time delays which are possible to measure; as this should be as long as possible the second method of implementation was chosen.

By the introduction of the discrete Fourier transform it is automatically assumed that the input data is periodic. To avoid overlapping(2), the number of points in the discrete correlation function, N, has to obey the following equation:

$$N \geqslant N_x + N_y - 1 \tag{8.3}$$

where

N_x is the number of sampling points in time series x.

N_y is the number of sampling points in time series y.

The number of samples in x and y can therefore be different. It would be uneconomical to use different Fast Fourier transform routines for each time series. The number of samples in each time series was therefore made equal by padding each time series with zeroes until the number of points was equal to N.

Fig. 8.2 shows a flow chart for a computer program OCOR2 which forms the cross-correlation function according to method (ii) i.e. the Fast Fourier transform method. This is an interactive program requesting control information from the operator. The number of records and the data file name for the recorded signal are requested first. The cross-correlation process is then performed, after padding the time series with zeroes. The Fourier transform of the two input signals is formed, the complex conjugate product of the Fourier transformed time series is carried out to obtain the cross-power spectrum and then finally the inverse Fourier transform of the cross-power spectrum is performed to obtain the cross-correlation function. The data-file name for the finished processed time series is then requested and the first processed record is stored. This procedure is now repeated for the requested number of times until the processing of the records stored under the input file name is finished. The output file is then closed, ready for further processing or inspection. A listing of the computer program OCOR2 is found under Appendix II.

The Fast Fourier transform is performed with the aid of a subroutine named FT01. Different methods were tested to make a Fast Fourier transform routine. Different versions of the Fast Fourier transform routines have appeared in the literature (see ref. in Chapter 7), some of these were tried for accuracy and speed of operation. The FFT routine,

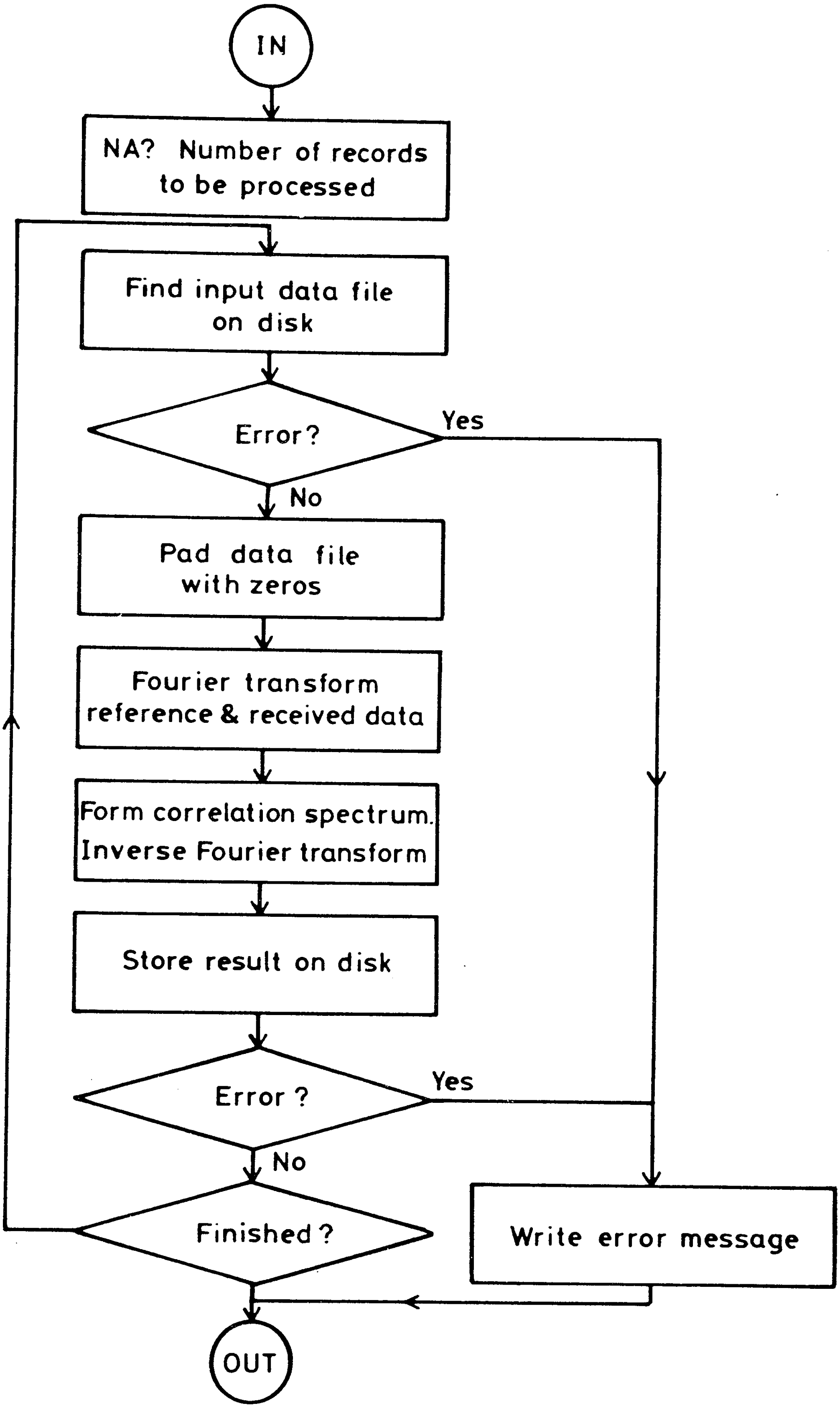

Figure 8.2 Flowchart for the correlation program OCOR2.

FT01, in Harwell's scientific subroutine library was found to be satisfactory and this was converted for the HP-1000 computer used in this experiment. The listing of the Fast Fourier transform named FT01 is found in Appendix II. To reduce requirements for data storage during processing, a technique using an extra routine for real time series points(3) was tried. This halves the number of data points to be temporarily stored and an approximate reduction in the processing time by 1.5. However, more processing of the data is required giving a more complicated experiment. As the main objective of this experiment was to show the usefulness of the processing principles this complication was not implemented. For a future implementation of the Harwell-Aston flaw detector this routine should be included.

To further process the cross-correlation functions, an averaging program was developed. This program was also an interactive program requiring the same control information as the cross-correlation program from the operator. The average of each data point in the cross-correlation domain was found and the resulting time series stored on disk. By making this a running average routine, the improvements in the final time series could be inspected as the number of input time series increased. Programs for display on the graphics terminal (shown in Fig. 8.1(b)) and on paper were also developed. These programs produced figures as shown in Figs 8.10 and 8.11.

8.1.5 The Random Noise Generator

To produce the random noise, different techniques were tested. First the noise produced in an electrical resistor was tried, this however did not have the required operational stability. Second, the noise from a zener diode when just conducting was tried for bandwidth and operational stability. After a number of trials without obtaining satisfactory operational stability, the commercially available Elgenco noise generator based on the same principle was brought in. This was however not matched to the rest of the equipment so a matching buffer was built. As seen from Fig. 8.3 the power spectrum (obtained by the Fast Fourier transform) from the noise generator/buffer had a more than satisfactory bandwidth. The power spectrum which is flat within 3 dB had a bandwidth exceeding 5 MHz.

To test the total equipment and computer programs several experimental runs were made. One of the test results is shown in Fig. 8.4. The auto-correlation function of the random noise signal was calculated and as shown in Fig. 8.4. there is a sharp, well defined peak with small sidelobe level. The main peak to sidelobe level is estimated to be in the order of 70 dB.

The main limitation for obtaining a sharp main peak in the correlation function is the limited bandwidth of the ultrasonic transducers, which are described next.

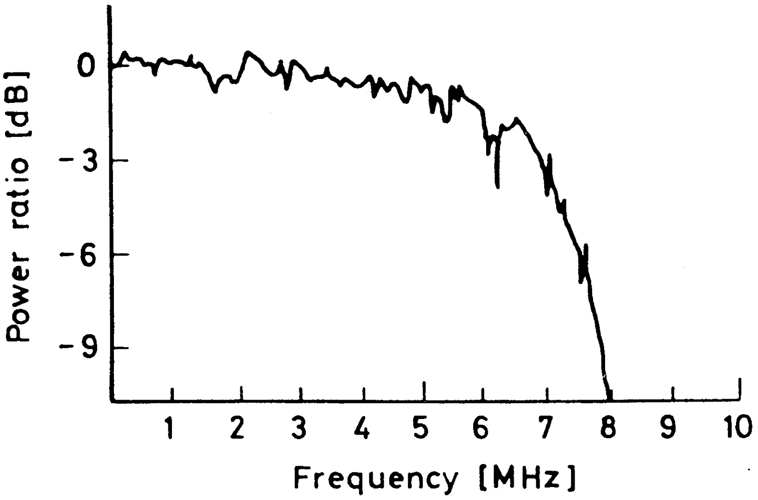

Figure 8.3 Power spectrum of the modulating noise signal.

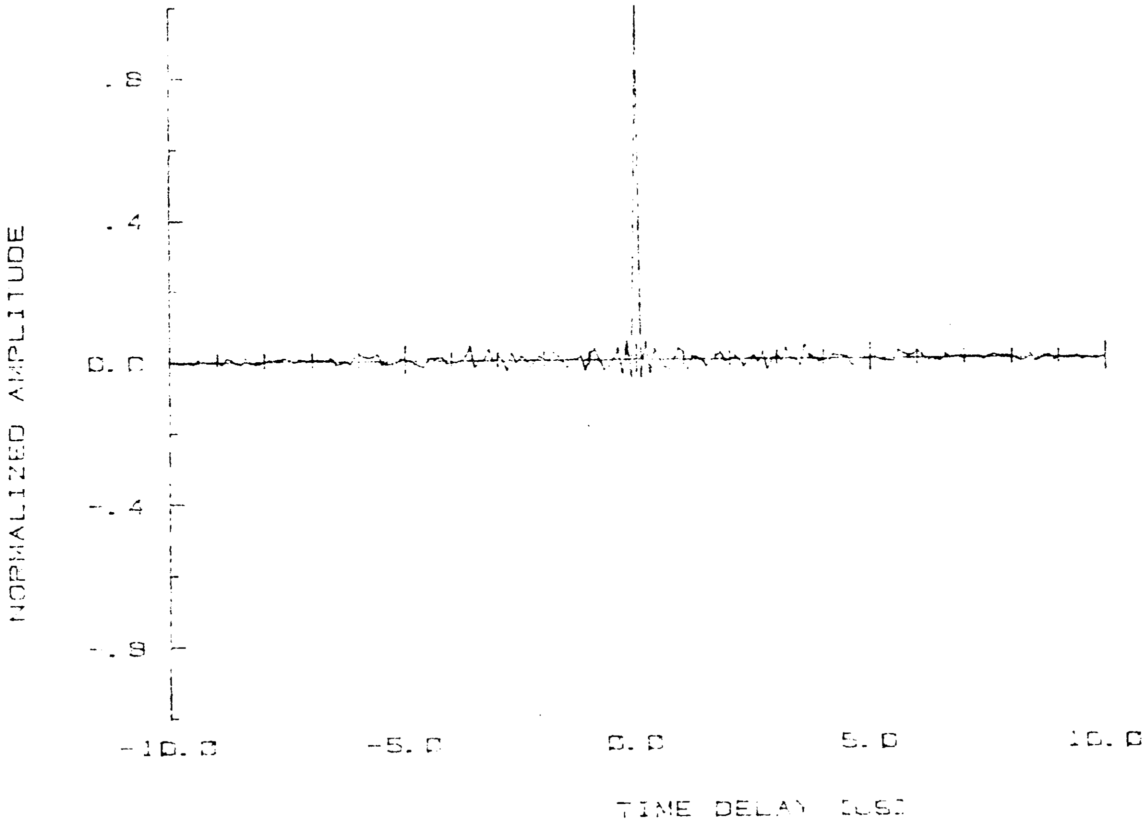

Figure 8.4. The autocorrelation function for the sent noise signal.

8.2 THE ULTRASONIC TRANSDUCERS

The ultrasonic transducers are a pair of Panametric longitudinal mode transducers with a diameter of 12.5mm and a stated resonance frequency of 5 MHz. Their power transfer function is shown in Fig. 8.5. The power transfer function was obtained by separating the transducers with an aluminium block 100 mm square. The sender-transducer was driven with a pulsed sinusoidal signal and the receiving transducer fed a sensitive power meter. The frequency response of the rest of the equipment was wider than the ultrasonic transducer's response, and as such Fig. 8.5 can be taken to be the frequency response of the whole system.

The beam profile of the sender transducers in water is shown in Fig. 8.6. The beam profile was obtained by using the transducer in a pulse-echo system. The reflecting target was the hemispherical end of a rod of 4.75 mm diameter. The reflector is moved in a raster pattern in front of the transducer and the amplitude of the reflected signal is recorded with a grey scale recorder as a function of the reflector position. The grey scale is quantized in 6 contours with 3 dB difference between each one, white being no signal. Figs. 8.6(a) and 8.6(b) show the longitudinal beam profiles with Fig. 8.6(a) perpendicular to Fig. 8.6(b). These beam profiles start 10 mm from the transducer face. Fig. 8.6(c) shows a transverse beam profile

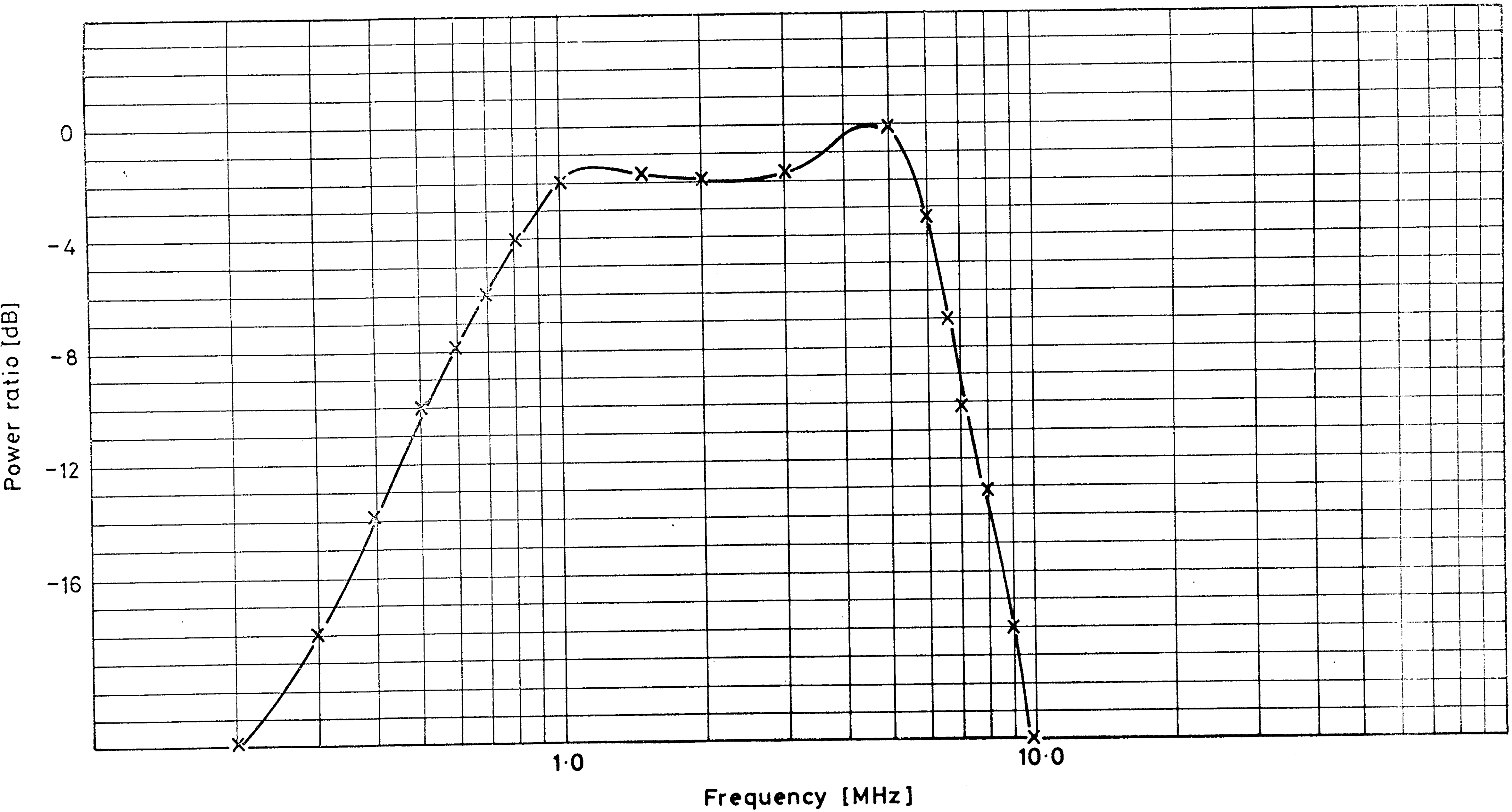

Figure 8.5 Frequency response of the sender and the receiver transducer, facing each other on a testblock.

FIGURE 8.6

(a) Longitudinal beam profile of the sender transducer in water.

(b) Longitudinal beam profile of the sender transducer perpendicular to Fig. 8.6(a).

Longitudinal scale 1:1.25

Transversal scale 1:0.3

(c) Transversal beam profile of the sender transducer; in water 100 mm from transducer face.

Scale 1:0.25

(d) Impulse response of sender transducer.

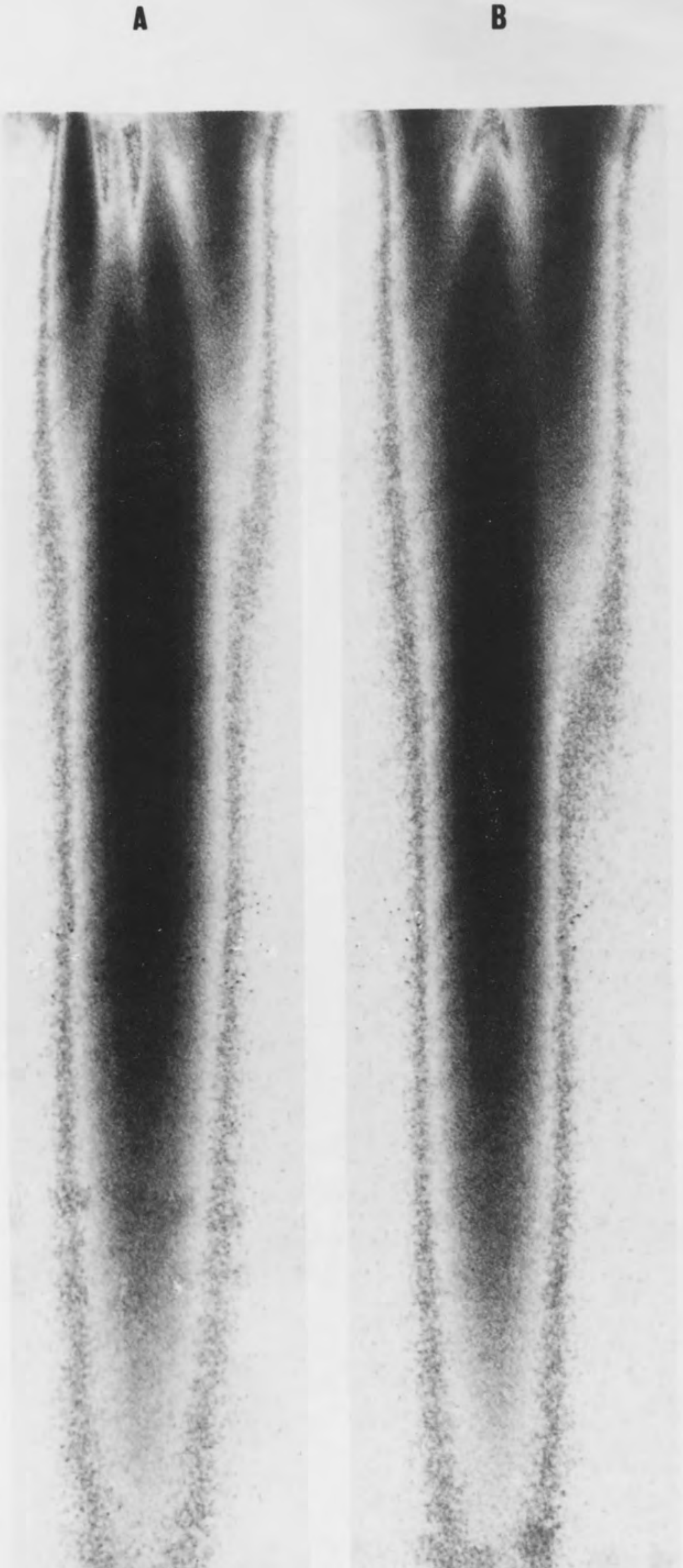
A
B

C

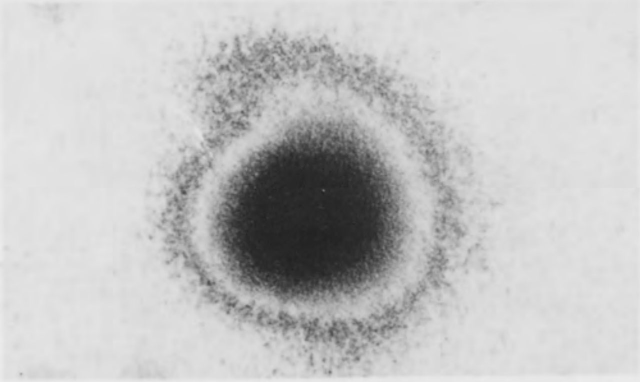

D

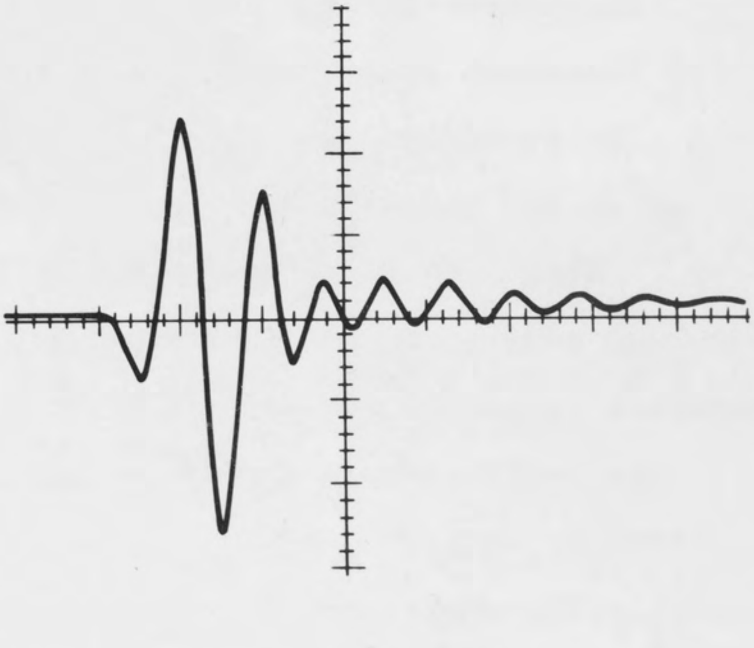

V. SCALE: 0.5 V/div.
H. SCALE: 0.2 μS/div.

120 mm from the transducer face. The received signal reflected from the same reflector as used for the beam profiles is shown in Fig. 8.6(d). The transducer is excited with an impulse of 40 V amplitude and a rise time of 15 ns, the falling edge is exponential with a time constant of 500 ns. The transducer is assumed to be excited with only the rising edge due to the slow decay time of the pulse.

8.3 PERFORMANCE TRIALS WITH THE HARWELL-ASTON EXPERIMENTAL FLAW DETECTOR

8.3.1 Early Performance Trials

Different experiments were conducted for performance trials of the flaw detector. However, only a few with metal test specimens were suitable for the transducer configuration used. Early experiments were conducted in water detecting different objects. One consisted of detecting two glass capillaries approximately 0.4 mm in diameter and separated by approximately 3 mm. Both capillaries were clearly visable with a small echo appearing closely behind the second main echo. It was later discovered that the second capillary was inadvertantly filled with water while the other capillary was air filled. As the separation of the main echo and the small echo corresponded to 0.7 mm in water it was inferred that the small echo was due to the back wall of the second capillary. This experiment was very encouraging since the capillaries could not be resolved when the same transducer was used in the conventional edge excitation mode. Tests proceeded to a metal test block.

8.3.2 Performance Trials on Metal Test Specimen

Fig. 8.7 shows a triangular aluminium block used to evaluate the basic usefulness of cross-correlation detectors for ultrasonic non-destructive testing. The transducers were placed symmetrically on the test block to give an approximate time delay of 36 (μs) as shown in Fig. 8.7 (The longitudinal velocity of elastic waves in aluminium is 6300 (m/s)).

Fig. 8.8 shows the source signal of duration 10(μs). This duration was chosen to be well within the requirements of equation (8.3). The received signal is shown in Fig. 8.9. It is difficult to detect the presence of any replica of the sent signal, and the precise arrival time would be impossible to determine. After the two signals have been processed with the correlation algorithm, the received signal is clearly visable as a peak in the correlation function shown in Fig. 8.10. The correlation peak gives a time of flight of 35.9(μs) which corresponds well with the location of the transducer. However, Fig. 8.10 shows a large noise level in the form of sidelobes of the correlation function. These sidelobes can be due to the

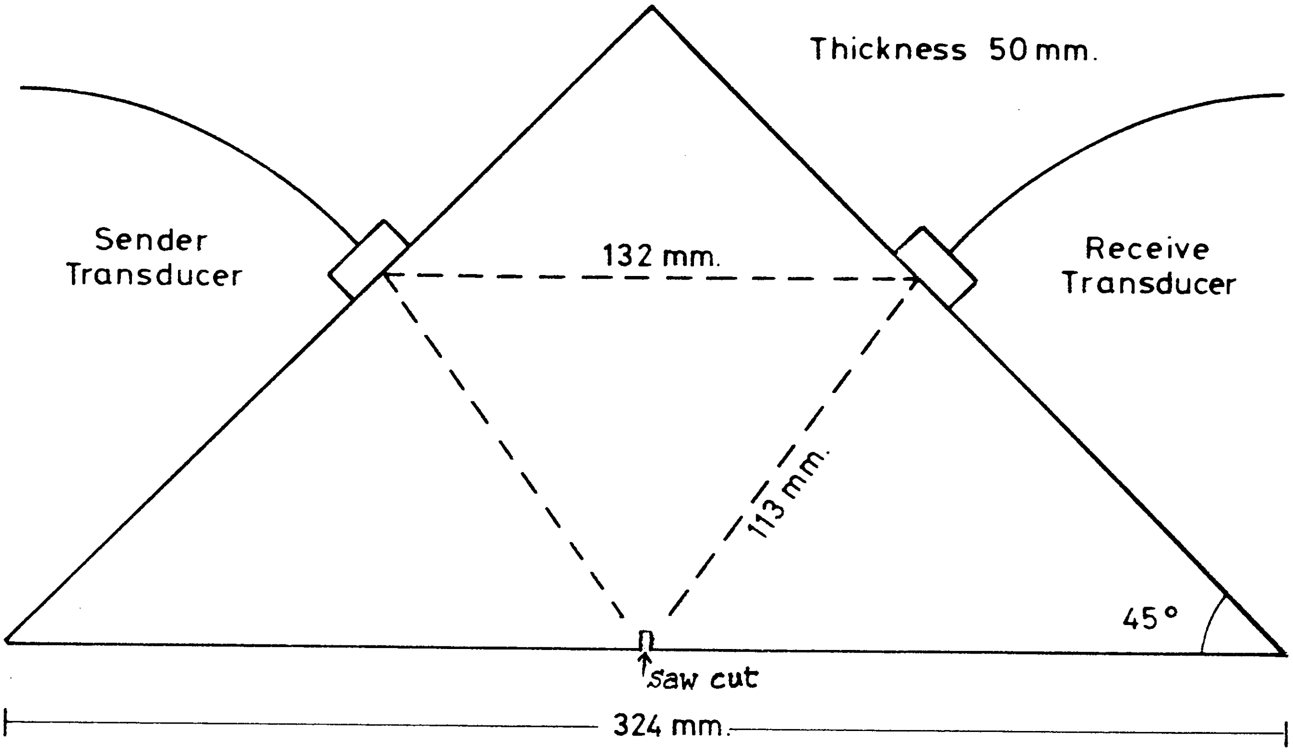

Figure 8.7 The testblock used for evaluation of the ultrasonic equipment.

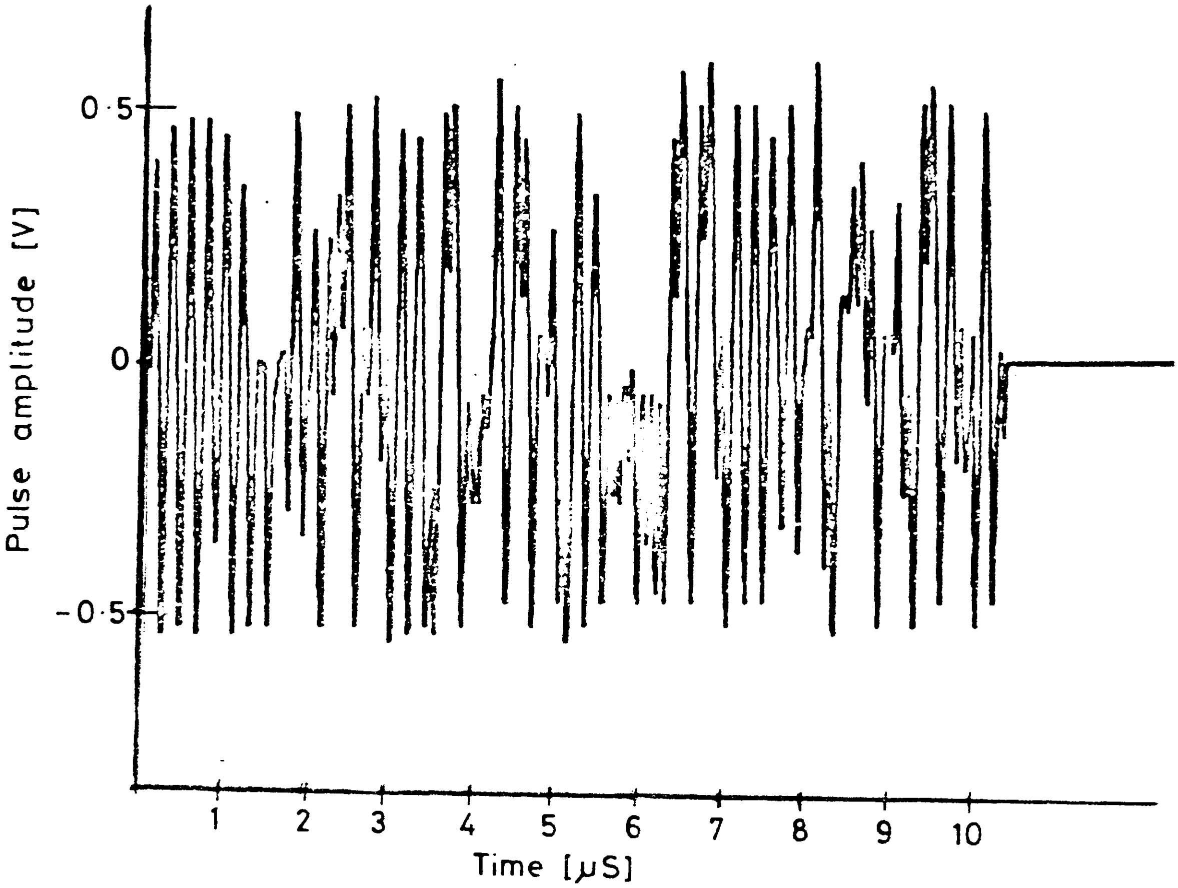

Figure 8.8 The electrical drive signal applied to the sending transducer.

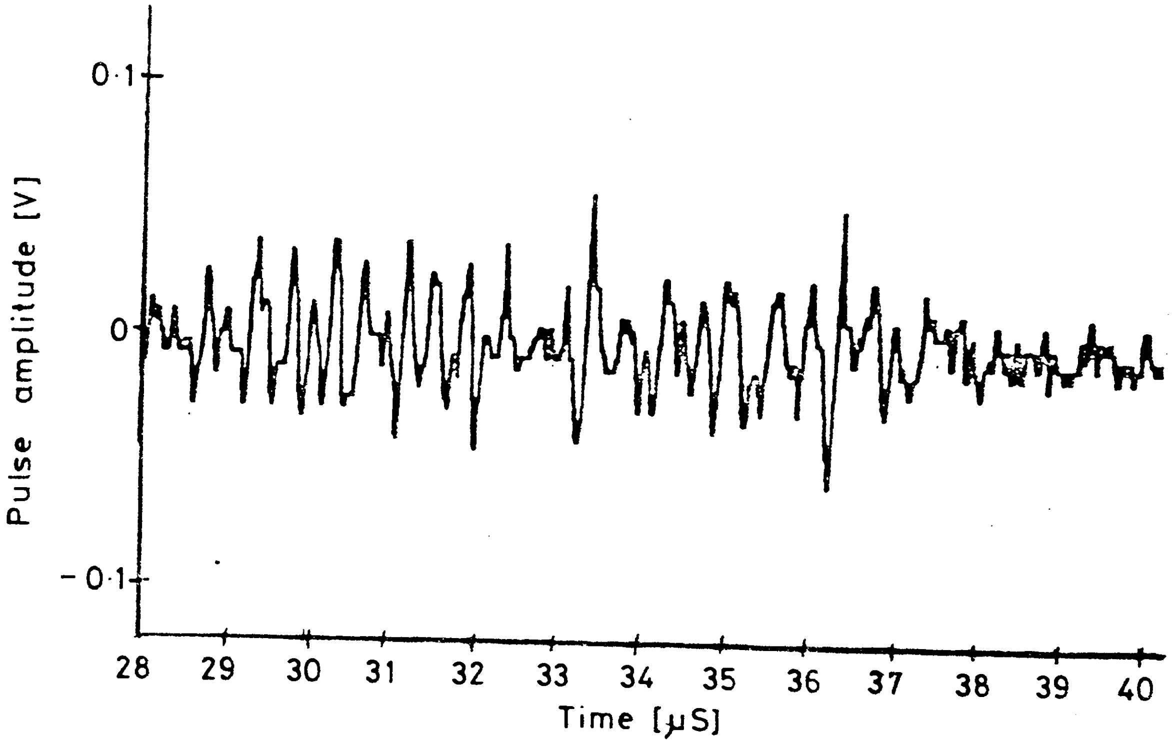

Figure 8.9 The received signal.

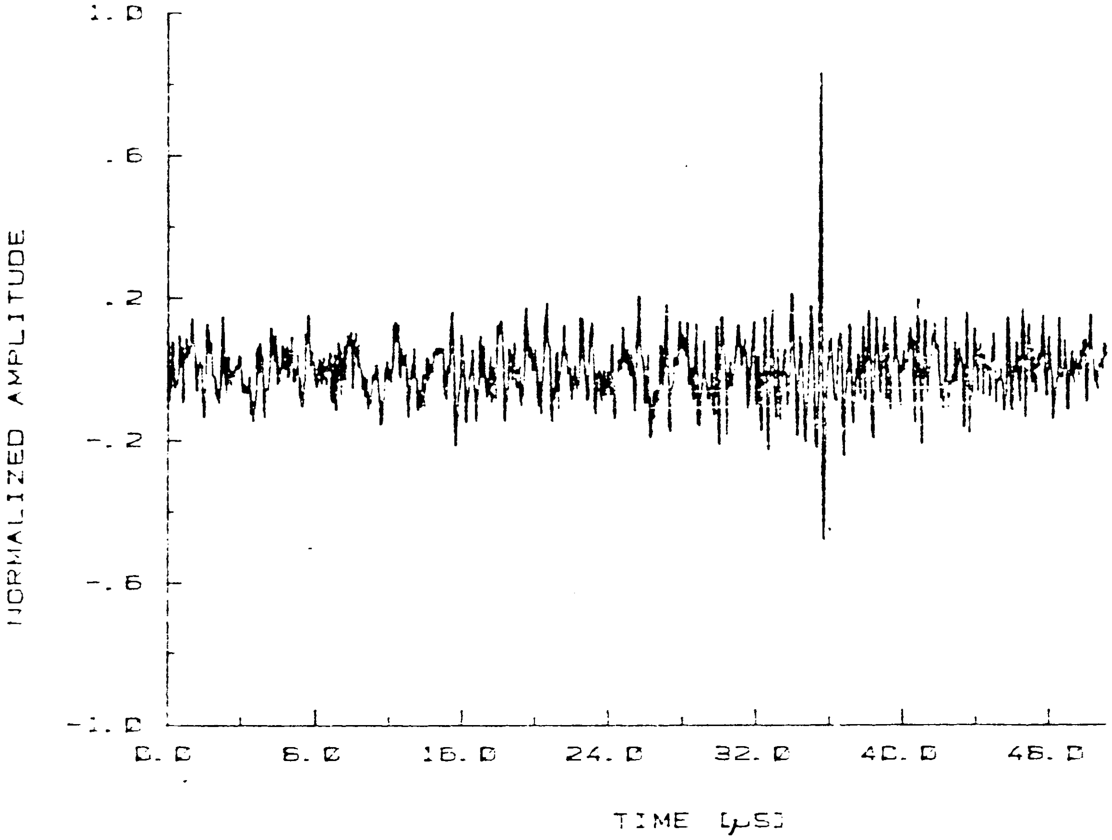

Figure 8.10. The cross-correlation function of the received and the sent signal.

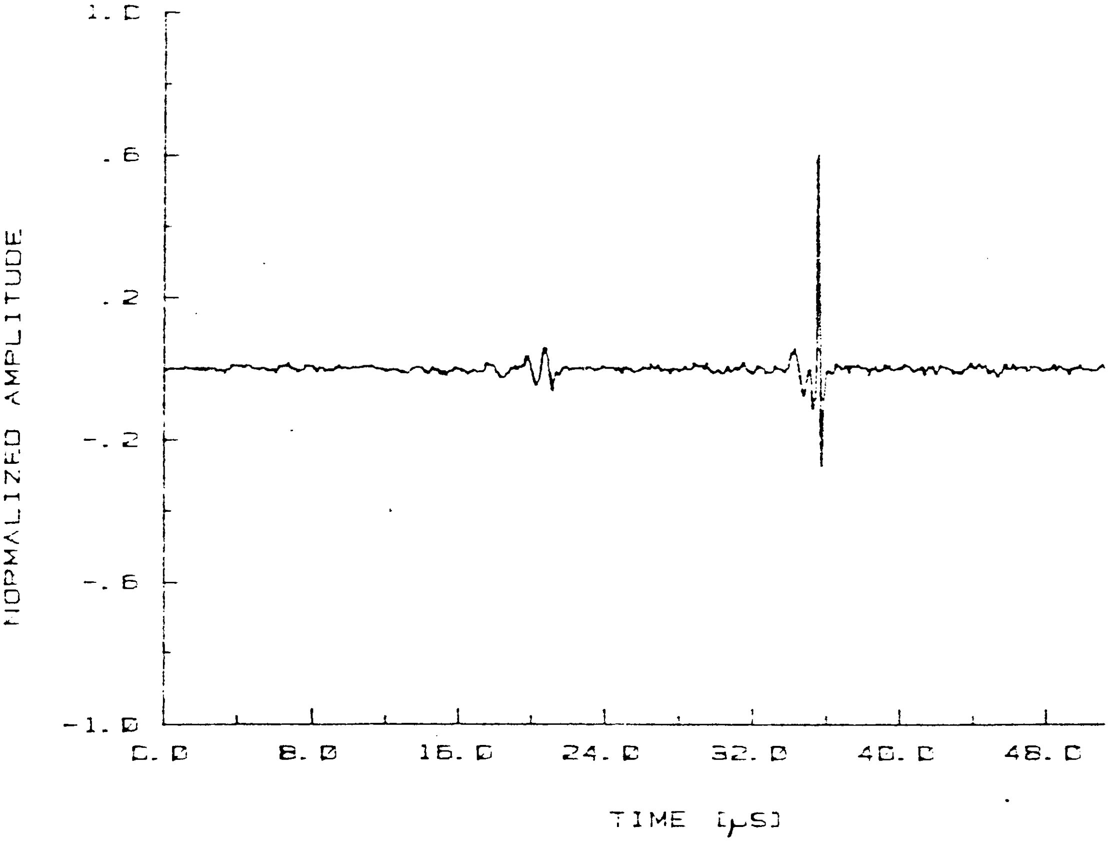

Figure 8.11. The average of 100 cross-correlation functions.

limited duration of the sent signal. An artificial lengthening of the sent signal was introduced by averaging a number, N of correlation functions, originating from the noise signal. The total sending time of the noise signal will be:

$$T_{Total} = T_{Single} \cdot N$$

Fig. 8.11 shows the resulting average of 100 correlation functions. A reduction in the sidelobe level of approximately $\sqrt{100} = 10$ is observed. The correlation peak at 21 (μs) corresponds to a path length of 132 mm for the elastic wave. This can be due to the direct path between the two transducers as shown in Fig. 8.7. The small peak at 34.9 (μs) near to the main correlation peak corresponds to a path length of 220 mm. This is attributed to a small saw cut in the block approximately 3 mm deep and 1.5 mm wide.

To show the considerable resolving power of the correlation based detector the same transducer was used in a conventional transmission mode employing edge excitation to the sender transducer. Neither the signal from the saw-cut nor the direct path signal could be detected. Even if the received signal was averaged 100 times no indication of the saw-cut nor transmission along the direct path could be detected. It is instructive to note that the energy of the edge excitation was approximately 7 times that of the random noise signal. The very great superiority of the cross-correlation technique is thus demonstrated and could well justify the cost of the advanced technology needed to achieve it.

CHAPTER NINE

CONCLUSION

Welds contain crystalline materials which cause attenuation and redirection of the elastic wave. This makes ultrasonic nondestructive testing of welded structures difficult.

This difficulty is mainly observed in two ways.

(i) The flaw cannot be detected.

(ii) If a flaw is detected the position is not where normal geometrical considerations would predict.

Emphasis has been given to the first point as this is most important for a safe operation of an engineering structure.

To improve the ability to detect flaws different methods can be employed. The transducer might be moved small distances and ultrasonic signals collected at a number of positions. These ultrasonic signals can be averaged after being delayed appropriately to account for the differences in propagation distance. This technique is similar to synthetic aperture focussing techniques, discussed in depth by other workers.

This thesis has mainly discussed detection methods not based on movements of the transducer, instead using signal processing techniques for single position signals. Compared with normal amplitude detection, cross-correlation detectors offer improvements of detection for signals with a lower signal-to-noise ratio. The estimation of the time of flight for the ultrasonic signal is also improved with cross-correlation detectors.

The signal used with a cross-correlation detector was investigated and two main categories were devised

(i) deterministic signals
(ii) random signals.

Deterministic signals, as frequency modulated sinusoidal signals and stepped frequency sinusoidal signals, offer the advantage of simple implementation at the cross-correlation detector. These signals do not, however, give the same signal processing possibilities as random signals. It has been shown (Chapter 6) that a bandlimited random noise signal, comparable in bandwidth and duration to the deterministic signals, gives a better detection for the same signal-to-noise ratio. The implementation of cross-correlating detectors for random signals is difficult. By using pseudo-random signals it is possible to simplify the detection process considerably. The problem of finding the best form for these pseudo-random signals is being studied.

To investigate further the use of cross-correlation detectors an experimental flaw detector was built. When two separate transducers were used there was an automatic reduction in the volume common to the two transducers and corresponding reduction in the background grain scattering. The transducers were heavily loaded to give a good bandwidth which exceeded half the resonant frequency.

In ultrasonic NDT the signals can have a dynamic range of as much as 100 dB. By using a digital system this range is achievable and subsequent signals can be processed arithmetically without error. The conversion of the analogue signals required a comparison between different analogue-to-digital conversion techniques. An experimental test of one of the currently adopted standard for converters such as the Biomation 8100 used in ultrasonic NDT established that this did not give adequate accuracy. A new analogue to digital converter (Lecroy 2256) gave an improvement in accuracy at higher signal frequencies (Chapter 7). It has since this test, been accepted as a standard for ultrasonic NDT.

Use of the flaw detector on test blocks showed that the random noise cross-correlation detector with long duration signals gave a spectacular improvement in signal detection (estimated at about 30 dB) with consequent improvement of the time of flight measurements.

Improvements arising from the cross-correlation detector in comparison to the normal amplitude detector are due to the following causes. White noise caused by electronic noise is effectively removed as shown in Chapter 5 By use of a long duration pulse more energy can be sent, the wide bandwidth of the signal and the correlation detector maintain the depth resolution. The scattering noise from small grains is changed from the source signal giving a lack of correlation, this gives an improvement in flaw signal to grain noise ratio. The following claims are therefore made (Compare with Chapter 6, section 6.5):

1. Smaller flaws are detected. These are of the order of millimeters in size even close to the surface.

2. Depth resolution is demonstrated to be better than ½. millimeter when detecting objects in water (frequency 5 MHz).

3. The application of averaging techniques has been demonstrated without reduction in resolution.

4. Electronic noise is effectively removed.

5. Partial coherent noise should be reduced.

The depth resolution is particularly important in engineering structures (Ref. Chapter 2) as the stress tend to be located near to the surface.

The use of two transducers is advantageous when inspecting materials with high grain noise, however, the necessity for two transducers reduces the simplicity of operation. Further work on the Harwell-Aston experimental flaw detector should therefore be concentrated on making a single transducer flaw detector.

APPENDIX I

THE WIENER-KHINCHIN RELATION

The definition of the power density spectrum is:

$$S_{xx}(w) = \frac{1}{2\pi} \lim_{T\to\infty} \frac{|F(w)|^2}{T} \qquad (A.I.1)$$

where F(w) is the Fourier transform of a truncated signal f(t) of duration T.

Rewriting the power density spectrum:

$$S_{xx}(w) = \frac{1}{2\pi} \lim_{T\to\infty} \frac{1}{T} \int_{-T/2}^{T/2} f(t)\, e^{-jwt} dt \int_{-T/2}^{T/2} f(t)\, e^{jwt} dt \qquad (A.I.2)$$

Replacing the variable t in the first integration by (t+τ) and rearranging the order of integration:

$$S_{xx}(w) = \frac{1}{2\pi} \lim_{T\to\infty} \frac{1}{T} \int_{-T/2}^{T/2} \int_{-T/2}^{T/2} f(t+\tau) f(t) e^{-jw(t+\tau)} e^{jwt} dt\, d(t+\tau) \qquad (A.I.3)$$

The first integration can be placed outside Lim.

$$S_{xx}(w) = \frac{1}{2\pi} \int_{-\infty}^{\infty} \lim_{T\to\infty} \frac{1}{T} \int_{-T/2}^{T/2} f(t+\tau) f(t) dt\, e^{-jw\tau} d\tau \qquad (A.I.4)$$

The mid term is the definition of the autocorrelation function, hence:

$$S_{xx}(w) = \frac{1}{2\pi} \int_{-\infty}^{\infty} R_{xx}(\tau)\ e^{-wj\tau} d\tau \qquad \text{(A.I.5)}$$

The power density spectrum $S_{xx}(w)$ and the auto-correlation function $R_{xx}(\tau)$ are Fourier transform pairs. The inverse of the above is obviously true.

APPENDIX II

Subroutine RECR2	:	Data recording routine
Subroutine OCOR2	:	Correlation routine
Subroutine FT01	:	Fourier transform routine

```
      SUBROUTINE RECR2(IDATA,ISW),11.12,79
C
C SUBROUTINE TO READ TWO LECROY 2256 WAVEFORM ANALYSERS
C IN CAMAC STATION NUMBER 1 AND 4.
C TRANSFER IS AT ONE WORD AT THE TIME AND
C THE DATA IS RETURNED IN INTEGER FORMAT IN THE ARRAY IDATA.
C O.MOEN,ATTACHED TO THE NDT CENTRE,AERE,HARWELL,1979
C THIS IS WRITTEN ON A HEWLETT PACKARD 1000 COMPUTER WITH A
C RTE-4 OPERATING SYSTEM.
C
      DIMENSION IDATA(1),IOUT(2)
      LU=38
C ENABLE THE HP INTERFACE BUS.
      CALL RMOTE(LU)
C ASK FOR 2 WORD RETURN FROM THE CAMAC-HPIB INTERFACE 8901.
      CALL EXEC(2,LU,60400B,1)
      CALL EXEC(1,LU,IA,1)
C INITIATE RECORDER 2 IN STATION 4.
C SEND OUT F=9,A=0,N=4!
      IOUT(1)=4400B
      IOUT(2)=2000B
      CALL EXEC(2,LU,IOUT,2)
      CALL EXEC(1,LU,IA,1)
C INITIATE RECORDER 1 IN STATION 1.
C SEND OUT F=9,A=0,N=1!
      IOUT(2)=400B
      CALL EXEC(2,LU,IOUT,2)
      CALL EXEC(1,LU,IA,1)
C SEND OUT F=26,A=0,N=1!
      IOUT(1)=15000B
      IOUT(2)=400B
      CALL EXEC(2,LU,IOUT,2)
      CALL EXEC(1,LU,IA,1)
C SEND OUT F=26,A=0,N=4!
      IOUT(1)=15000B
      IOUT(2)=2000B
      CALL EXEC(2,LU,IOUT,2)
      CALL EXEC(1,LU,IA,1)
C TEST LAM BY SENDING OUT F=8 TO RECORDER 1.
      IOUT(1)=4000B
      IOUT(2)=400B
      CALL EXEC(2,LU,IOUT,2)
10    CALL EXEC(1,LU,IA,1)
C READ Q AND TEST IF SET.
      CALL EXEC(1,LU,IB,1)
      IB=IAND(IB,3B)
      IF(IB.NE.3) GOTO 10
C SEND OUT F=2,A=0,N=1!
      IOUT(1)=1000B
      IOUT(2)=400B
      CALL EXEC(2,LU,IOUT,2)
C READ THE DATA.
      DO 20 I=1,1024
      CALL EXEC(1,LU,IDATA(I),1)
      IDATA(I)=IDATA(I)/256
C MASK OUT THE MOST SIGNIFICANT BYTE.
      IDATA(I)=IAND(IDATA(I),377B)-128
```

```
20      CONTINUE
        IF(ISW.EQ.1)GOTO 40
C READY TO READ 2ND. RECORDER?
C SEND OUT F=2,A=0,N=4!
        IOUT(1)=1000B
        IOUT(2)=2000B
        CALL EXEC(2,LU,IOUT,2)
C READ THE DATA.
        DO 30 I=1025,2048
        CALL EXEC(1,LU,IDATA(I),1)
        IDATA(I)=IDATA(I)/256
C MASK OUT MOST SIGNIFICANT BYTE.
        IDATA(I)=IAND(IDATA(I),377B)-128
30      CONTINUE
40      RETURN
        END
```

```
      PROGRAM OCOR2,,,,,,,,,,11.3.80
C
C THIS PROGRAM FINDS THE CORREALTION FUNCTION
C OF A REFERENCE SIGNAL AND A DATA SIGNAL.
C WHERE BOTH ARE STORED CONSECUTIVELY
C IN A DISK FILE,WITH THE REFERENCE FILE FIRST.
C O.MOEN,ATTACHED TO THE NDT CENTRE,AERE,HARWELL,1980
C THIS IS WRITTEN ON A HEWLETT PACKARD 1000 COMPUTER
C WITH A RTE-4 OPEREATING SYSTEM.
C TO RUN THIS PROGRAM AFTER LOADING IT,TYPE
C RU,OCOR2,9
C WHERE 9 IS THE LOG.UNIT NUMBER OF THE TERMINAL.
C
      DIMENSION REF(2048),REF1(1024),DAT(2048),DAT1(1024)
      EQUIVALENCE(REF(2048),REFI(1024)),(DAT(2048),DATI(1024))
      DIMENSION IPRAM(5),IDCB(144),NAMEDR(3),NAMERE(3),IBUF(2048)
      CALL RMPAR(IPRAM)
      LU=IPRAM(1)
      IF(LU.EQ.0)LU=1
C
C OBTAIN INFORMATION AS TO WHERE THE DATA IS STORED
C ON THE DISK.
C
      WRITE(LU,1)
1     FORMAT("HOW MANY RECORDS DO YOU WANT TO PROCESS?")
      READ(LU,*)NA
5     WRITE(LU,10)
10    FORMAT("TYPE DATA FILE NAME!")
21    READ(LU,20)NAMEDR
20    FORMAT(3A2)
      WRITE(LU,30)
30    FORMAT("TYPE CARTRIDGE REFERENCE NUMBER!")
      READ(LU,*)IREF
      IN=1
31    CALL OPEN(IDCB,IERR,NAMEDR,0,0,IREF)
      IF(IERR.LT.0)CALL ERROR(LU1,IERR,2)
32    NUM=IN*16-(16-1)
C WRITE CONTENT OF THE DISK FILE TO IBUF.
      CALL READF(IDCB,IERR,IBUF,2048,LEN,NUM)
      IF(IERR.NE.-12)GO TO 33
      WRITE(LU,50)
50    FORMAT("THIS RECORD NUMBER DOES NOT EXIST")
      CALL CLOSE(IDCB)
      GOTO 5
C
C FIND THE FOURIER TRANSFORM OF THE REFERENCE SIGNAL.
C
C FIRST SUBTRACT THE DC COMPONENT I.E. THE MEAN.
C
33    SUMR=0.
C TRANSFER THE REFERENCE SIGNAL TO THE ARRAY REF.
      DO 35 I=1,1024
      REF(I)=FLOAT(IBUF(I))
      SUMR=SUMR+REF(I)
35    CONTINUE
      SUMR=SUMR/1024.
      DO 36 I=1,1024
```

```
      REF(I)=REF(I)-SUMR
      REFI(I)=0.
36    CONTINUE
C FOURIER TRANSFORM THE REFERENCE DATA.
      CALL FT01(1024,2,REF,REFI)
      CALL CLOSE(IDCB)
C
C FIND THE FOURIER TRANSFORM OF THE RECEIVED SIGNAL.
C
C FIRST SUBTRACT THE DC COMPONENT I.E. THE MEAN.
C
37    SUMD=0.
      DO 38 I=1,1024
C TRANSFER THE RECEIVED SIGNAL TO THE ARRAY DAT
      DAT(I)=FLOAT(IBUF(I+1024))
      SUMD=SUMD+DAT(I)
38    CONTINUE
61    SUMD=SUMD/1024.
      DO 150 I=1,1024
      DAT(I)=DAT(I)-SUMD
      DATI(I)=0.
150   CONTINUE
C FOURIER TRANSFORM THE SIGNAL DATA.
      CALL FT01(1024,2,DAT,DATI)
C FORM THE CORRELATION SPECTRUM.
      DO 200 I=1,1024
      AR=DAT(I)
      ARI=DATI(I)
      BR=REF(I)
      BRI=REFI(I)
      DAT(I)=(AR*BR+ARI*BRI)
      DATI(I)=(BR*ARI-AR*BRI)
200   CONTINUE
C  INVERSE FOURIER TRANSFORM THE CORREATION SPECTRUM.
      CALL FT01(1024,1,DAT,DATI)
      DO 202 I=1,1024
      J=1025-I
      IBUF(I)=INT(DAT(I)/512.)
202   CONTINUE
      WRITE(LU,550) IN
550   FORMAT("RECORD NUMBER",I3," IS PROCESSED")
C
C STORE THE RESULT ON THE DISK.
C
      IF(IN.GT.1) GOTO 810
      ISIZE=NA*8
400   WRITE(LU,500)
500   FORMAT("TYPE RESULT DATAFILE NAME (6 CHARACTERS)")
      READ(LU,600)NAMERE
600   FORMAT(3A2)
      WRITE(LU,510)
510   FORMAT("TYPE CARTRIDGE REFERENCE NUMBER!")
      READ(LU,*)IREF
      GO TO 800
700   WRITE(LU,710)
710   FORMAT(21HFILE ALREADY EXISTS !,/,
     247HIF YOU WANT TO OVERWRITE OLD FILE TYPE (RETURN),/,
```

```
     323HIF NOT, TYPE ANY NUMBER)
      READ(LU,*)IFI
      IF(IFI.NE.0)GO TO 400
      CALL PURGE(IDCB,IERR,NAMERE,0,IREF)
800   CALL CREAT(IDCB,IERR,NAMERE,ISIZE,1,0,IREF)
      IF(IERR.EQ.-2)GO TO 700
      IF(IERR.LT.0)CALL ERROR(LU,IERR,1)
810   CALL OPEN(IDCB,IERR,NAMERE,0,0,IREF)
      IF(IERR.LT.0)CALL ERROR(LU,IERR,2)
      NUMRES=8*IN-(8-1)
      CALL WRITE(IDCB,IERR,IBUF,1024,NUMRES)
      IF(IERR.LT.0)CALL ERROR(LU,IERR,3)
      CALL CLOSE(IDCB)
C INCREASE THE RECORD COUNTER
C
      IN=IN+1
C ARE ALL THE RECORDS PROCESSED ?
C IF NOT GOTO 31
      IF(IN.LE.NA)GOTO 31
      WRITE(LU,900)NAMERE
900   FORMAT(34HTHE DATA RECORDED IS NOW STORED ON,/,
     122HDISK IN A FILE CALLED ,3A2)
      END
      SUBROUTINE ERROR(LU,IERR,N)
      WRITE(LU,40)N,IERR
40    FORMAT(9HFMP ERROR,I1,2X,I3)
      STOP
      END
```

```
      SUBROUTINE FT01(IT,INV,TR,TI),FIT 17.9.79
C         THIS SUBROUTINE CALCULATES THE FOURIER TRANSFORM OF
C        EQUALLY SPACE F(N) N=0,1,.......IT-1.
C          *******ARGUMENTS SET BY CALLING PROGRAM *******
C          IT IS NUMBER OF SAMPLES,POWER OF 2.
C          INV=2  FOR DIRECT TRANSFORM.
C          INV=1  FOR INVERSE TRANSFORM.
C          TR(I)  CONTAINS REAL DATA,THE TRANSFORMED DATA
C                 IS RETURNED IN THE SAME ARRAY.
C          TI(I)  CONTAINS IMAGINARY DATA,THE TRANSFORMED DATA
C                 IS RETURNED IN THE SAME ARRAY.
C          ********ARGUMENTS SET BY FT01*******
C          IF IT IS NOT POWER OF 2,
C          INV IS SET TO -1 AND FT01 RETURNS TO
C          THE CALLING PROGRAM.
C THIS SUBROUTINE IS TAKEN FROM HARWELLS SUBROUTINE LIBRARY,
C ORIGINATOR A.R. CURTIS,HARWELL. ADOPTED TO A
C HEWLETT PACKARD 1000 COMPUTER WITH A RTE-4 OPERATING SYSTEM BY
C O.MOEN,ATTACHED TO THE NDT CENTRE,AERE,HARWELL,1979
      DIMENSION TR(4),TI(4),UR(15),UI(15)
100   UM=0.5
      DO 50 I=1,15
      UM=0.5*UM
      TH=6.283185307178*UM
      UR(I)=COS(TH)
      UI(I)=SIN(TH)
50    CONTINUE
200   UM=1.0
      IF(INV.GT.1) GOTO 2
1     UM=-1.0
2     I0=2
      DO 3 I=2,16
      I0=I0+I0
      IF(I0-IT)3,4,5
3     CONTINUE
C       ERROR IN IT - SET INV=-1 AND RETURN.
5     INV=-1
      WRITE(1,1000)
1000  FORMAT("INV=-1")
      RETURN
C   IT=2**I -INITIALISE OUTER LOOP.
4     I0=I
      II=I0
      I1=IT/2
      I3=1
C       START MIDDLE LOOP
10    K=0
      I2=I1+I1
C       CALCULATE TWIDDLE FACTOR E(K/I2).
11    WR=1.
      WI=0.
      KK=K
      J0=I0
24    IF(KK)21,22,21
21    J0=J0-1
      KK1=KK
      KK=KK/2
```

```
      IF(KK1-2*KK)23,21,23
23    WS=WR*UR(J0)-WI*UI(J0)
      WI=WR*UI(J0)+WI*UR(J0)
      WR=WS
      GOTO 24
22    WI=WI*U
C START INNER LOOP
      J=0
C       DO 2*2 TRANSFORM
31    L=J*I2+K
      L1=L+I1
      ZR=TR(L+1)+TR(L1+1)
      ZI=TI(L+1)+TI(L1+1)
      Z=WR*(TR(L+1)-TR(L1+1))-WI*(TI(L+1)-TI(L1+1))
      TI(L1+1)=WR*(TI(L+1)-TI(L1+1))+WI*(TR(L+1)-TR(L1+1))
      TR(L+1)=ZR
      TR(L1+1)=Z
      TI(L+1)=ZI
C       INDEX J LOOP
      J=J+1
      IF(J-I3)31,12,12
C       INDEX K LOOP
12    K=K+1
      IF(K-I1)11,6,6
C       INDEX OUTER LOOP
6     I3=I3+I3
      I0=I0-1
      I1=I1/2
      IF(I1)51,51,10
51    J=1
C       UNSCRAMBLE
      UM=1.
      IF(INV.GT.1) GOTO 52
61    UM=1./FLOAT(IT)
52    K=0
      J1=J
      DO 53 I=1,II
      J2=J1/2
      K=2*(K-J2)+J1
53    J1=J2
54    IF(K-J)66,56,55
56    TR(J+1)=TR(J+1)*UM
      TI(J+1)=TI(J+1)*UM
      GOTO 66
55    ZR=TR(J+1)
      ZI=TI(J+1)
      TR(J+1)=TR(K+1)*UM
      TI(J+1)=TI(K+1)*UM
      TR(K+1)=ZR*UM
      TI(K+1)=ZI*UM
66    J=J+1
      IF(J-IT+1)52,57,57
57    TR(1)=TR(1)*UM
      TI(1)=TI(1)*UM
      TR(IT)=TR(IT)*UM
      TI(IT)=TI(IT)*UM
      RETURN
      END
```

APPENDIX III

Reprint from conference proceedings Ultrasonics International '79. Graz., Austria, 15-17 May, IPC Business Press Limited, 1979.

APPENDIX IV

List of principal symbols used.

In general only symbols which are used in more than one chapter are included.To agree with accepted standars some symbols have a double meaning.The relevant one should be clear from the content.

A	Amplitude.
B	Bandwidth.
C_{ik}	Elastic constant.
C_o	Electrical capacitance.
D	Electrical displacement.
E	Young's modulus; electrical field strength.
F	Force.
G	Material fracture toughness.
$G(j\omega)$	Transfer function.
I	Intensity.
M	Modulation index.
N	Number of samples in a digitiser.
N_{lev}	Number of levels in a digitiser.
P	Pressure.
Q	Electrical charge.
R	Electrical resistance.
R_{xy}	Cross-correlation function between x and y.
T	Temperature; pulse length.
T_s	Sampling period.
V	Electrical voltage.
X	Electrical reactance.
Z	Impedance.

a	Area.
c	Phase velocity.
f	Frequency.
h	Piezoelectric conversion constant.
j	$\sqrt{-1}$
k	Wave number; Boltzmans constant.
p	Wave pressure.
r	Reflection coefficient.
t	Time.
u	Displacement vector.
z	Characteristic impedance.
α	Attenuation constant.
ε	Dielectric constant.
λ	Wavelength.
μ	Absorption constant.
ν	Poisson's ratio.
ρ	Density.
σ	Mechanical stress; root mean squared amplitude.
τ	Time delay.
ω	Angular frequency.
ΔA	Amplitude change during 't.
ΔV_h	Voltage drop.
Δt	Aperture time.
$\Delta 't$	Aperture uncertainty time.

APPENDIX V

Electronics specifications and wiring diagram.

Receive amplifier,Harwell 95/0187-1:

Gain = 20-50 dB
Input impedance = 50 ohm.
Output impedance = 50 ohm.
Bandwith = 0.2-40 MHz.

Filters were used to reduce the bandwidth,these were set to give a bandwidth of 0.2-6 MHz.

Sender amplifier,Harwell 95/2153-1:

Gain = 20-73.5 dB
Input impedance = 100 ohm.
Output impedance = 100 ohm.
Bandwidth = 0.5 kHz- 8 MHz.

Filters were used to reduce the bandwidth,these were set to give a bandwidth of 0.03-8 MHz. This corresponds to a second order differentiation time constant of 5 µS and an integration time constant of 0.02 µS.

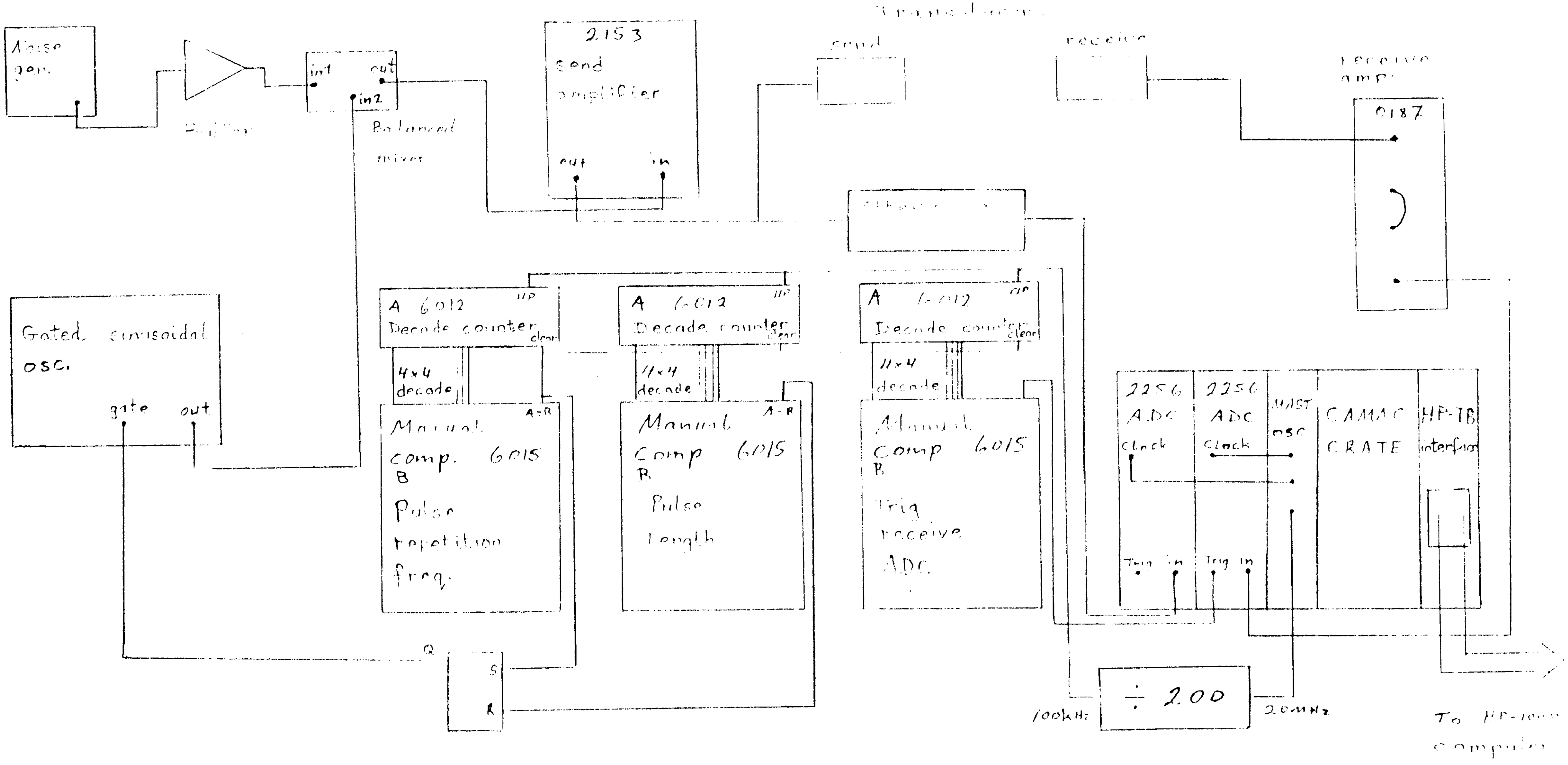

Electrical wiring diagram for the experimental cross-correlation flaw detector.

REFERENCES

CHAPTER 2

1. Knott, J. F.
Fundamentals of fracture mechanics.
Butterworth, 1973.

2. McMaster, R. C.
Nondestructive testing handbook.
The Ronald Press Company, Vol. 1 and 2, 1959.

3. Halmshaw, R.
Physics of industrial radiology.
Iliffe books Limited, 1966.

4. Sokoloff, S.
Means of indicating flaws in materials.
U.S. pat. no. 2 164 125, 1939.

5. Firestone, F. A.
The supersonic reflectoscope, an instrument for inspecting the interior of solid parts by means of sound waves.
Journ. Acoust. Soc. Am., 17(3), pp. 287-299, 1946.

6. Kinsler, L. E. and Frey, A. R.
Fundamentals of acoustics.
John Wiley and Sons Inc., 1962.

CHAPTER 3

1. Gooberman, G. L.
Ultrasonic, theory and application.
The English University Press, London, 1968.

2. Pollard, H. F.
Soundwaves in solids.
Point Limited, London, 1977.

3. Silk, M. G., Lidington, B. H. and Hammond, G. F.
A time domain approach to crack location and sizing in austenitic welds.
B. J. NDT, 22, pp. 55-61, 1980.

4. Silk, M. G.
The propagation of ultrasound in austenitic weldments.
UKAEA, Harwell, rep. R9391, 1979.

5. Wagg, A. R., Tomlinson, J. R. and Whittle, M. J.
Ultrasonic inspection of austenitic welds.
B. J. NDT, 22, pp. 119-127, 1980.

6. Mason, W. P., and McSkimin, H. J.
Energy losses of sound waves in metals due to scattering and diffusion.
Journ. App. Phy., 19, pp. 960-946, 1948.

7. Merkulov, L. G.
Investigation of high-frequency scattering.
Soviet Techn.-Phys., 1, pp. 59-66, 1956.

8. Bhatia, A. B.
Scattering of high-frequency sound waves in polycrystalline materials.
Journ. Acoust. Soc. Am., 31(1), pp. 16-23, 1956.

9. Papadakis, E. P.
Ultrasonic attenuation caused by scattering in polycrystalline media.
Phy. Acoust., ed. Mason and Thurston, 15, pp 269-328.

10. Papadakis, E. P.
Ultrasonic attenuation caused by scattering in polycrystalline metals.
Journ. Acoust. Soc. Am., 37(1), pp. 711-717, 1965.

11. Serabian, S., and Williams, R. S.
Experimental determination of ultrasonic attenuation characteristics using the Roney generalised theory.
Materials Evaluation, pp. 55-62, July 1978.

12. Neuman, E., Roemer, M., Just, T., Matthies, K., Nabel, E. and Mundry, E.
Development and improvement of ultrasonic testing techniques for austenitic nuclear components.
ASM/ASTM/ASTN/ANS Conf. Nondestructive evaluation in the nuclear industry, Salt Lake City, 13-15 Feb. 1978.

Chapter 4

1. Whittington, K. R.
Ultrasonic inspection of hot steel.
B.J. NDT, 20(5), pp. 242-247, 1978.

2. Breazeale, M. A., and Cantrelle, J. H.
Elimination of transducer bond corrections in accurate ultrasonic-wave velocity measurements by use of capacitive transducers.
Journ. Acoust. Soc. Am., 61(2), pp. 403-406, 1977.

3. Curtis, G.
A broadband polymeric foil transducer.
Ultrasonic, 12(4), pp. 148-154, 1974.

4. Bar-Cohen, Y.
Non-destructive testing of microwelds using Laser-induced shock waves.
B.J. NDT, 21(2), pp.76-78, 1979.

5. Berlincourt, D. A., Jaffe, B., Jaffe, H., and Krueger, H. H. A.
Transducer properties of lead titanate zirconate ceramics.
IRE Trans. Utrason. Eng., VE7(1), pp. 1-6, 1960.

6. Redwood, M.
A study of waveforms in the generation and detection of short ultrasonic pulses.
Appl. Mat. Research, 2, pp. 76-84, 1963.

7. Kazhis, R. I., and Lukoshevichyus, A. I.
Wideband piezoelectric transducers with an inhomogeneous electric field.
Sov. Phys. Acoust., 22(2), pp. 167-168, 1976.

8. Redwood, M. and Mitchell, R. F.
The generation of sound by non-uniform piezoelectric materials.
Ultrasonics, 7(2), pp. 123-24, 1969.

9. Bainton, K. F., and Silk, M. G.
Some of the factors which affect the performance of ultrasonic transducers.
B. J. NDT, 22(1), pp. 15-20, 1980.

10. Kossof, G.
The effect of backing and matching on the performance of piezoelectric ceramic transducers.
IEEE Trans. Sonic and Ultrason, SU-13(1), pp. 20-30, 1966.

11. Kinsler, L. E., and Frey, A. R.
Fundamentals of acoustics.
John Wiley and Sons, Inc., 1962.

12. Manufactures Data
Vernitron Limited, Thornhill, Southampton, England.

13. Gooberman, G. L.
Ultrasonics theory and application.
The English Univ. Press Limited, 1968.

14. Fraser, W.
Telecommunications
Macdonald and Co. Limited, 1967.

15. Mason, W. P.
Electromechanical transducers and wave filters.
Van Nostrand, 1948.

Chapter 5

1. Crowther, J. G., and Whidington, R.
Science at war.
His Majesty's Stationary Office, London,1947.

2. Tucker, D. G.
Sonar
The New Encyclopaedia Britannica, 15th Ed., 17, pp.1-4, 1977.

3. Graff, K. F.
Ultrasonics:Historical aspects.
IEEE Ultrasonic Symposium Proc.,pp. 1-10, 1977.

4. Whealer, G. J.
Radar
The new Encyclopaedia Britannica, 15th Ed., 17, pp.1-4, 1977.

5. Sachse, W., and Ceranoglu, A. N.
Experiments with a well-characterised acoustic emission system.
Proc. Ultrasonics Int., Graz, pp.138-145, 1979.

6. Wadley, H. N. G., Sruby, C. B., and Speake, J. H.
Acoustic emission for the physical examination of metals.
UKAEA, Harwell, Report 9335, 1979.

7. Kinsler, L. E., and Frey, A. R.
Fundamentals of acoustics.
John Wiley and Sons, Inc., 1962.

8. Inst. of Acoustics
Transducer arrays and array processing.
Proc. of the specialist meeting; underwater acoustics group held at the University of Birmingham,13-14 December 1978.

9. Steinberg, B. D.
Principles of aperture and array system design.
John Wiley and Sons, 1976.

10. Waugh, T. M., Kino, G. S., De Silets, G. S., and Fraser, J. D.
Acoustic imaging techniques for nondestructive testing.
IEEE Trans. sonic and ultrasonics, SU-23(5), pp.313-317, 1976.

11. Plummer, J. D., Swartz, R. G., Maginness, M. G.
Beaudouin, J. R., and Meindly, J. D.
Two-dimensional transmit/receive ceramic piezoelectric arrays: Construction and performance.
IEEE Trans. sonci and ultrasonics, SU-25(5), pp.273-280, 1978.

12. Brown, W. M., and Porcello, L. J.
An introduction to synthetic aperture radar.
IEEE spectrum, pp. 52-62, 1969.

13. Fredrick, J. R., Vanden Brock, G., Ganapathy, S., Elzinga, M., Devrise, W., Papworth, D., and Hamano, N.
Improved ultrasonic nondestructive testing of pressure vessels.
U.S. Nuclear regulatory commission, NUREG/CR-0908, 1979.

14. Jackson, J. L.
Program for field validation of synthetic aperture focussing technique testing.
U.S. NUREG/CR-0290, 1978.

15. Moose, P. H.
Signal processing in reverberant environments.
Signal processing, Academic Press, London, 1973.

16. Ermolov, I. N., and Pilin, B. P.
Ultrasonic inspection of materials with coarse grain anisotropic structures.
NDT International, 9(6), pp. 275-280, 1976.

17. Bilgutay, N. M., Furgason, E. S.,and Newhouse, V. L.
Evaluation of a random signal correlation system for ultraonic flaw detection.
IEEE Trans. on sonic and ultrasonic, SU-23(5), pp.329-333, 1976.

Chapter 6

1. Abramowitz, M., and Stegun, I. A.
Handbook of mathematical functions.
Dover Pub., Inc., New York, 1970.

2. Lathi, B. P.
An introduction to random signals and communication theory.
Int. Textbook comp., London, 1968.

Chapter 7

1. Betts, J. A.
Signal processing, modulation and noise.
Hodder and Stoughton Limited, London, 1970.

2. Shannon, C. E.
Communication in the presence of noise.
Proc. IRE, 37(1), pp. 10-21, 1949.

3. Bingham, C., Godfrey, M. D. and Tukey, J. W.
Modern techniques of power spectrum estimation.
IEEE Trans. audio, el, acous., AU-15(2), pp. 56-66, 1967.

4. Welch, P. D.
The use of fast Fourier transform for the estimation of power spectra:A method based on the time averaging over short, modified periodograms.
IEEE Trans. audio, el. acous., AU-15(2), pp. 70-73, 1967.

5. Burgess, J. C.
On digital spectrum analysis of periodic signals.
J. Acoust. Soc. Am., 58(3), pp. 556-567, 1975.

6. Harris, F. J.
On the use of windows for harmonic analysis with discrete Fourier transform.
Proc. IEEE, 66(1), pp. 51-83, 1978.

7. Ricci, D. W., and Nelson, G. E.
Standard instrument interface simplifies system design.
Electronic internation, 47(23), pp. 95-106, 1974.

8. Klessmann, H.
Introducing CAMAC: An international instrument standard for on-line data acquisition and process control.
CAMAC seminar of KVIV-Technologisch Institut, Antwerpen, 23rd March 1977.

9. Elsley, R. K.
Accurate ultrasonic measurements with the Biomation 8100 transient recorder.
Report SC-PD-78-70, Science Centre, Rockwell Int., 1978.

Chapter 8

1. Oppenheim, A. V., and Schafer, R. W.
Digital signal processing.
Prentice-Hall, Inc., New Jersey, 1975.

2. Bringham, O. E.
The fast Fourier transform.
Prentice-Hall, Inc., London, 1974.

3. Singelton, R. C.
An algorithm for computing the mixed radis fast Fourier transform.
IEE trans. audio,el. acous.,AU-17(2), pp.93-103, 1969.